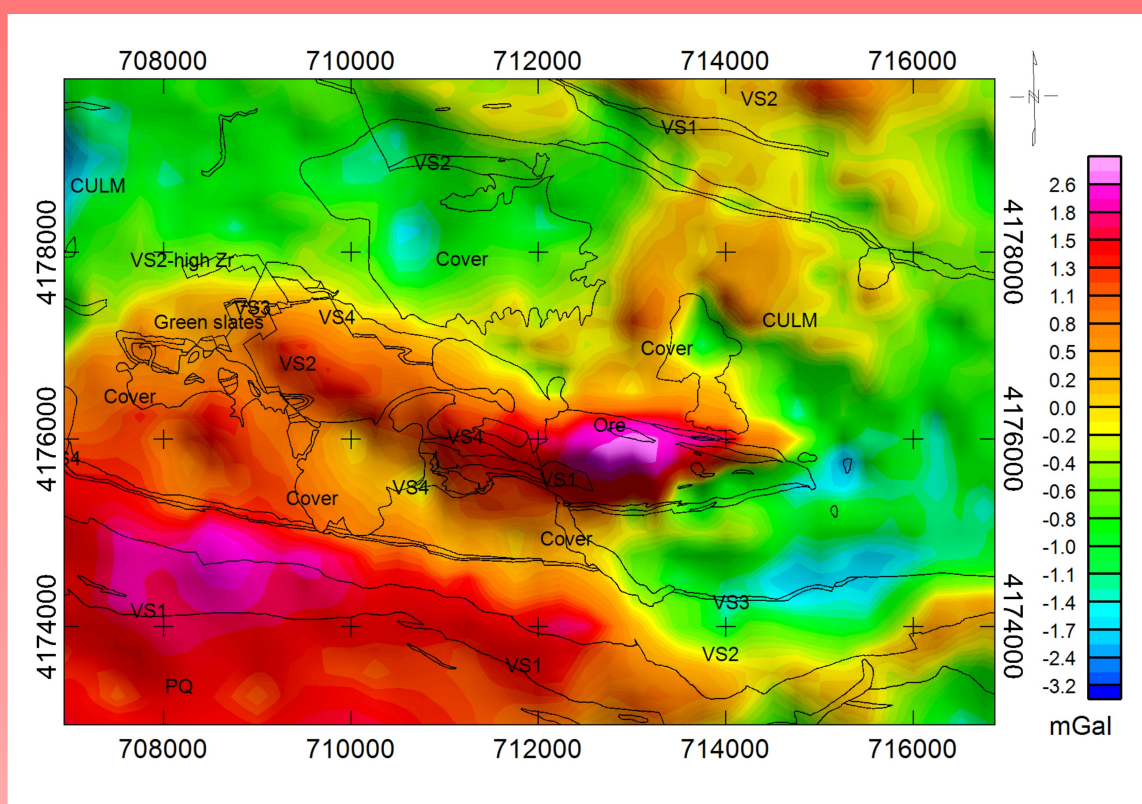# Characterization of geological structures from gravity and magnetic data of Riotinto, Iberian Pyrite Belt (Huelva, Spain)

Autores: Teresa Sánchez-García
                Concepción Ayala Galán
                Alejandro Díez Montes
                Jose Luis García Lobón
                Carmen Rey Moral
                Jesús García Crespo
                Félix Bellido Mulas
                Félix Manuel Rubio

MINISTERIO DE ECONOMÍA, INDUSTRIA Y COMPETITIVIDAD

Instituto Geológico y Minero de España

Characterization of geological structures from gravity and magnetic data of Riotinto, Iberian Pyrite Belt (Huelva, Spain)

Characterization of geological structures from gravity and magnetic data of Riotinto, Iberian Pyrite Belt (Huelva, Spain)

Autores:

Teresa Sánchez-García
Concepción Ayala Galán
Alejandro Díez Montes
Jose Luis García Lobón
Carmen Rey Moral
Jesús García Crespo
Félix Bellido Mulas
Félix Manuel Rubio

San Dionisio orebody

Filon Sur orebody

Purple shales

Epiclastic rhyolites

Rhyolites-Dacites

Basalts

P-Q fm.

Eduardo fault

1 km

N
W   E
S

INDEX

1. INTRODUCTION. BACKGROUND

The Spanish Geological Survey (IGME) has been involved during the last years in many infrastructure and metalogenetic research projects located in the South-Portuguese and Ossa-Morena zones of the Variscan Iberian Massif. These zones are characterized by the exceptional mine and metalogenetic orebodies. In fact, in the southwest of Spain are located some of the most important massive sulphurs of the world and some remarkable metallic crustal anomalies.

Following this events, the 6th of May 2009, IGME signed as a co-partner the project "*Nano-particle products from new mineral resources in Europe*" (ProMine, NMP-2008-4.0-5) (contract 228559) of the seventh UE Forward Program, together with 25 partners. The project was led by the Finland geological survey (GTK). Out of the 7 work packages of Promine, the IGME has been actively involved in WP1, WP2 and WP4.

The objective of WP2 was to obtain the 3D model of the main orebodies representative of the Ossa Morena Zone and South Portuguese Zone. Specifically the work was focused in Aguablanca and Cala Mine of the Ossa Morena Zone and the Río Tinto orebody of the Pyritic Belt.

This report is the result of the geological and geophysical investigation and the 2.5 and 3D geological and geophysical models of the Río Tinto area, within the WP2.

2. OBJECTIVES. METHODOLOGY

2.1. Objectives. Study area

The aim of this study is to obtain the geophysical characterization of the geological structures in Río Tinto mine (Huelva). To that end, we have analysed and interpreted magnetic and radiometric

airborne data together with gravity and petrophysical data from the IGME databases as well as newly acquired gravity and petrophysical data specifically for this work.

The figure 2.1 shows the reduced to the pole total field aeromagnetic map, scale 1:200.000 of the Pyritic Belt. With a green rectangle the study area is depicted, covering the southwest sector of the geological map of Nerva (sheet number 938).

The study area, covering c. 86 km^2 (green rectangle of ~11x7.65 km, in figure 2.1) is located in the southwest sector of the geological map of Nerva (geological sheet number 938). This area has been previously investigated for its high interest in economic mineralizations of Cu, Pb, Zn, Fe and Au.

The distribution of the gravity stations compiled and new, is shown in figure 2.2.
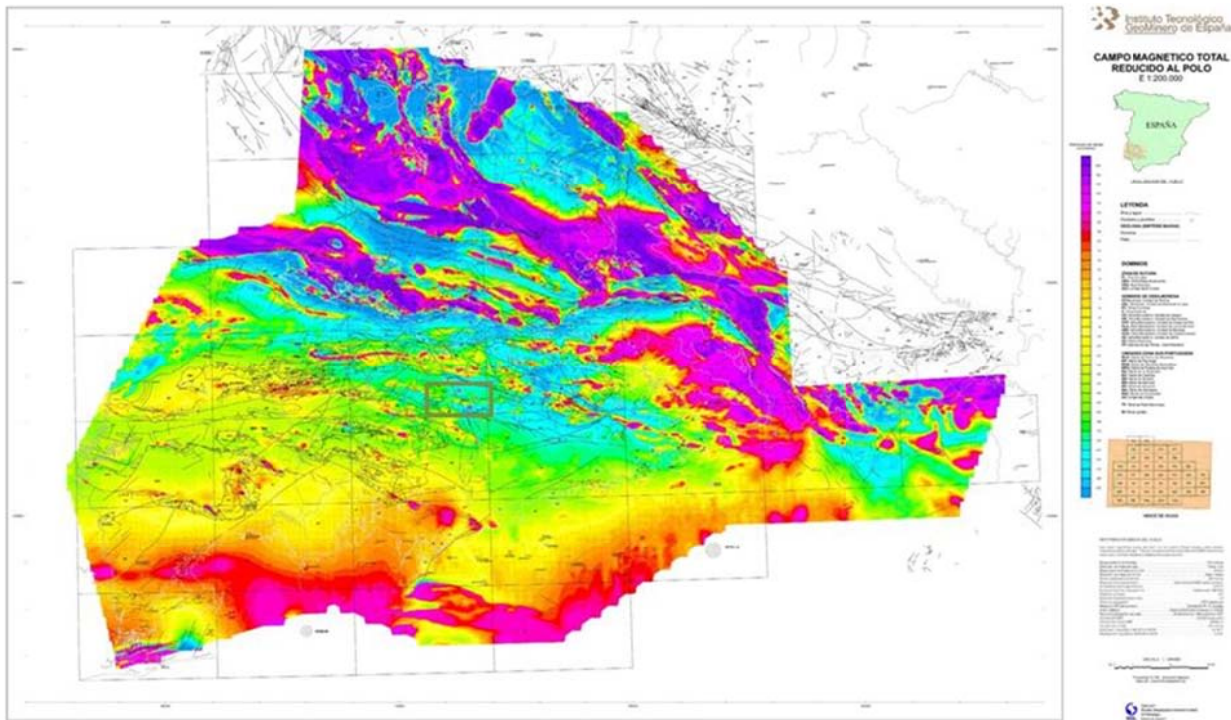
Figure 2.1: Reduced to the pole aeromagnetic map, scale 1:200.000. The green rectangle shows the area included in this project.

2
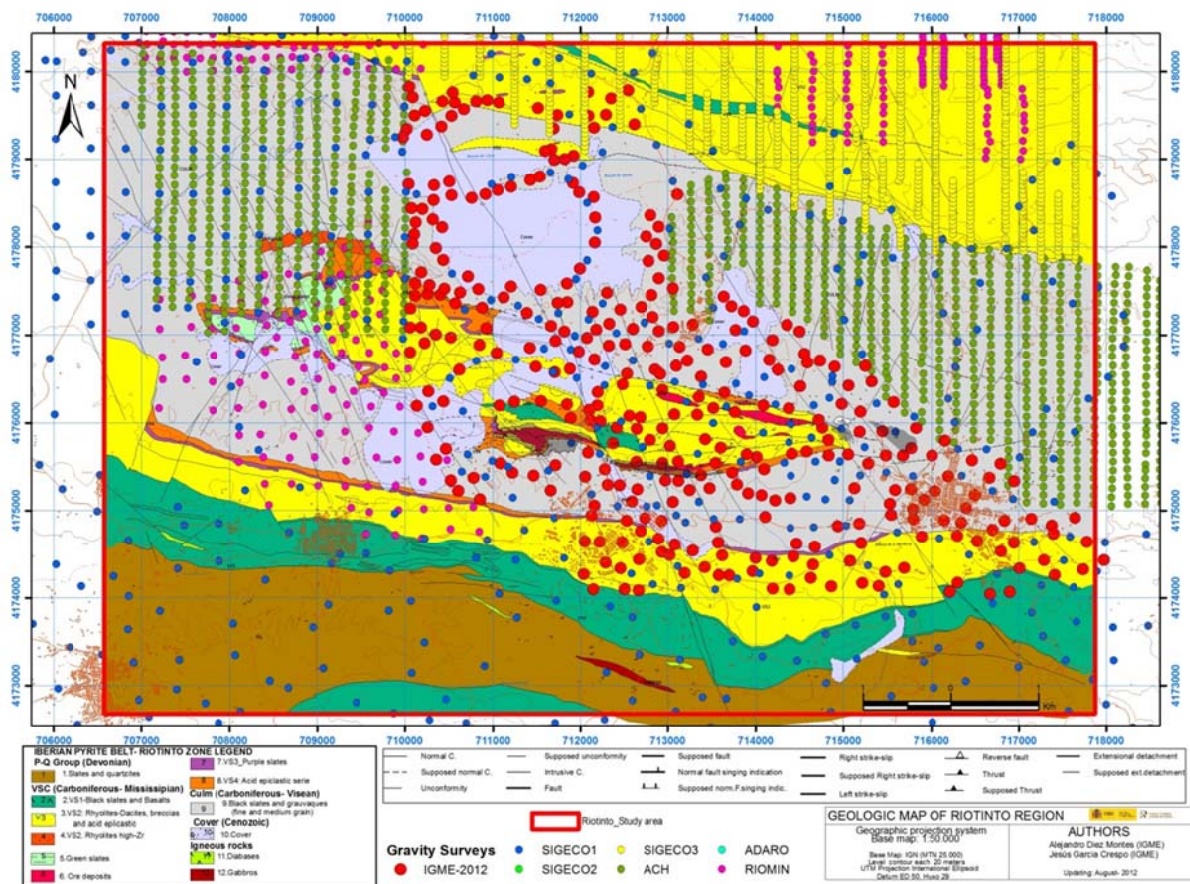
Figure 2.2 Available gravity data in the study area.

The table 2.1 is a summary of the compiled and new acquired gravity data.

2.2. Metodology

The methodology involves:

- Compilation of geological and geophysical data. Revision of the geological cartography and structure of the area.

- Acquisition of new gravity data with and appropriate distribution of points per km2 (see chapter 3 of this report).

- Acquisition of GPS topographic data together with the gravity data (see chapter 3 of this report).

- Acquisition of rock samples in order to make the petrophysical analysis.

- Processing of the gravity and GPS data using the appropriate software. Regional-residual gravity separation.

- Qualitative interpretation of the gravimetric, magnetic and radiometric maps. Interpretation of the isoanomaly maps based on the comparison between the anomalies and the corresponding surface geology.

3

- Petrophysical study of the mapped units.

- 2.5D and 3D modelling (see chapter 6). Geophysical models are the best way to test the geological structures in depth, providing a final model consistent with all the geological and geophysical observations.

To achieve these goals IGME has a proven experience in field work and also in processing, interpretation and modelling. We have the adecuate instrumentation for geophysical data acquisition (gravity meter, radiometric sensor, etc.), the expertise for the geological mapping and rock sampling and the specific software for data processing, interpretation and 2.5D and 3D modelling.

All the maps coordinates on this report are referred to UTM Projection International Elipsoid, Datum ED50, zone 29.

2.3. Geological and geophysical data

The geological and geophysical data used in this work (see summary in Table 2.I) are:

- MAGNA geological sheet number 938 (Navarro Vázquez and Ramírez Copeiro del Villar, 1982), Geological Map FAJA Project (Junta de Andalucía-IGME, 1982).

- New geological map of the Río Tinto area, made by the ProMine geologist's team, scale 1:10.000 (see figure 2.2).

- Digital Elevation Model, 100 m x 100 m grid (Instituto Geográfico Nacional, MDT 100) and digital Elevation Model, 25 m x 25 m grid (Instituto Geográfico Nacional, MDT 25))

- Compiled gravity, magnetic and natural gamma radiation data (SIGECO: geophysical data bases IGME, online, http://cuarzo.igme.es/sigeco/). The most relevant for this work is the 1996-97 flight (see figures 2.1, 5.3 and 5.4, 5.5, 5.6 and 5.7, Bates, M., García Lobón, J.L., 1998.

 Gravimetric Data from previous surveys:

1. Data from SIGECO geophysical database:

   - Regional gravity (1976 points, 4 point/km^2)
   - Detailed gravity (2528 points, about 30 points/km^2)

2. Gravimetric data from previous surveys made by others companies, and compiled for this study:

   - Atlantic Copper (2199 points)
   - ADARO (316 points)

4

- RIOMIN (401 points)

Topographic corrections were made using the DTM of the RIOMIN IBÉRICA, digitizing the 1:10.000 Junta de Andalucia topographic maps.

- Published petrophysical data (Plata and Navas, 1996).
- New acquired gravity, radiometric and petrophysical data (see table 2.I): A new gravity survey was carried out in the southern part of the study area, where no gravity data were available. 327 stations were measured using a Scintrex CG5 gravity meter. Bouguer anomaly was calculates into account also measures from previous surveys (Table I), using the GRS67 geodetic system and with a density reduction of 2.60 g/cm^3. From Bouguer anomaly, a suitable residual gravity anomaly was obtained (See Chapter 5 of this report).

Data	New acquired	Compiled
Gravity	327 points	SIGECO: 4504 points; Riomin-ACH-Adaro: 2916 points
Magnetic	-	Grids flight 1996-97
Radiometric	-	Grids flight 1996-97
Petrophysics	67samples	167samples

Table 2.I. Geophysical and petrophysical data used for the characterization of the Río Tinto area.

The Table 2.II summarizes the gravity data used in the Río Tinto area (figure 2.2)

Gravimetric surveys of RÍO TINTO Zone	Origin-data	UTMXmin	UTMXmáx	UTMYmin	UTMYmáx	Nº points
IGME-2012	IGME	709803	718534	4174728	4179822	327
SIGECO1	SIGECO	704324	719156	4171634	4183097	1976
SIGECO2	SIGECO	705806	719161	4172818	4182799	492
SIGECO3	SIGECO	709694	718459	4177445	4183097	2036
ADARO	ADARO	707205	719205	4174000	4181189	316
ACH	Atlantic Copper	706990	718641	4175040	4181052	2199
RIOMIN	Riomin Ibérica	706834	717449	4174196	4181012	401

Table 2.II. Coordinates UTM zone 29. Some of the areas have irregular limits so these coordinates represent the encompassed data limits.

The airborne survey from which the aeromagnetic and radiometric data has been taken comes from a flight covering an area of 15.185 km^2 including the Pyritic Belt and adjacent areas (within the Badajoz, Huelva and Sevilla provinces). Its aim was to obtain geophysical information in order to find new orebodies sites. The flight was carried out during 1996-97, by the Sander Geophysics Ltd., Canadian company, and it was supervised and interpreted by IGME (Bates, M.and García Lobón, J.L., 1998). A total of 69019 km of lines (N-S trend) were flown, with 250 m spacing between the lines. The altitude clearance was 80 m. The processing of the radiometric data (levelling and gridding, at 50*50 m) was also done. The radiometric data were processed with reduction, micro levelling and gridding (100*100 m).

As final products, the maps were: total magnetic field, reduced to the pole magnetic field, vertical gradient and radiometric data, scale 1:50.000, 1:100.000 and 1:200.000.

The reduced to the pole aeromagnetic map (nT) in the study area could be seen in the Figure 5.3. The radiometric maps of the Río Tinto Area, Potassium, Thorium and Uranium could be seen in figures 5.4, 5.5 and 5.6 respetively of this report. Ternary map could be seen in the Figure 5.7.

3.   ACQUISITION OF NEW DATA. CALCULATION OF GRAVITY ANOMALIES

3.1.   GPS topografic survey

The Bouguer anomaly calculation requires knowing the coordinates of each gravimetric station with great precision; especially in relation to the elevation of the station.The number of points measured in the gravimetric survey was 327, which distribution is shown in Figure 3.1.

The GPS system provides coordinates in WGS84 (World Geodetic System of 1984 year) global system associated to the ellipsoid in the year 1984.

For gravimetric data, the value of the normal gravity is established from the existing values on a reference surface or geoid (approximated by revolution ellipsoid), at sea level, and depends on the geographical latitude. The use of different ellipsoids and/or G values, gives rise to different systems of reference for the gravimetric surveys. The standard UNE 22-611-85, "Prospección Geofísica Terrestre, método gravimétrico", sets the geodetic system GRS67 for the calculation of the normal gravity. This system use for the calculation of the normal gravity the expression of the International Gravity Formula of 1967 (with Datum Potsdam 981260 mGal) and with the latitude in the reference system ED50.
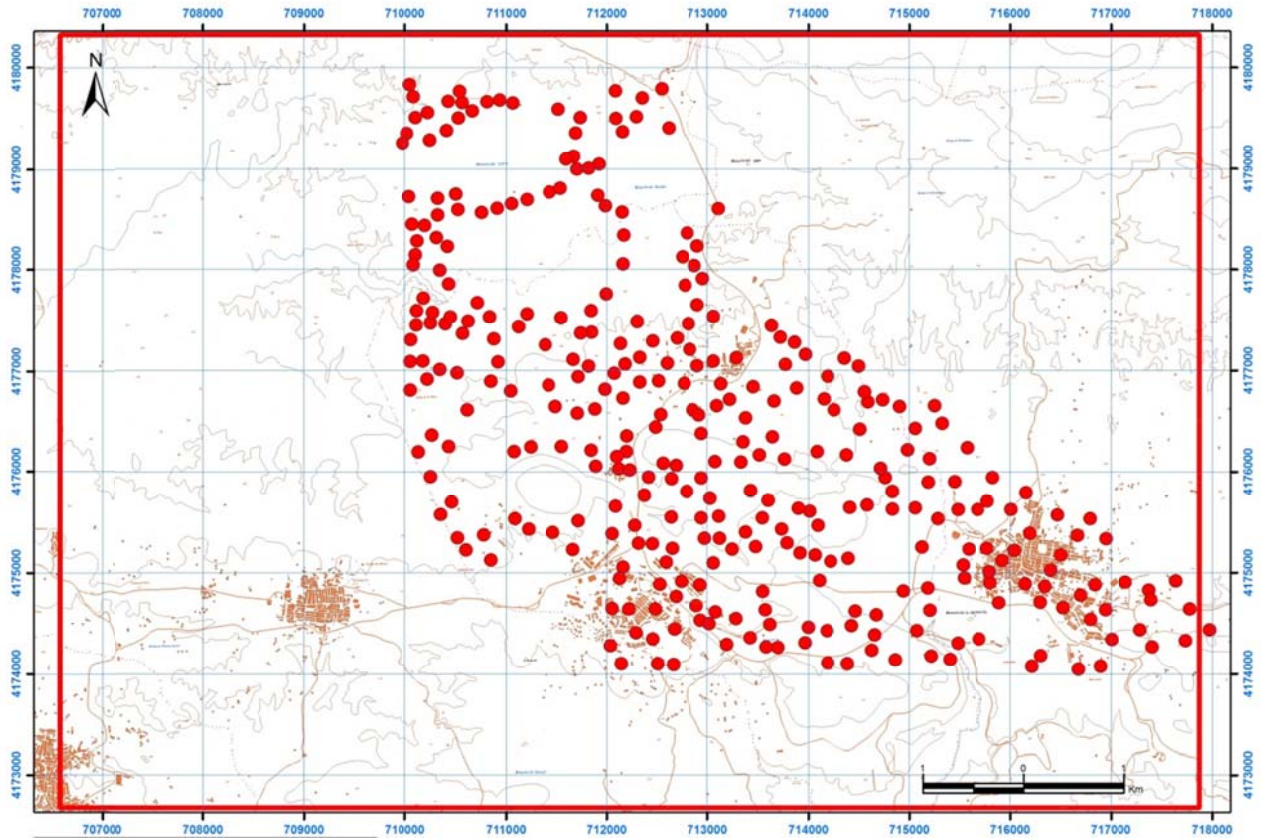
Figure 3.1. Point distribution of the IGME survey (2011-2012): a total of 327 were measured.

Orthometric height, H, is the height referred to the geoid (in Spain is taken as a reference the mean sea level in Alicante), while the ellipsoidal height, h, is referred to the reference ellipsoid height. The height measured with GPS provides the h referred to the international ellipsoid WGS84.

To convert ellipsoidal heights into ortometric heights is required to know the height of the geoid N (separation between the geoid and the ellipsoid), so:

$$H = h - N$$

The problem is that the surface of the geoid is not usually well known, and its calculation is constantly updated (Fairhead et al., 2003). In this work the IGN REDNAP EGM08 geoid model has been used. Usually, the heights are expressed in metres. The calculation of the coordinates has been referred to the ED50 system (by transforming from WGS84 into ED50) and calculation of normal gravity to the geodetic system GRS67.

3.1.1 Instrumentation. Description of the methodology adopted

The instruments used have been receptors Triumph from JAVAD. This GPS instrument reads and stores the signal with milimetrical accuracy and has the ability to work in static or cinematic mode.

We used two instruments, with the idea of using one of them as a base and other as mobile along with the gravity meter.

A control point has been used as a base. This point has been established by measuring in static mode with a receiver for 6 hours and performing differential correction with values from the GNSS base of Aracena. Figure 2.3 shows a picture of the point. Its coordinates are, UTM (WGS84) 29 N, and ellipsoidal height:

X= 712831.40 m

Y= 4176889.41 m

Z= 501.69 m

The procedure we followed was to place a stationary receiver at this control point, as a base, and to move with the mobile receiver to the measurement points. Calculation of the differential correction and the coordinates of the stations is being done in postprocessing at the office. The software used for the post-processing has been the JUSTIN developed by Javad. The program made the calculation of the differential corrections, obtaining the following coordinates for all points of the survey in the WGS84 system:

X e Y in UTM projection, Huse 29 North, ellipsoidal height.

After that, we perform the transformation to ED50 UTM coordinates. For transforming to orthometric height, we have used the geoid model from the Instituto Geográfico Nacional (IGN) EGM08 REDNAP.

A
B

Figure 3.2 A) GPS instrument Triumph from JAVAD B) Gravimetry and GPS measurement at a point in the survey.

Figure 3.3. Control point used as topographic base in the survey.

3.1.2. Points distribution and quality Control of GPS measurements

In accordance with the objectives of the study we have sought to have a distrubution of field data through the area that complete and complement the data already available. The number of points measured in the survey has been 327, and its distribution is shown in Figure 3.1.

The number of repeated points of topography has been 24, which is more than 7% of the points of the survey:

As shown in Figure 3.4, displaying the histograms of the differences obtained in repeats for the coordinates X and Y (ED50 UTM) and the elevation Z, the result has been as follows:

The formule used for the calculation of the root mean square error is the indicated in the standard UNE 22-611-85, "Prospección Geofísica Terrestre, método gravimétrico", and is the same for the gravity control:

$$Ecm = \pm \sqrt{\frac{\Sigma d^2}{2N}}$$

d= differences between repeats measured

N=numbers of repeats points

The X-coordinate (UTM ED50):

- Average value of differences 0.41 m

- A root mean square error of 0.39 m

The Y-coordinate (UTM ED50):

- Average value of differences 0.26 m

- A root mean square error of 0.25 m

Height Z (Orthometric):

- Average value of differences 0.04 m

- A root mean square error of 0.04 m.
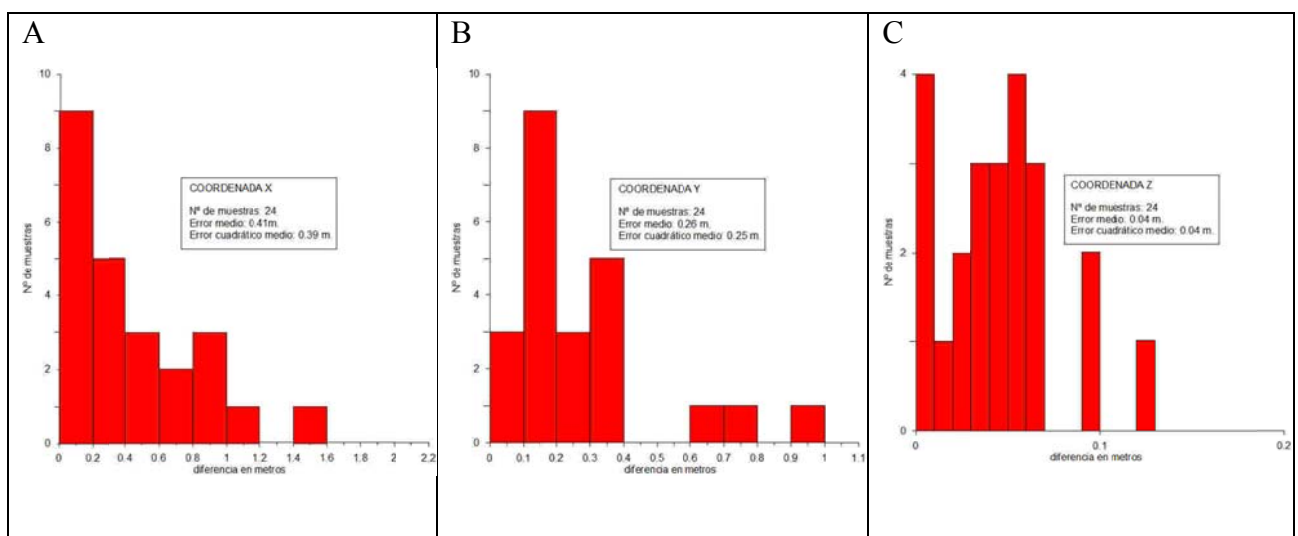
Figure 3.4. Histograms of the differences in m of the repeated points for: A) Coordenate X (UTM ED50 huse 29; B) Coordenate Y (UTM ED50 huse 29); C) Height Z (orthometric).

3.2.   Gravity meter. Observed gravity.

In gravimetry, we want to determine the density distribution of subsurface rocks through the observation of the perturbations that the geological structures cause in the Earth's gravitational field, measured on the surface (Plata et al., 2002). The gravity meters are the instruments used for this task and, are, in essence, mechanical escales with a mass supported with a spring. The gravity changes will produce variations in the weight of the mass, and therefore in the length of the spring, being this variation what is measured by the gravity meter. The gravity meters measure the vertical gravity.

In this work, for the acquisition of the gravity data has been used the Scintrex CG5 gravity meter of IGME. Originally this gravimeter Scintrex was a CG3 model, which was upgraded to the CG5 model in 2009. The nominal features of this device are:

Reading accuray: 1 microGal

Repeatability of standard field: < 5 microGal

The gravity meters are instruments of very high sensitivity, and should be used with great care since they are affected from variations over time, reflected in the values of the readings, phenomenon which is called drift. Different types of drift can be determined depending on the type of control that is carried out with the gravity meter. If the gravity meter is kept repeating the measurement at the same fixed point, the drift is called static, which gives an idea of the mechanical condition of the device. During a survey, drifting of mechanical and tidal origin can be called instrumental drift. In order to minimize the working drift, each working day is divided in what we call programme which duration (from one to several hours) depends on each gravity meter and on the accuracy we need for each survey. The alternation of the gavity meter measures at a fixed point and during the survey, controlled every 24 h provides the secular drift.

Figure 3.5 shows the registration at a fixed point of the facilities of the IGME carried out in April 2012, before one of the surveys. The record presents a drift less than 0.05 mGal/24 hours, proving the stability of the gravity meter.

During the field survey, control of the instrumental drift (the drift of each programme), and secular drift (control at fixed point, in this case the base of opening and closing of programs) has been made. Graph of the secular drift is shown in figure 3.6.

Lectura efectuadas el 8/4/2012 en el punto fijo del IGME
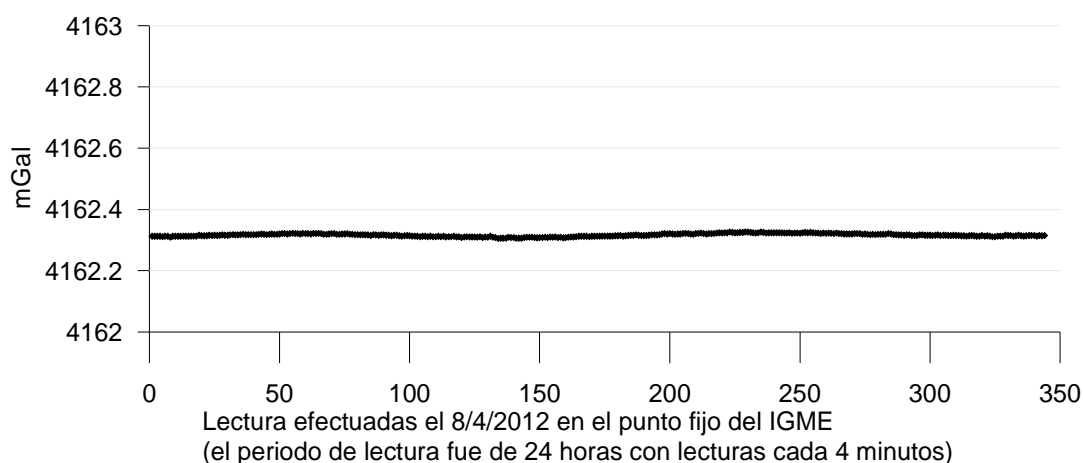(el periodo de lectura fue de 24 horas con lecturas cada 4 minutos)

Figure 3.5. Measurement at fixed point for 24 hours with Scintrex CG-5 gravity meter. In x-axis are represented sequentially the gravity meter readings, taken at 4 minute intervals during the April 8, 2012.

Figures 3.5 and 3.6 demonstrates that the gravity meter has shown a normal behavior, not seen large drifts or sudden jumps throughout the survey. More rigorous control is carried out through the repetitions, as it will indicate later.
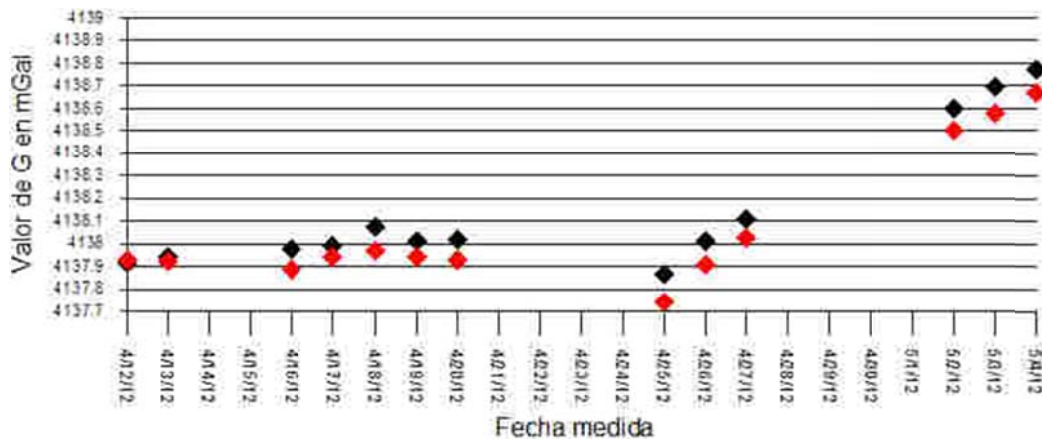
Figura 3.6. Graph of secular drift of the gravimeter Scintrex during the different programs of the survey. Measures were carried out in the gravimetric base when you open (black point) and close (red dot) the daily programme.

3.2.1. Measurement points. Bases. Control of repetitions of field survey

During the survey, a single base has been used. It is located in the town of Nerva and its characteristics can be observed in the figure 3.7. This base was established by the Metalogenia cátedra of the E.T.S.I.M. in November 1989 and belongs to the network of gravimetric bases of the Spanish pyrite belt, linked to the IGRS67.

The UNE 22-611-85, referred to the gravimetric method, establishes: "the accuracy of the measurements will be checked as follows: at least 5% of the stations will be measured twice in the course of different programmes". In the case of gravimetric data acquired in this project, scale 1:50000 of work and 2 points for km^2, the recommendation of the UNE norm states that the root mean square (RMS) of differences in the observed gravity obtained by two readings at the same point should be less than 0.15 mGal

In this regional survey the total number of gravity stations measured was 327, of which 27 have been repeated, which represents more than 8%. The study of the repetitions' value is presented in Figure 3.8. According to the calculation of the repetitions' value, the RMS is 0.03 mGal.

Figure 3.7. Characteristics of the gravimetric base of Nerva.
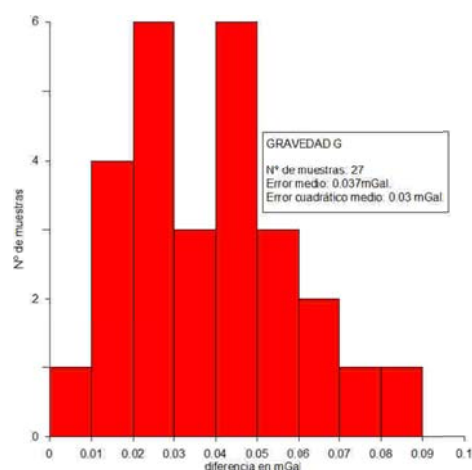
Figure 3.8 Histogram of the distribution of the repetitions' values of the gravimetric measures of the regional survey.

3.2.2. Calculation of the observed gravity

The gravity meter employed in this work measures relative gravity values. A gravimetric survey aims to measure gravity variations between a specific point and the remaining station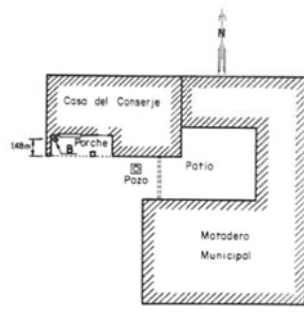s of the area. This specific point is called the base, and is a field point in which the absolute value of gravity is known.

The gravity value observed at a point is given by the following expression:

$$g_{obs} = ((l_p - l_b)k \pm CLS \pm D + g_b$$

g_{obs} = is the observed gravity at the point of measure p
l_p = reading of the gravity meter at the point p
k = calibration constant of the gravity meter
l_b = reading of the gravity meter on the base
g_b = absolute value of gravity at the base.

D is the drift correction of the gravity meter. It is used for correcting the reading variations of the gravity meter due to mechanical and thermal effects, during the reading period from the first reading in the base and the reading at the station. This correction is applied through readings of opening and closing a programme on the base and it is distributed between readings considering a lineal variation.

CLS is the tide correction, which takes into account the influence exerted by the Moon and the Sun on the terrestrial gravity. The gravity meter Scintrex provides the value of $l_p k + CLS$, since it has implemented in the device the program for its calculation.

The formulas used are based on 1959 Longman equation (Longman, 1959) to predict the values of the acceleration of tides for certain intervals of time at any point on the Earth's surface.

3.3. Calculation of the Bouguer anomaly

The observed gravity (g_{obs}) is a measured value that depends on several factors: geographical latitude, elevation of the station, the actual distribution of densities under it and its surroundings, and the time of the acquisition (corrected for drift and tide variation).

This value should be compared with a theoretical one g_t obtained from normal gravity g_0 into the geoid (g_n) but corrected to the height where g_{obs} has been measured. This correction takes into account the difference of height z between the measured point and the geoid, the existing mass between these heigths and the influence of the surrounding topography. The value

$$B = g_{obs} - g_t$$

is called Bouguer anomaly and should rely solely on theoretical and real densities relationship.

The aim of the gravimetric data process is to get the value of the Bouguer anomaly in each of the measurement points. With these values we can build the map of Bouguer anomalies, the basemap on gravimetric cartography. Based on this cartography, documents with which to perform the analysis and interpretation of anomalies located by gravimetric prospecting can be obtained.

3.3.1. Normal gravity. Corrections: air free, Bouguer, and topographic

The data procedure to calculate the Bouguer anomaly has been made using the software OASIS MONTAJ from Geosoft Company, complemented with some software developed by IGME.

Value of the normal gravity

Theoretical gravity is established from the normal g_0 gravity existing on a surface of reference or geoid (approximated by an ellipsoid of revolution) and depends on the geographical latitude.

In this work the normal gravity has been calculated using geodetic reference syatem GRS67 (Datum Potsdam g = 981260 mGal):

This system used for the calculation of the normal gravity the expression of the international gravity Formula 1967 (Formula Somigliana (Somigliana, 1929) developed in series):

$$g_0 = 978031.85 * [1 + 0.005278895 * sen^2(\varphi) + 0.000023462 * sen^4(\varphi)]$$

where φ is the latitude in the ED50 reference system.

Correction of altitude (free air correction)

Historically, the altitude correction has been called free-air correction and is defined as the difference between the gravity observed at one point of the Earth's physical surface and the normal gravity on a reference surface, ellipsoid or the geoid.

For its calculation has been used the so-called first order formula:

$$\delta g_{FA} = 0.30854 * h;$$

where is h the orthometric height in meters and δg_{FA} it is expressed in mGal.

Bouguer correction

Bouguer correction corrects the gravitational efect of the landmass between the datum plane and the station. To calculate the effect of this mass, it is considered an infinite slab of thickness h and density ρ (known as reduction density). The effect of this slab in the station is given by:

$$\delta g_{BA} = 2\pi * G * h * \rho \text{ (mGal)}$$

where G is the constant of universal gravitation, $(6.673 \pm 0.001) \ 10^{-11} \ m^3 kg^{-1} s^{-2}$, h is the height of the station in m and ρ is the density of the plate in kg/m^3. Substituting G and π the formula becomes:

$$\delta g_{BA} = 4.192 \ 10^{-5} * h * \rho \text{ (mGal)}$$

Calculation of topographic correction

The topographic correction accounts for the variations in the observed gravity caused by variations in the topography near each observation point. Because of the assumption made during the slab correction, topographic correction is always positive regardless whether the local topography is a mountain or a valley.

The topographic correction is performed following Hammer's method (Hammer 1939), based on determining the gravity effect of a series of segmented annular rings, called zones, centered on the station. We have considered the total topographic correction as the sum of three distances: near topographic correction (up to 53.3 m, zones A to C), medium topographic correction (up to 4668.8 m, zones D to I) and far topographic correction (21943 m, zones J to M).Near topographic correction (up to 53.3 m) is performed in the field, through estimation of the field operator. For medium and far topographic correction, it has been used the CCT program (Plata, 1991). In the calculations, height is in meters and the results of the correction are given in cmGal.

CCT gives the topographic correction for a reduction density of 2.0 g/cm^3. When the topographic correction is needed with a different reduction density ρ, we can use the followin expression (ρ in g/cm^3):

$$CT(\rho) = (\rho/2.0) * CT(2.0).$$

3.3.2 Integration of data from other surveys

The surveys that we have joined together for this work have been described in section 2.3., and summarized in table II. Here is, again, the list as a reminder (see also figures 2.1 and 3.1):

Gravimetric data from previous surveys:

* Data from the IGME geophysics database, SIGECO:

- Regional_938.xls (1976 points)
- Gravi_JM.xls (492 points)
- Minera_938_coordenadas.CSV (2036 points)

 * Data from previous studies carried out in the area:

- Data by Atlantic Copper (ACH_Datos.xls). A total of 2199 points
- Data by ADARO (Regional_datos.xls). A total of 316 points
- Data by RIOMIN (Riomin_datos .xls). A total of 401 points

Data from previous studies have been given by Riotinto, in the form of data files with the following format:

X29ED50;Y29ED50; Zorto; Station; B26, BGR26.

Where BGR is the Bouguer anomaly with topographic correction and a density of reduction of 2.6 g/cm^3.

Data from the database of the IGME (SIGECO) also have been calculated with a density of reduction of 2.6 g/cm^3.

A file has been a file with all the gravimetric data homogenized, with the following format:

X, and Y; elevation Station, BGR26, LongETRS89, LatETRS89.

Where X and Y are the ED50 UTM coordinates huse 29 North; Elev is the orthometric height in meter; station is the station number; BGR26 is the value of the Bouguer anomaly with density reduction of 2.6 g/cm^3; LongETRS89 and LatETRS89 are the longitude and latitude geographical coordinates in the ETRS89 system.

The study area is somewhat smaller than the extension of the aforementioned surveys. It encompasses the following coordinates:

Xmin: 704500
Xmax: 720000
Ymin: 4171000
Ymax: 4183000

3.4. Gravimetric data processing

3.4.1 Bouguer anomaly map

Once calculated the value of the Bouguer anomaly in each measured point, next step is to obtain a regular grid in order to create the Bouguer anomaly map. The chosen grid spacing has been 250 m. The gridding algorithm selected was Minimum Curvature that has been considered the one that best fits the available point distribution. The density of reduction chosen is 2.6 g/cm^3. Figure 3.9 shows the anomalies of Bouguer map.

3.4.2. Regional-Residual separation

The Bouguer anomaly map reflects the superposition of the anomalies produced by different sources at different depths. To make the interpretation of gravimetric map, we need to separate the contribution from deep sources (regional anomalies) from the sources in the upper crust (residual anomalies), which are the target of the present study. There are different methods of regional-residual separation: graphs, polynomial surfaces, derivation of digital filtering, potential field, continuation of fields, etc. In this work it has been applied the method of polynomical surfaces adjust.

The anomalies of Bouguer map (fig. 3.9), shows a clear gradient SW-NE. Therefore to the Bouguer anomaly was subtracted a polynomial of degree 1, assumed to be the regional field, obtaining the residual Bouguer anomaly map (figure 3.10).
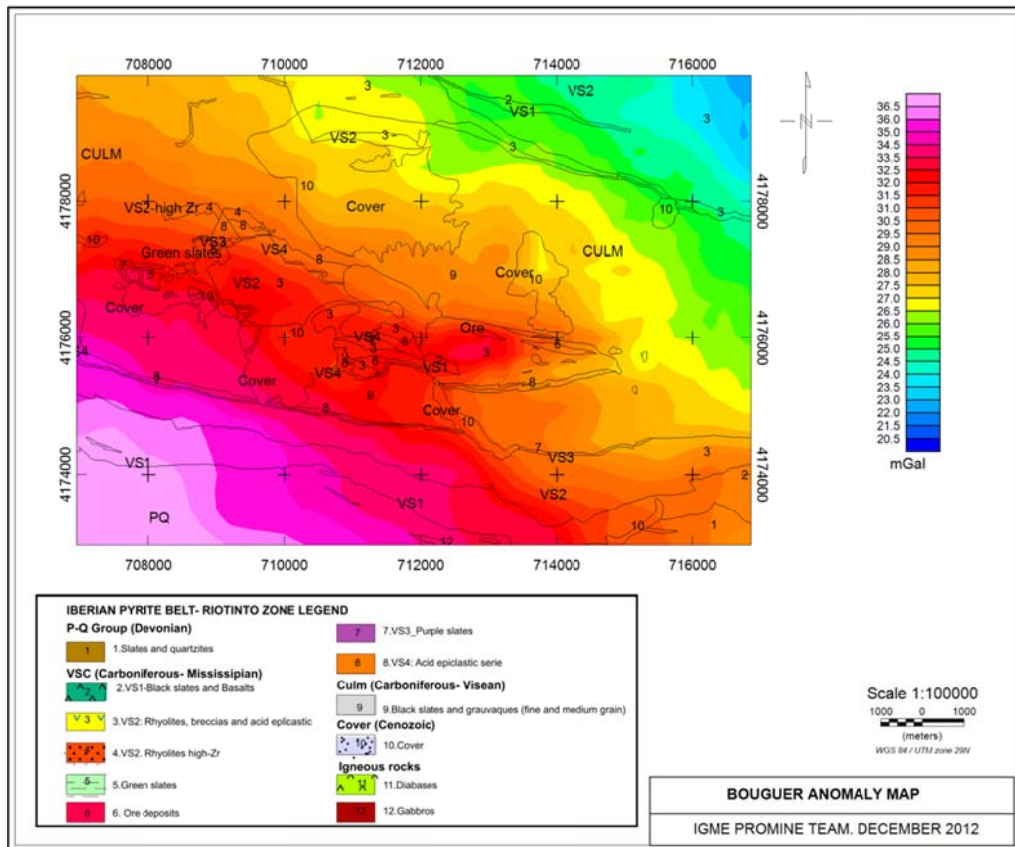
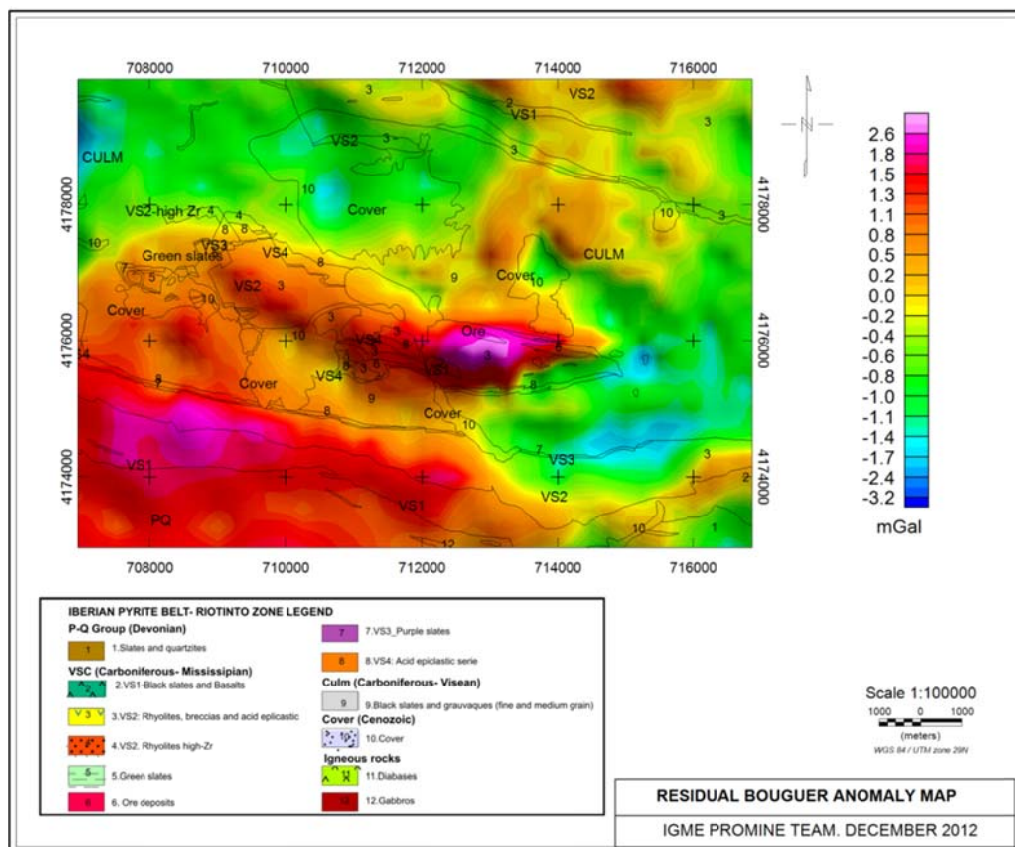Figure 3.9. Map of anomalies of Bouguer for density reduction of 2.6 g/cm^3.

Figure 3.10. Bouguer residual anomaly map for density reduction of 2.6 g/cm^3.

4. PETROPHYSICS OF RÍO TINTO AREA

4.1. Introduction

This section describes the variation of petrophysical properties (density and magnetic susceptibility) measured in laboratory from 234 surface rocks collected in the Río Tinto area (Iberian Pyrite Belt). The purpose of this analysis is twofold: on one hand, the interpretation of available geophysical data and on the other hand, to build the regional 3D geological model of the area with the appropriated petrophysical properties. It is shown how the natural variation of the measured parameters explains some gravity anomalies recorded in recent years, and the data obtained from in flight radiometric and magnetic surveys carried out in the region of Río Tinto (including Río Tinto mines). A new gravimetric survey was carried out under the project ProMine (7EUFP) in order to complete the coverage of previous surveys.

The sampling presented here includes gravity and magnetic susceptibility from the main outcropping geological units targeted in the modelling. For this work, it has been collected and measured 67 rock samples for petrophysical study. It also has been analyzed data from a previous IGME project (167 samples, see Plata and Navas, 1996 and other references therein).

Some references on Natural gamma radiometric characteristics of igneous rocks and minerals, acquired "in-situ", are also included. A radiometric survey was carried out with a handheld spectrometer: 360 samples were measured, of which 90 correspond to specific measurements and 270 measurements through continuous profiles.

The study area is located within the Iberian Massif (Figure 4.1A), in the central sector of the South Portuguese Zone (SPZ) (Figure 4.1B), more specifically in the Iberian Pyrite Belt (IPB). In this report we have used the information contained in the IGME geophysical and petrophysical database (Figures 4.1C and 1D and point 2.3 and tables 2.I and 2.II, data available on SIGECO, Geophysical databases, online IGME, 2014).

The Pyrite Belt is about 250 km long by 20-70 km wide and is bounded to the north by the Pulo do Lobo Domain (PLD), which is among the SPZ and Ossa Morena Zone (OMZ). The dimensions of the Río Tinto study area are approximately 86 km^2 (11.3 by 7.6 km).

In general terms, the Iberian Pyrite Belt has a relatively simple stratigraphic column that consists of three major lithostratigraphic units, which botton to top are: the shale and greywacke group (PQ Group), the Vulcano Sedimentary Complex (VSC) and the Culm group. In detail, those sequences

can show a very complex structure, due to the multiple tectonic faults and thrusts resulting from the Variscan deformation that affects them.

The lower unit (PQ Group) is mainly composed of dark shales with interbedded packages of quartz-sandstones and cuarzowacas, siltstones and, more rarely, conglomerates and carbonate nodules on top.

The Volcano-Sedimentary Complex (VSC) is composed of shales and siltstones together with thin levels of volcano-sedimentary rocks. The volcanic rocks are dominantly felsic (rhyolites, dacites and rhyodacites), but, from bottom to top, also include mafic rocks (basalts and dolerites) of the massive sulfide (VHMS) and lesser amounts of andesite. The Iberian Pyrite Belt (IPB) is intruded by large volumes of plutonic and sub-volcanic rocks grouped in the Sierra Norte Batholith (SNB) (Simancas, 1983, de la Rosa, 1992). The VSC was generated in an extensional tectonic setting, Fameniense mid-upper Viséan in age, within graben type basins (Oliveira, 1990) in relation to an oblique continent-continent collision (the South Portuguese Zone terrane against the Ossa-Morena Zone) (Silva et al, 1990, Quesada, 1998. Lathe et al, 2005).

The upper unit (Culm) consists of black shales and greywackes of fine to medium grain. Represents a foreland basin developed along a Variscan tectonic inversion, which occurred during the Upper Viséan-Moscovian (Oliveira et al, 1978; Silva et al 1990, Pereira et al, 2008.). They are composed of turbidite sandstones and shales that filled the foreland basin with multiple sources in the SW edge of the Ossa-Morena zone, in the Iberian Pyrite Belt and Avalonia plate (Jorge et al., 2012).

The study area (filled yellow rectangle in Figure 4.1 and red rectangle in figure 4.2) is in the Río Tinto area, within the syncline of the same name, where the core is formed by volcano-sedimentary rocks (CVS) and flanked by Carboniferous metasediments (Culm) (Navarro and Vázquez Ramírez Copeiro del Villar, 1982).
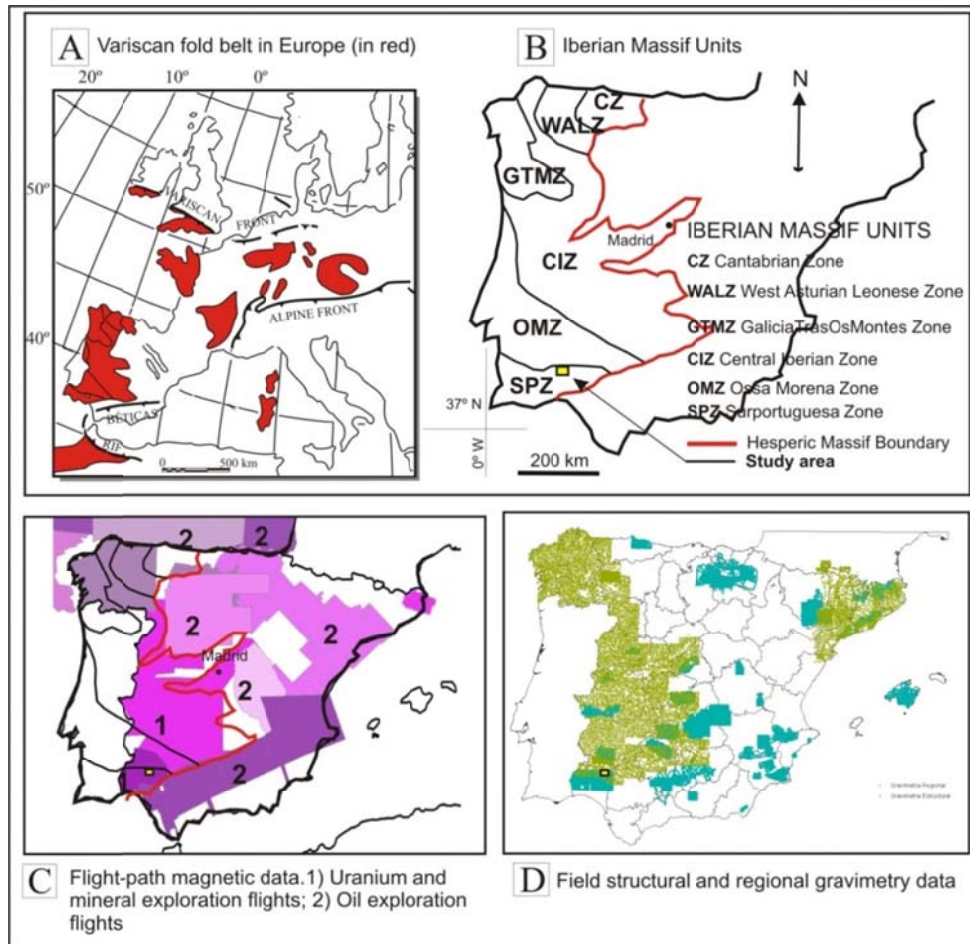
Figure 4.1. – A) General location of the study area (small yellow rectangle) in Variscan fold belt in Europe ; B) In the Iberian Massif; C) Flight-path magnetic data; D) Gravimetry data

The petrophysical study presented in this work includes data measured and analyzed on the surface from different rock types: from metamorphic to volcanic rocks, sampling all lithologies outcropping in the region of Río Tinto (Figure 4.2). A more detailed description of the different lithologies can be found in the geology report of this project (Díez Montes et al, 2014).

The petrophysical sampling has focused on the vulcano-sedimentary sequences, in order to properly characterize the lithologies that will be included in the models.

The legend in Figura 4.2 corresponds to a simplification of the geological legend Río Tinto area, reflecting the units that have been considered in the modelling.

Figure 4.2.-Geological map of the study area, i.e., Río Tinto Region (Iberian Pyrite Belt). Dots: location of petrophysical samples (234 samples). See text for explanation: Letters in bold relevant units (VS1, VS2, Culm, etc).

Since one of the objectives of the petrophysical analysis is to constrain the regional potential fields modelling, in the following sections we will describe the petrophysical character of the samples grouped by formations rather than the more usual approach based on lithology. Because this approach, in this study we have included 167 samples from a previous project (STRIP Project, Plata and Navas, 1996) some of which are outside the Río Tinto region (not shown in Figure 4.2), but that are important for the interpretation of the geophysical data and the modelling. GAZA project samples were taken within the 1:50000 geological sheet 938 (Nerva). In this project we have taken 67 new samples in the study area.

Figure 4.3 shows an example of one of the geological sections (PERFIL14) that will be used as an input for the 3D modeling of the Río Tinto area, before (B) and after (A) the geophysical setting (2.5 D modeling with GM-SYS, e.g. Talwani et al.; 1959, Talwani and Heirtzler, 1964; Won and Bevis, 1987).
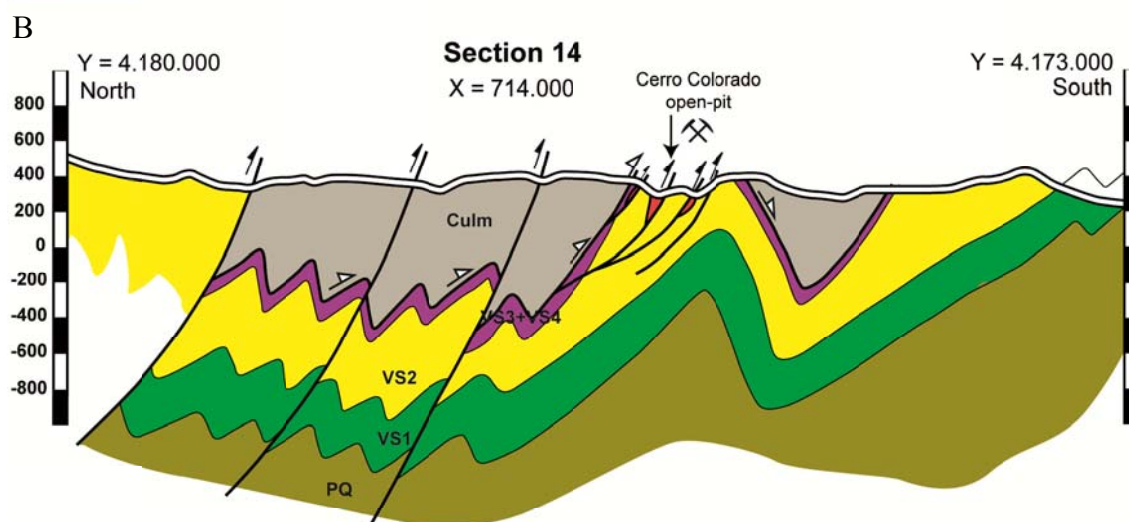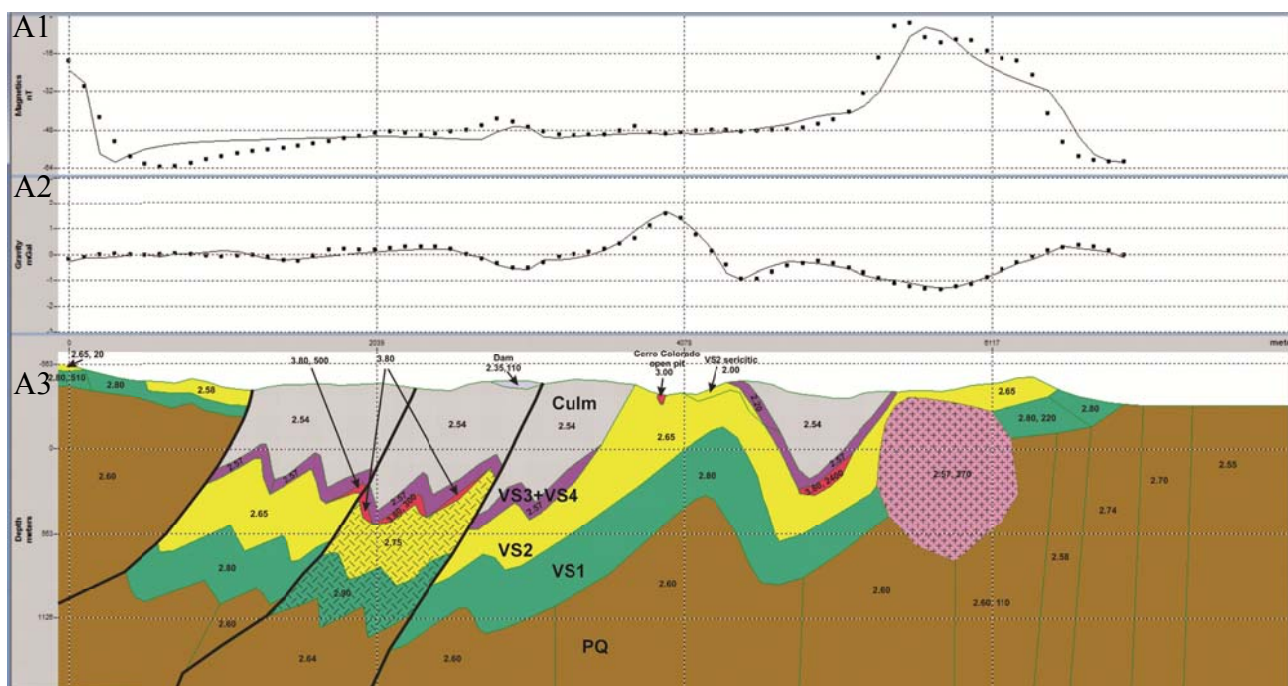
4.2.   Measurements. Sampled units and lithologies

Collected samples come from the geological record exposed in the studied Río Tinto area, within the ProMine project (red rectangle in figure 4.2). Laboratory measurements of density have been made on hammer-cut samples (0.3–0.6 kg) by weighing them in air and water (Archimedes principle). These samples come from 3-4 kg of rock collected in the field. From each of these samples, powder (2 mm grid pass) is obtained and magnetic susceptibility determined in a kappabridge (KLY-3 instrument of AGICO); the mass of the powder is measured, and the kappabridge values are converted to a mass susceptibility, then multiplied by the density of the sample to obtain volume susceptibility. Sensitivities are of the order of 0.01 g/cm^3, and $2*10^{-7}$ cgs units, respectively. Precisions are 0.02 g/cm^3 for density, and better than 5% for the magnetic measurements. Figure 4.3 displays samples and sampled groups ordered by age.

The complete petrophysical sampling referred to in figure 4.4 and used in this study consists of 234 measurements of density and magnetic susceptibility. The sample specifically collected for the ProMine project comprises 67 rocks from an area of c.86 km^2 (part of sheets 938, of the Topographical Spanish National Map, 1:50.000 scale series: red rectangle in figure 4.2).

As far as some lithologies are not entirely represented in the area of figure 4.2, the sample has been reinforced with 167 rocks collected and analyzed in an IGME previous project (Plata and Navas 1996).

Figure 4.3.A. Results of the gravity and magnetic modelling across section 14: A1- magnetic anomalies; A2: gravity anomalies; A3- modelled cross-section. Dotted line: observed anomalies; continuous line: calculated anomalies. B- Initial geological cross section. Labels and numbers correspond to the lithologies labelled in figure 4.2.

		Measured Density d (g/cm³)		Measured Susceptibility k (*10-6 ucgs)		
Sampled units	Nº	range	avg	range	avg	Main ferromagnetic mode
P-Q (1)	12	2,92-2,27	2,60	117,00-8,00	35,51	-
VS1-Basalts (2)	55	3,00-2,34	2,80	2.115,00-3,00	118,11	-
VS2-Rhyolites-Dacites (3)	77	2,96-2,32	2,65	630,00-0,00	61,86	-
VS2-Rhyolites high-Zr (4)	7	2,77-2,42	2,64	31,83-0,00	9,78	-
Green slates (5)	2	2,56-2,21	2,38	21,49-0,00	10,74	-
ORE- RIOTINTO (6)	10	4,86-3,45	4,30	86,00-1,59	44,79	-
VS3-Purple slates (7)	37	3,00-2,07	2,57	100,00-4,00	33,35	-
VS4-Acid Epiclastic serie (	27	2,84-2,31	2,63	655,00-2,00	66,63	-
Culm (9)	7	2,70-2,24	2,41	60,00-0,00	24,57	-

25

Iberian Pyrite Belt- Riotinto Zone - Legend

Culm (Carboniferous- Mississipian) / d=2.41 g/cm^3) (7 Samples) (Unit 9)

VS4 (Carboniferous- Mississipian)
Acid epiclastic serie /d=2.63 g/cm^3 / 27 Samples (Unit 8)

VS3 (Carboniferous- Mississipian)
Purple slates / d=2.57 g/cm^3 / 37 Samples (Unit 7)

VSC- Ore deposits (Carboniferous- Mississipian) / d=4.30 g/cm^3 / 10 Samples (Unit 6)

VS (Carboniferous- Mississipian)
Green slates / d=2.38 g/ cm3 / 2 Samples (Unit 5)

VS2 (Carboniferous- Mississipian)
Rhyolites with high Zr content/ d=2.64 g/cm^3 / 7 Samples (Unit 7)

VS2 (Carboniferous- Mississipian)
Rholites, breccias and acid epiclastic rocks / d=2.65 g/cm^3 / 77 Samples (Unit 3)

VS1 (Carboniferous- Mississipian)
Black slates and basalts/ d=2.80 g/cm^3 / 55 Samples (Unit 2)

P-Q Group (Middle-Upper Devonian)
d=2.60 g/cm^3 / 12 Samples (Unit 1)

Figure 4.4.-Sample distribution by group, ordered by age. Names and ages correspond to the legend of the revised geology map of figure 4.2. (Units Coloured as in figure 4.2)

In summary:

- 68 samples of metasedimentary sucessions: 12 from PQ Group (sands, quarzites, breccias and slates), 7 from Culm (black and sericiticed slates) and 49 from CVS (slates, purples and green slates, epiclastics rocks, sands and quartzites)

- 156 samples of Vulcanosedimentary Complex: 108 from acid rocks (Rhyolites, dacites, tuffs and chert) and 47 from basic rocks (basalts, andesites, trachyandesites and diabases).

- 10 samples from ore deposits

In relation to gamma natural radiation 360 sites have been measured. From these measurements, 90 correspond to single measurements and 270 to measurements through continuous profiles (Table 4.II).

Sampled units	Nº
P-Q Group (unit 1)	12
VS1-Basalts (unit 2)	55
VS2-Rhyolites-Dacites (unit3)	77
VS2-Rhyolites hight Zr (unit 4)	7
Green slates (unit 5)	2
ORE- RÍO TINTO (unit6)	10
VS3-Purple slates (unit 7)	37
VS4-Acid Epiclastic serie /unit 8)	27
Culm (unit 9)	7
Total	234

Tabla 4.I. Summary of the distribution of petrophysical sampling units (Units coloured as in Figure 4.2).

- -128 from metasedimentary rocks

- - 30 from ore deposits

- - 202 from volcanosedimentary rocks

Sampled units Río Tinto	N (all)	N (only point)
VS1-Basalts	52	7
VS2-Rhyolites-Dacites	99	14
VS2-Rhyolites sericitic alteration	7	7
VS2-Rhyolites cloritic alteration	6	6
VS2-Rhyolites hight Zr	11	11
VS1.Rhyolite dome	5	5
Green slates	4	4
ORE- RÍO TINTO	30	10
VS3-Purple slates	8	3
VS4-Acid Epiclastic serie	23	3
Culm	88	13
Tailings & Cover	27	7
Total samples	360	90

Table 4.II. Summary of the distribution of gamma natural sampling (colour code as in Figure 4.2).
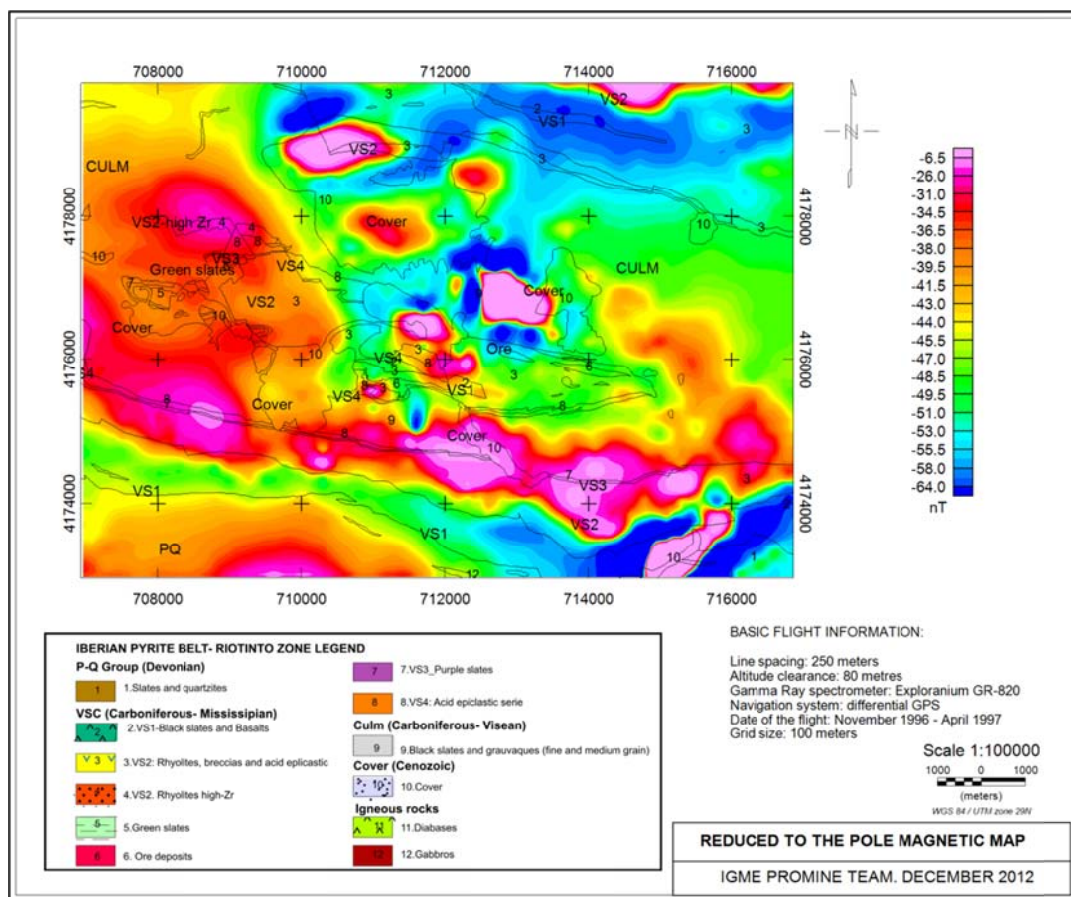
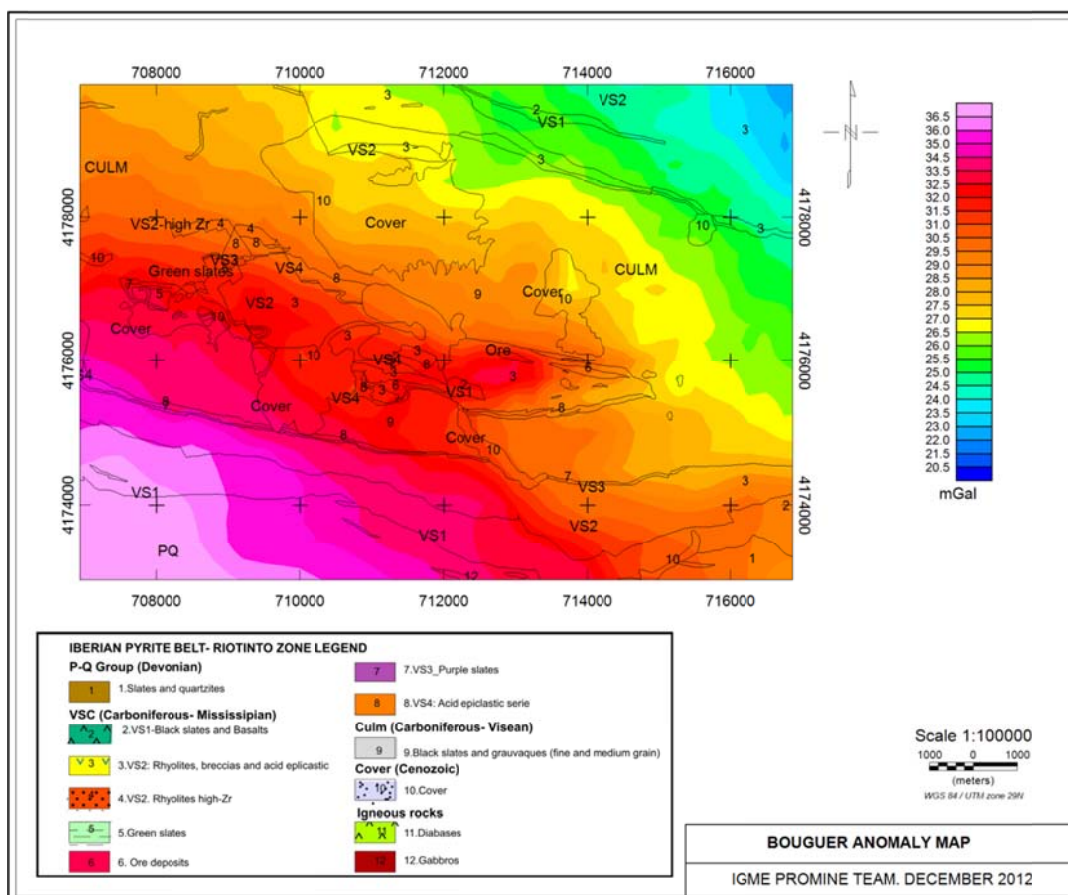Figure 4.5.- Total field reduced to pole magnetic map. Río Tinto region. Dots: sampling sites.

Figure 4.6.- Residual Bouguer anomaly map of studied area in the Río Tinto region (reduction density of 2.6 g/cm^3) Dots: sampling sites.

4.3. Density, magnetic susceptibility and natural gamma radiation classified by rocks group

Petrophysical results (average, median and ranges) are presented in Table 4.III and in a comprehensive summary, in Figure 4.7.

Figure 4.7 is a Density versus Magnetic susceptibility graph sorted by group, from bottom to top of the stratigraphic sequence, depicted in different colours, and represented by different symbols corresponding to different lithologies, within each group. One digit enclosed in parentheses shows the number of samples, while the other displays average density (g/cm^3). Blue bar represents average density of the whole sample. The two purple bars over magnetic susceptibility scale represent ferromagnetism limits: samples of first left side are paramagnetic (susceptibility k <250*10^{-6} ucgs); samples between both bars are weak to moderate ferromagnetic (0.1<% Fe$_3$O$_4$<1), and right side second bar samples is ferromagnetic (k>2500*10^{-6} ucgs; % Fe$_3$O$_4$> 1%).

| Sampled units | Nº | Measured Density d (g/cm^3) | | Measured Susceptibility k (*10-6 ucgs) | | Main ferromagnetic mode |
		range	avg	range	avg	
P-Q (1)	12	2.92-2.27	2.60	117.00-8.00	35.51	-
VS1-Basalts (2)	55	3.00-2.34	2.80	2115.00-3.00	118.11	-
VS2-Rhyolites-Dacites (3)	77	2.96-2.32	2.65	630.00-0.00	61.86	-
VS2-Rhyolites hight Zr (4)	7	2.77-2.42	2.64	31.83-0.00	9.78	-
Green slates (5)	2	2.56-2.21	2.38	21.49-0.00	10.74	-
ORE-(6)	10	4.86-3.45	4.30	86.00-1.59	44.79	-
VS3-Purple slates (7)	37	3.00-2.07	2.57	100.00-4.00	33.35	-
VS4-Acid Epiclastic serie (8)	27	2.84-2.31	2.63	655.00-2.00	66.63	-
Culm (9)	7	2.70-2.24	2.41	60.00-0.00	24.57	-
Total	234	4.30-2.38	2.78	2115.0-21.5	45.04	

Table 4.III. Density (g/cm^3) and Magnetic Susceptibility (ucgs.10^{-6}) of 234 rock samples belonging to the studied groups (Numbers within brackets indicates the cartography unit)

The results of natural gamma radiation (average, maximum and minimum) are presented in Table 4.IV. A total of 360 "in situ" measurements of K, Th and U have been done in the studied area;. Notice that in some groups field radiometric data are not available. These measures include isolated measures 360 (90) (figures 4.9, 4.11 and 4.13) and the rest (270) are profiles made along different paths. In the figures 4.8, 4.10 and 4.12 it can see all measures.
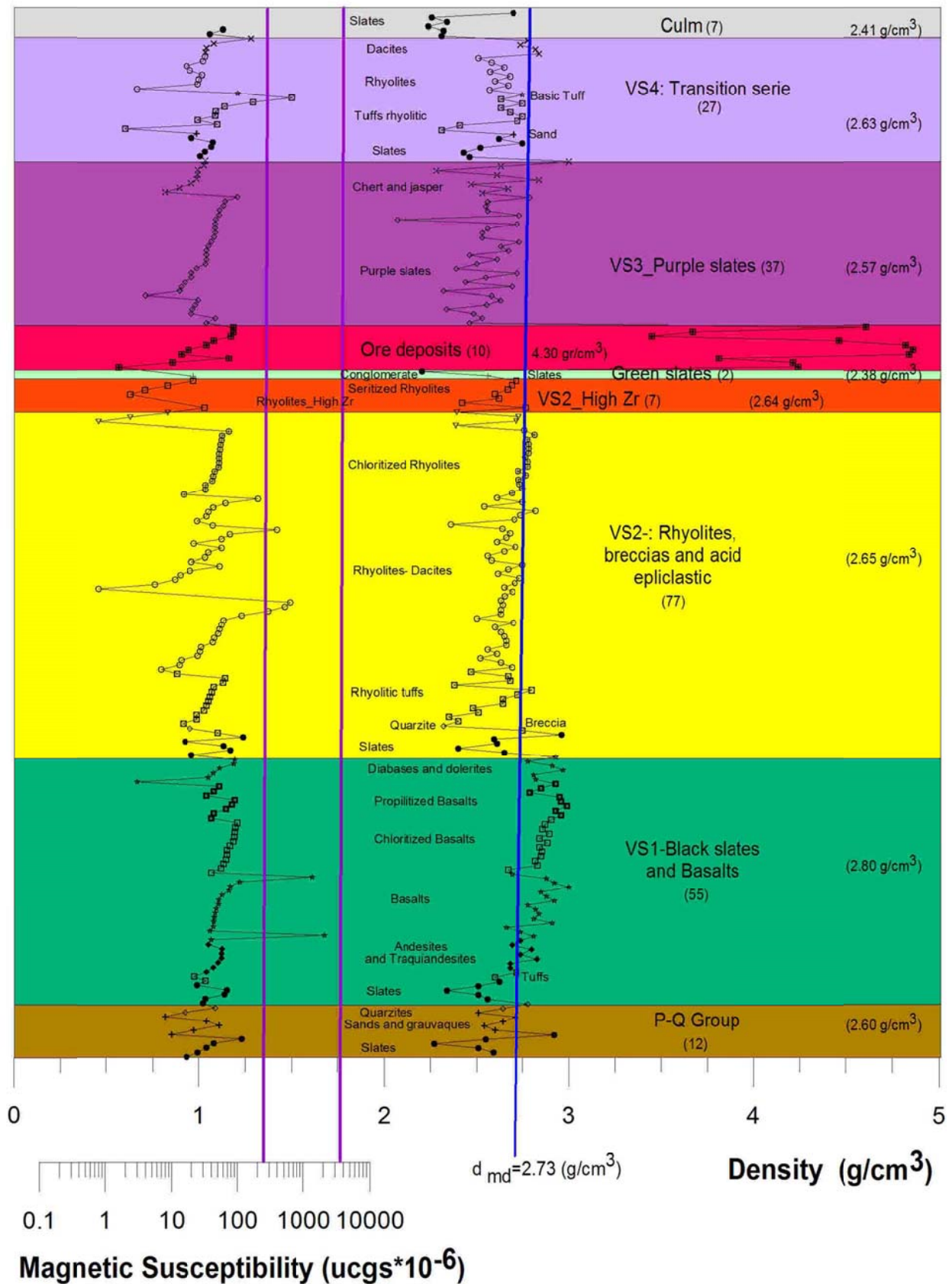
Figure 4.7. - Double graph with Density and Magnetic susceptibility results (234 samples). Samples are sorted by group from bottom to top in different colours, and according to lithology, represented by different symbols, within each group. One digit enclosed in parentheses shows the number of

samples of each group, while the other displays average density (g/cm^3). Blue bar represents average density of the whole sample. The two purple bars over magnetic susceptibility scale represent ferromagnetism limits: samples of first left side are paramagnetic (susceptibility $k<250*10^{-6}$ ucgs); samples between both bars are weak to moderate ferromagnetic ($0,1<\%\ Fe3O4<1$), and right side second bar samples are ferromagnetic ($k>2500*10^{-6}$ ucgs; $\%\ Fe_3O_4> 1\%$).

Sampled units Río Tinto	N	K_{min}	K_{max}	K_{av}	U_{min}	U_{max}	U_{av}	Th_{min}	Th_{max}	Th_{av}
VS1-Basalts (unit 2)	52	0.0	3.0	0.3	0.0	4.4	1.4	0.0	16.8	2.7
VS2-Rhyolites-Dacites (unit 3)	99	0.0	4.2	1.2	0.0	6.7	2.4	2.3	22.5	9.5
VS2-Rhyolites sericitic alteration (unit 3)	7	2.1	4.6	3.6	0.4	6.6	4.0	12.3	23.4	18.4
VS2-Rhyolites cloritic alteration (unit 3)	6	0.1	9.0	2.5	2.9	11.9	5.2	10.9	23.2	15.1
VS2-Rhyolites hight Zr (unit 4)	11	1.5	4.4	3.1	0.9	4.1	2.3	11.7	19.3	14.1
VS1.Rhyolite dome (unit 3)	5	2.0	5.1	3.6	2.4	20.5	6.8	16.6	25.3	21.4
Green slates (unit 5)	4	1.8	2.8	2.2	1.6	3.6	2.4	9.1	14.4	11.6
ORE- (unit 6)	30	0.0	4.9	1.1	0.0	29.3	3.7	3.3	15.5	6.5
VS3-Purple slates (unit 7)	8	1.2	3.8	2.4	0.0	6.1	2.2	5.2	14.4	11.1
VS4-Acid Epiclastic serie (unit 8)	23	0.5	2.8	1.7	0.4	6.0	2.4	4.2	16.4	9.8
Culm (unit 9)	88	0.4	3.5	2.1	0.0	8.5	2.6	4.3	22.3	12.2
Tailings & Cover (unit 10)	27	0.7	3.4	2.4	0.7	8.5	3.9	5.4	19.2	10.3
	360									

Table 4.IV.-Natural gamma radiation measurements (average, maximum and minimum) for the different groups.

Using the appropriate software and the calibration parameters (both provided by the company RS-125 of Radiation Solutions Inc) the K (%), Th (ppm) and U (ppm) have been obtained. In the next chapter the description of each geological group is linked with the radiometric analysis related to ternary map (Broome, J. H., 1987, 1990; Darnley, A. & Ford, K. L. 1989).

PQ Group

The PQ Group (12 samples) includes sandstones (4), quartzites (3) and slates (5) (Unit 1 in Figure 4.2). Density ranges between 2.27 and 2.92 g/cm^3, with an average of 2.60 g/cm^3. The sample that has higher density corresponds to a sericític-chloritic slate (sample num. 1234) (in Campofrío massif), and also corresponds to the maximum magnetic susceptibility group (117 x 10-6 ucgs). In the Iberian Pyrite Belt, this formation always shows a minimum in the Bouguer anomaly maps. All samples are paramagnetic ($k<250*10^{-6}$ ucgs), as shown in figures 4.5 y 4.7. This unit has not been sampled for natural gamma radiation.

VSC. VS1.Basalts

This group includes 55 samples, comprising 5 slates, 2 tuffs, 7 andesites and trachyandesites, 35 basalts and 6 diabases (Unit 2 in Figure 4.2). Density ranges between 3.0 and 2.34 g/cm^3, averaging 2.80 g/cm^3. The minimum values correspond to the sedimentary and volcano-sedimentary group, and if we exclude these components, the average is around 2.84 g/cm^3. This unit shows a gravimetric maximum throughout the Iberian Pyrite Belt and a relative maximum at the outcrops west of the study area.

Most of the samples are paramagnetic (k <250 x 10-6 ucgs), with only 4 samples in the range of weak to moderately ferromagnetic (0.1 <Fe3O4 <1), although these are the rocks that present relative maxima in the reduced to the pole magnetic map (Figure 4.5).

This unit is also well reflected in the ternary radiometric maps (Figure 5.7), where it coincides with the white colors.

Regarding natural gamma measures, it should be noted that in maps (Figures 4.14 to 4.16) and graphs (Figures 4.8 to 4.13) we have distinguished single measured points from measures along continuous profiles.
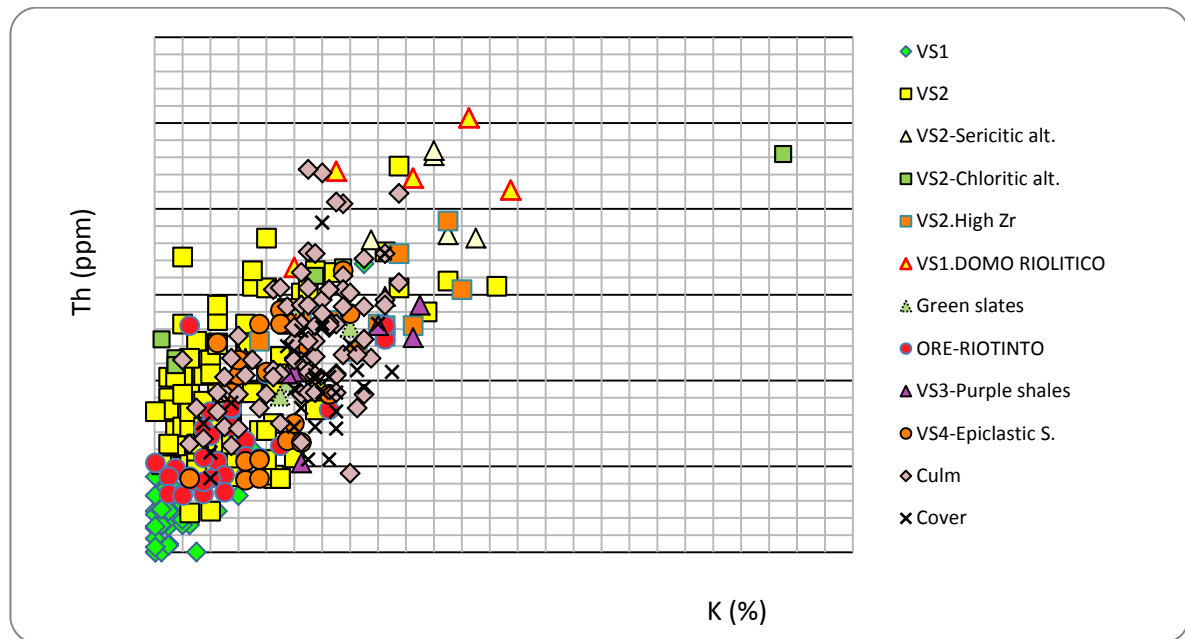
Figure 4.8.-Th-K Diagram of 360 samples of metasedimentary rocks (RS-125) in situ measurements.

In this unit 52 samples of natural gamma radiation have been taken. The mean values for all measured elements are low. The value of K is very low, being 0.3%, 1.4 ppm and 2.7 ppm U Th (Table 4.IV). The graph Th-K (Figures 4.8 and 4.9) shows a positive relationship between the contents of both elements, with an increase of Th with the K.

In the graph K / Th-U / Th of 4.12 Figure, some samples with high values have been eliminated, the ones where the Th value was very low (values from 10 to 340).

Similarly, the same applies to some values in Figures 4.11 y 4.12 where there is a positive relationship between Th y U.

VSC. VS2.Rhyolite-Dacites, breccias and acid epiclastic

This unit (number 3 in Figure 4.2) contains 77 samples with great lithological variety, including 5 slates, 1 quartzite, 1 breccia, 13 rhyolitic tuffs, 34 rhyolites 5 dacites and 18 chloritized rhyolites. Density ranges vary between 2.96 and 2.32 g/cm^3, averaging 2.65 g/cm^3. Most of the samples are below the average, as seen in Figure 4.7, except the breccia and the samples corresponding to the chloritized rhyolite.

This unit does not show a homogeneous behavior on the geophysical maps, presenting both highs and lows on the Bouguer anomaly map (Figure 4.6). In the central and southern part of the study area relative maxima can be seen, while in the northeastern part there is a minimum. Because it is a less dense unit, the maximum should reflect denser basic rocks that do not crop out.

This unit is paramagnetic, with only four samples in the range of weak to moderately ferromagnetic (0.1 < Fe3O4 <1) (Figure 4.7). In the reduced to the pole magnetic map (Figure 4.5) is can be observed a different behavior of this unit in different areas. In the central band, there is a relative maximum to the west, whereas to the east it shows a relative minimum. Both zones are divided by the Eduardo Fault (see Figure 4.2). The Atalaya-La Ponderosa fault also seems to delimit different magnetic fabrics. To the southern part, the unit is characterized by a maximum while in the northeastern part you can see both a maximum and a minimum. This may suggest differences in the lithologies that make up the unit. These differences in behavior in different areas are also reflected in the radiometric maps of Th, U, and K (Figures 5.4, 5.5 and 5.6) and in the Ternary map (Figure 5.7).
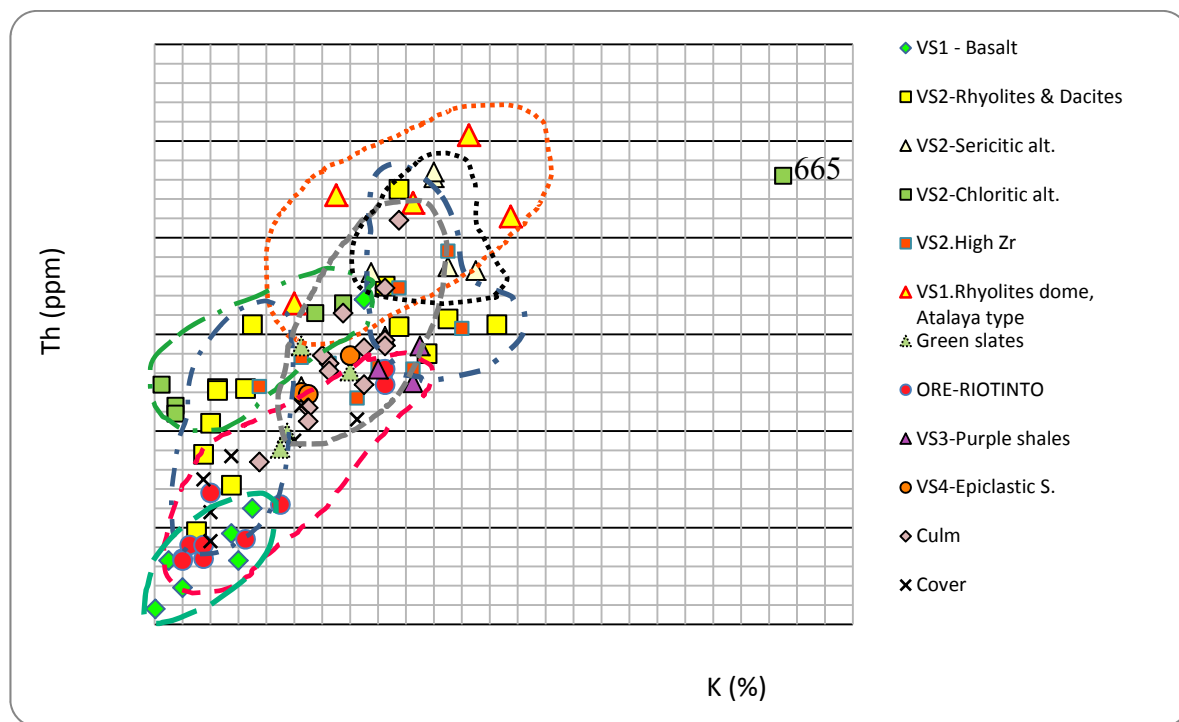
Figure 4.9.-Th-K Diagram of 90 samples of metasedimentary rocks (RS-125) in situ measurements, considering only measure at a point.

In this unit 116 samples have been measured for natural gamma radiation, within which we have differentiated 7 samples having a sericitic alteration, 5 a chloritic alteration, and 5 that form Corta Atalaya-like domes, with ryolithic-dacitic compositions, intersecting all other acidic rocks (VS2) and mineralizations.

The value of K is low, being 1.2%. We have measured 2.4 ppm for U and 9.5 ppm for Th (Table 4.IV4 and Figures 4.8 and 4.9). The rhyolites-dacites of this unit form two distinct populations, as shown in Figure 4.9, but this does not correspond to any relationship found on the field and we have not bee able to determine any. In Figure 4.8, that includes all samples, these two populations do not appear to be so clearly related. The rhyolites that are high in Zr (mapping unit # 4) are located between the two groups.

In Figure 4.9 it can be seen as different groups' rhyolites having a sericitic alteration or of having a chloritic alteration. Dacites and rhyolites with sericitic alteration have higher K values and lower values of U and Th than those showing chloritic alteration (see table 4.IV).

In Figure 4.10 sample num. 628 shows higher values of U, which sigles it out from the rest of the chloritic alterated rhyolites. This sample was within one of the rhyolite-dacite domes, and was collected next to the contact.

34

Also the rocks that form the rhyolitic-dacitic domes like Corta Atalaya, also differ from other VS2 rocks, showing generally higher Th values than the rest, both in relation to the K and the U (Figures 4.8 to 413). The sample num. 627 corresponds to an area of contact between one of the domes and the host rock.

These features, as well as a study of the spatial distribution of samples in the different maps (Figures 4.14 to 4.16) show that in general, all the elements, especially the U, are mobilized and concentrated in fault areas and in the contacts between the different units.
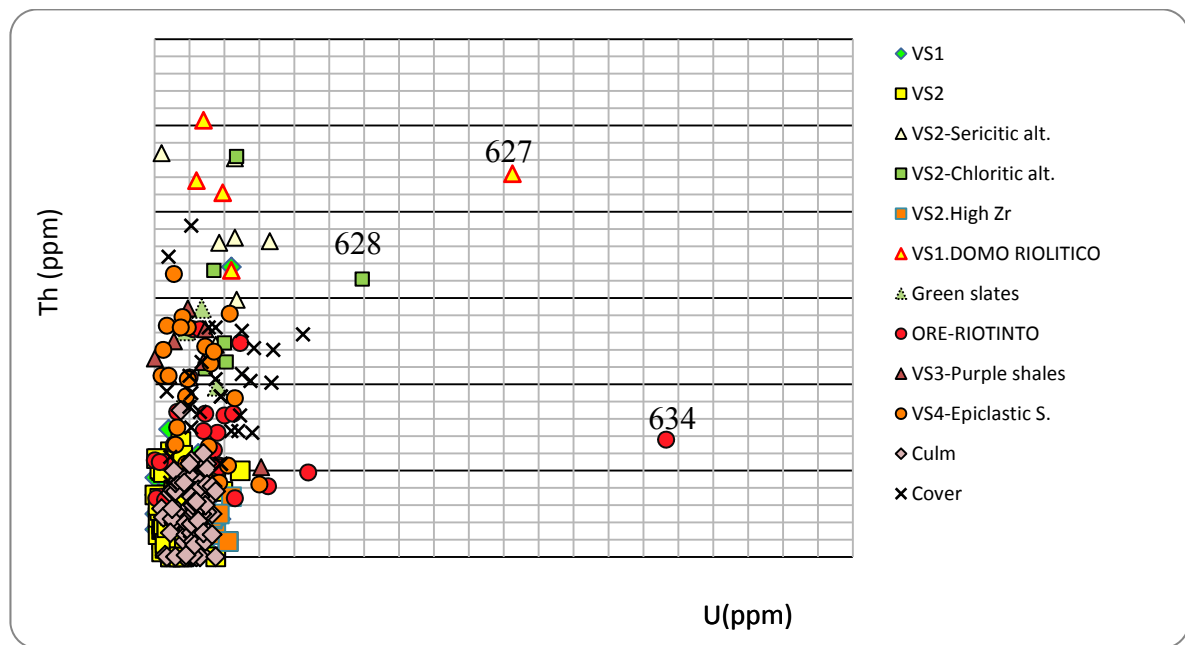
Figure 4.10.-Th-U Diagram of 360 samples of rocks (RS-125) in situ measurements.

The Th-K graphic show a positive relationship between the contents of both elements, with an increase of the Th with K. The same pattern applies to the Th and U (Figures 4.10 y 4.11).

VSC. VS2. High Zr Rhyolites

This unit (No. 4 in Figure 4.2) includes 7 rhyolite samples with high Zr content and having a sericitic alteration. Density ranges vary between 2.77 and 2.42 g/cm^3, with an average of 2.64 g/cm^3, very similar to the rhyolites from VS2 group. This unit can not be singled out on the Bouguer anomaly map (Figure 4.5).

The magnetic map shows a relative maximum although the values of magnetic susceptibility are low, always showing a paramagnetic behavior (k <250 x 10-6 ucgs).
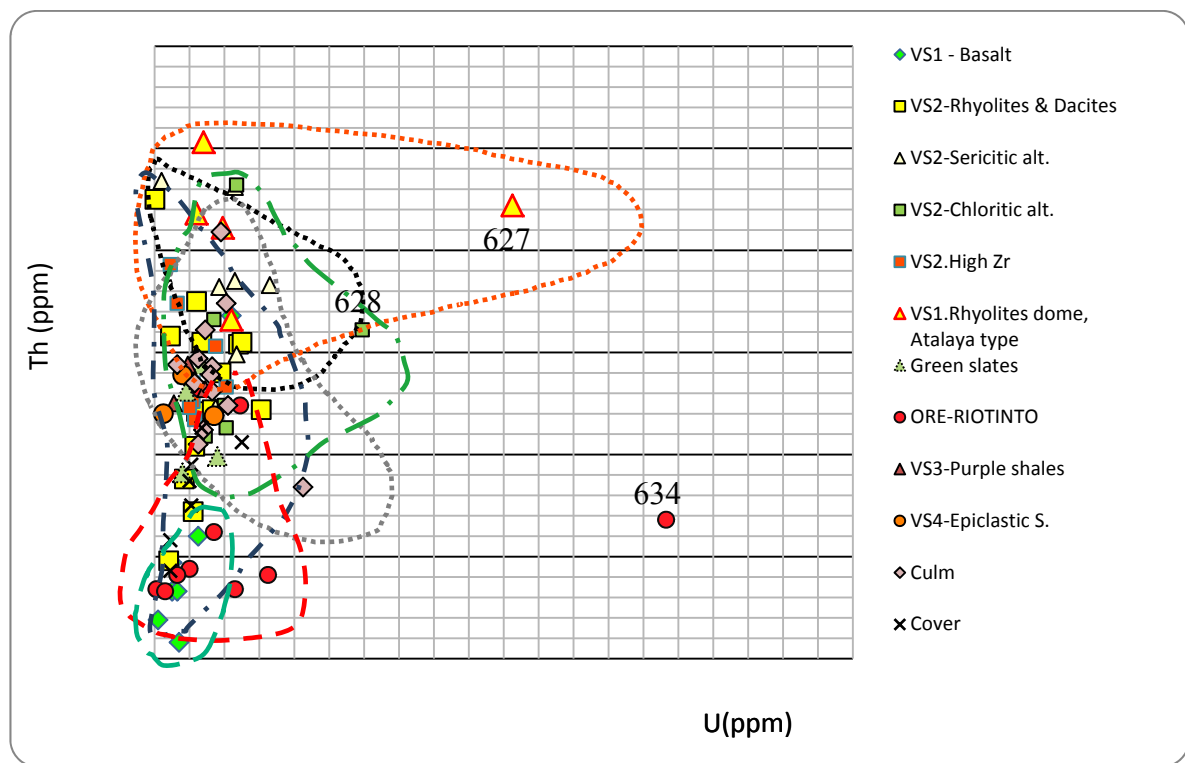
Figure 4.11.-Th-U Diagram of 90 samples of rocks (RS-125) in situ measurements considering only measure at a point.

In the radiometric maps, this rocks show a different behaviour than the rest of the VS2 with a higher content of U and Th (Figures 4.15 and 4.16), but not in the K content (Figure 4.14).

From this unit, 11 samples of natural gamma radiation have been taken. The mean values for all measured elements of this group are larger than the median. The value of K is close to the maximum value being 3.1%; values are 2.3 ppm for U and 14.1 ppm for Th (Table 4.IV). In the charts Th-K (Figures 4.8 and 4.9), Th-U (Figures 4.10 and 4.11) and K/Th-U/Th (Figures 4.12 and 4.13) a positive relationship between the contents of both elements can be observed: Th increases with K and U.

According with its petrophysical properties, this group of samples can not be clearly differenciated from other VS2 rocks. This contrasts with its distinct geochemical signature that make this samples stand out from the other VS2 rocks.

VSC. Green slates

This unit (Number 5 in Figure 4.2) includes only 2 samples of green slates. Density ranges vary between 2.56 and 2.21 g/cm³, averaging 2.38 g/cm³. This unit crops out mainly in two zones, one in the east and one in the center. In the Bouguer anomaly map both areas are characterized by a

maximum, which must be produced by the mineralization and / or basic rocks (VS1) both outcropping and subcropping.

The behavior of this unit in the radiometric maps (Figures 4.14, 4.15 and 4.16) shows differences over the eastern and central outcrops, presenting a relative maximum of U at the east while in the central part U has a relative minimum. Potassium and thorium present a maximum in the central area and a minimum in the east. In the ternary radiometric map, this unit shows a green color (Figure 4.8).

From this unit, 4 samples of natural gamma radiation were taken. The mean values of all measured elements are close to the average values of all samples, with values of 2.2% K, 2.4 ppm U and 11.6 ppm Th. In general a positive correlation between all elements can be observed (Figures 4.8 to 4.13).

Regarding the magnetic properties of this unit, the rocks are paramagnetic (k <250 x 10-6 ucgs) and in the magnetic map (Figure 4.5), the pattern is similar for the eastern in central outcrops.
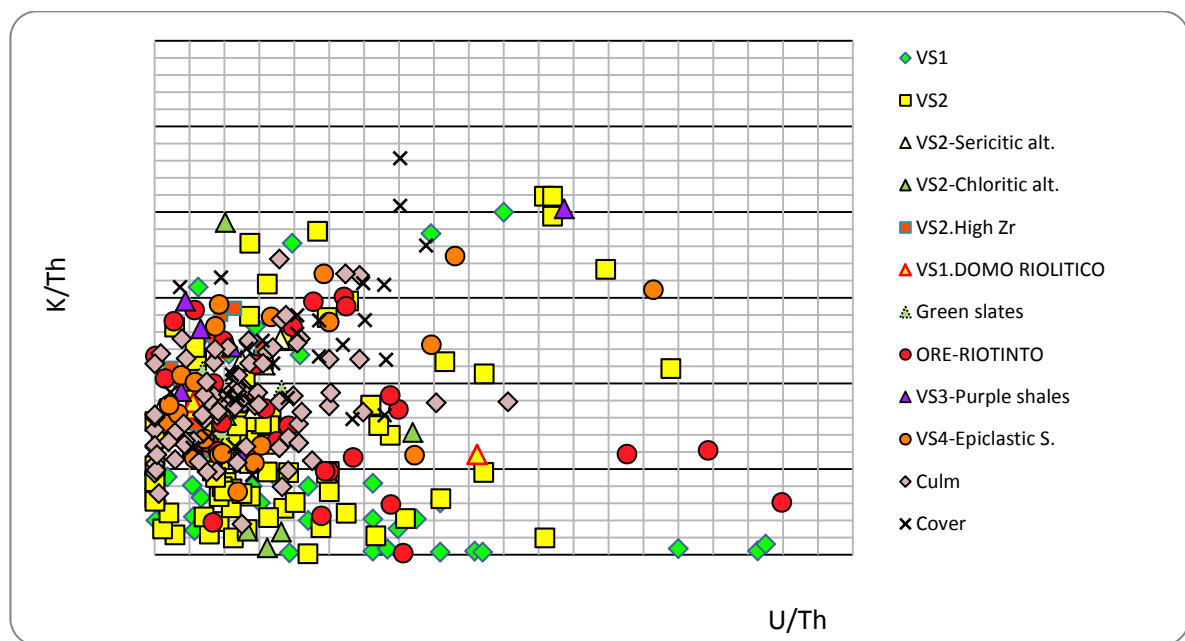
Figure 4.12.-K/Th-Th/U Diagram of 360 samples of rocks (RS-125) in situ measurements

VSC. Ore deposits

This unit (number 6 on Figure 4.2) includes 10 samples of mineralizations, which in this case are massive sulphides. The samples show high density values, ranges varying between 4.86 and 3.45 g/cm^3, averaging 4.30 g/cm^3.

All samples are paramagnetic (k <ucgs 250 x 10-6), althoug in the reduced to the pole magnetic map (Figure 4.6) the mineralizations are located in an area of maximum magnetic. This could be interpreted by the subcropping volcanic rocks located in the thrust fronts.
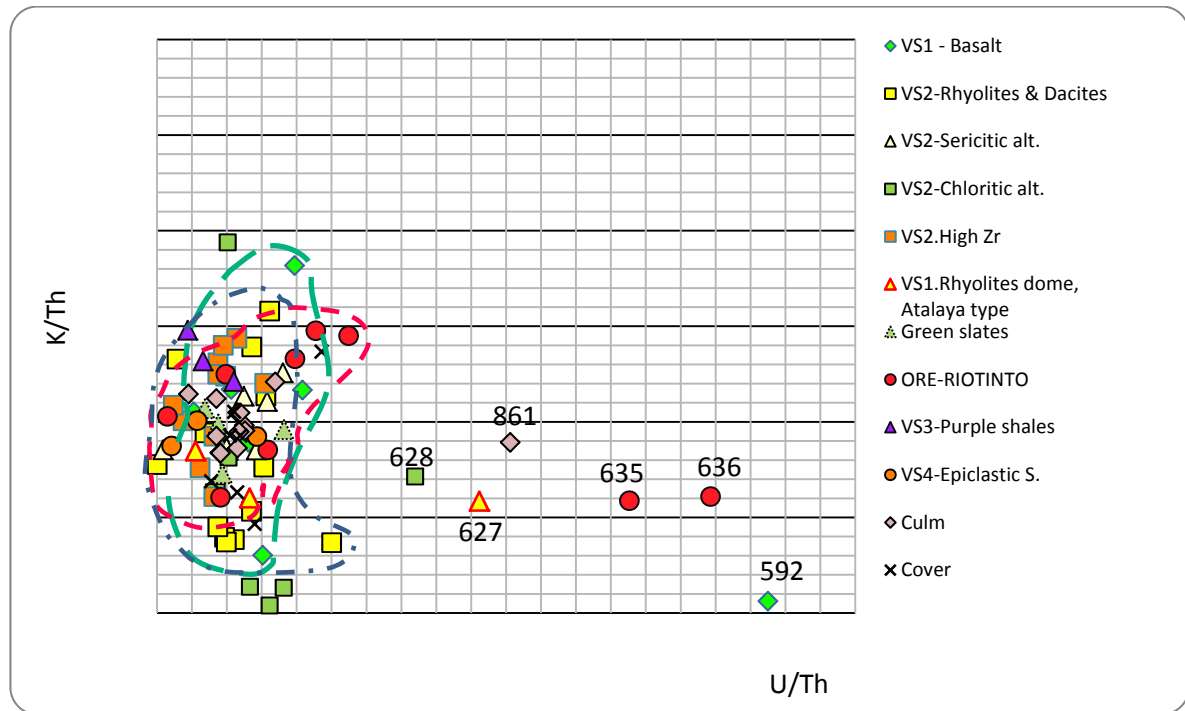

Figure 4.13.-K/Th-Th/U Diagram of 90 samples of rocks (RS-125) in situ measurements considering only measure at a point.

From this unit, 30 samples of natural gamma radiation have been taken, presenting values of K lower than the average (1.1%), values of U somewhat above average (3.7 ppm) and values of Th well below (11.6 ppm). Although the graphics are not shown, we separated the stockwork from the massive sulfides, but there are no significant differences between their properties, being the relationships between the elements positive and rather similar (see Figures 4.8 to 4.13). In Figures 4.10 and 4.11, sample num. 634 U stands out with values greater than the rest of the group. This sample corresponds to a zone of brecciaceous massive sulphide with fragments of chalcopyrite.

In Figure 4.13 there are two conspicuous samples, numbers 635 and 636, which belong to a small level of sulfides north of Filón Norte. As discussed above, in that chart we have removed some samples with very high values of U/Th, especially from the VS1 group, but also sample num. 634 (values of U / Th = 4.31), which as mentioned above, corresponds to a zone of massive sulphides and is in contact with a purple slates.

VSC.VS3. Purple slates

This unit (No. 7 in Figure 4.2) includes 37 samples of purple slates and jasper. Density ranges vary between 3.00 and 2.07 g/cm^3, averaging 2.57 g/cm^3. If we considered only the slates, average density is 2.53 g/cm^3 and for the jaspers subgroup, average is 2.63 g/cm^3.

In this unit, 11 samples of natural gamma radiation were taken. The mean values are fairly close to the overall average values (2.2 ppm U and 11.1 ppm Th) except for U which is slightly lower: 2.4% K, (Table 4.IV). This group does not have any oustanding feature of any of the three elements and there is a positive correlation between all measured elements (see Figures 4.8 to 4.13).

Regarding the magnetic properties of this unit, most of the samples are paramagnetic (k <250 x 10-6 ucgs), with only a sample out of the range. Nonetheless, the reduced to the pole magnetic map (Figure 4.5) presents a band of relative maxima.
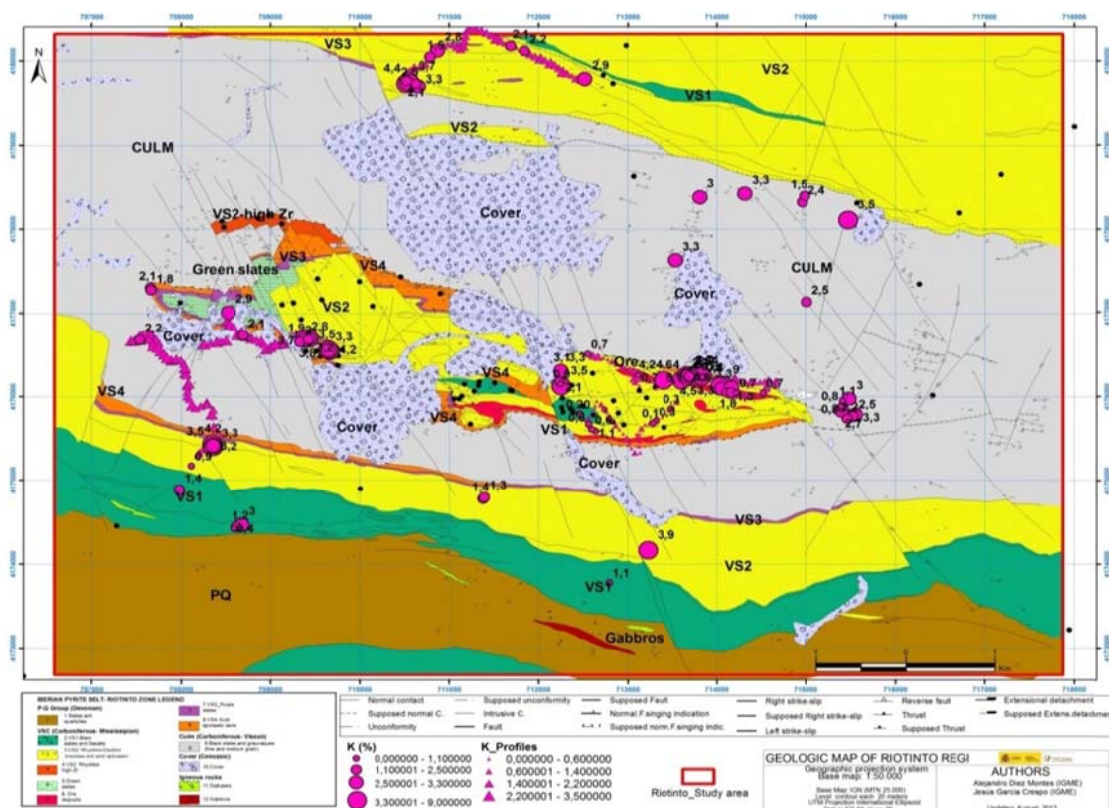
Figure 4.14.-Potassium radiometry measurements on the geological map.
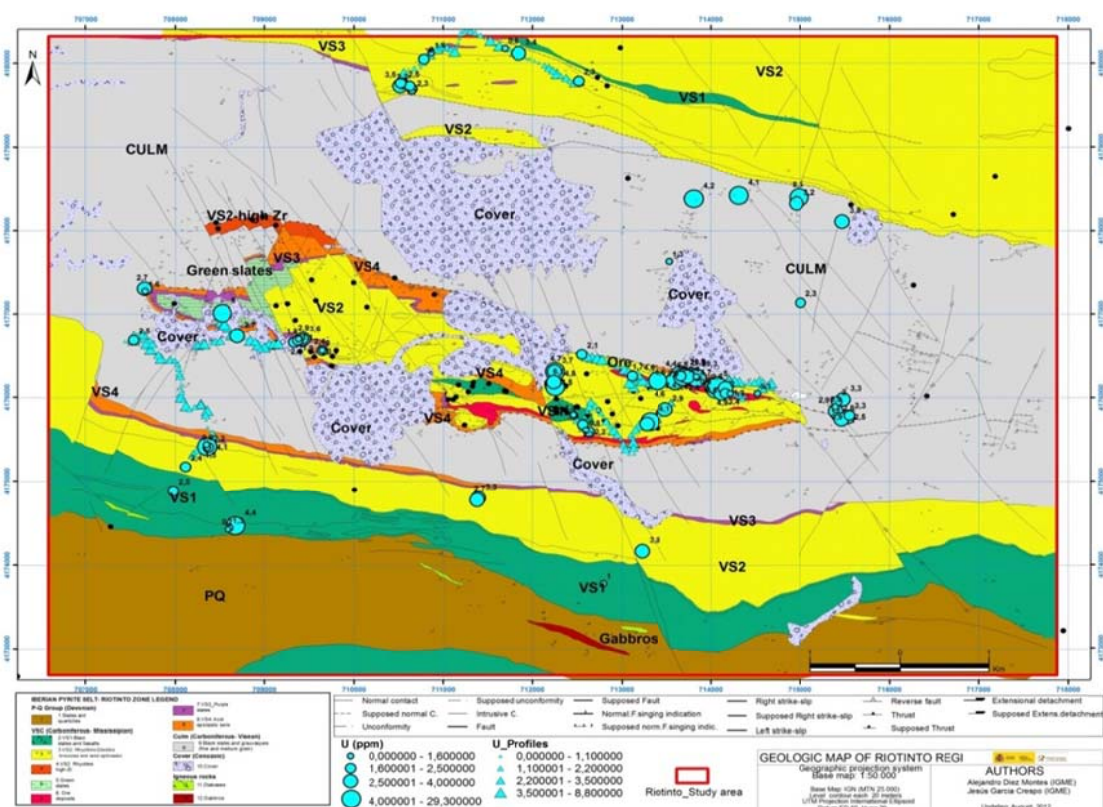
Figure 4.15. Uranium radiometry measurements on the geological map.
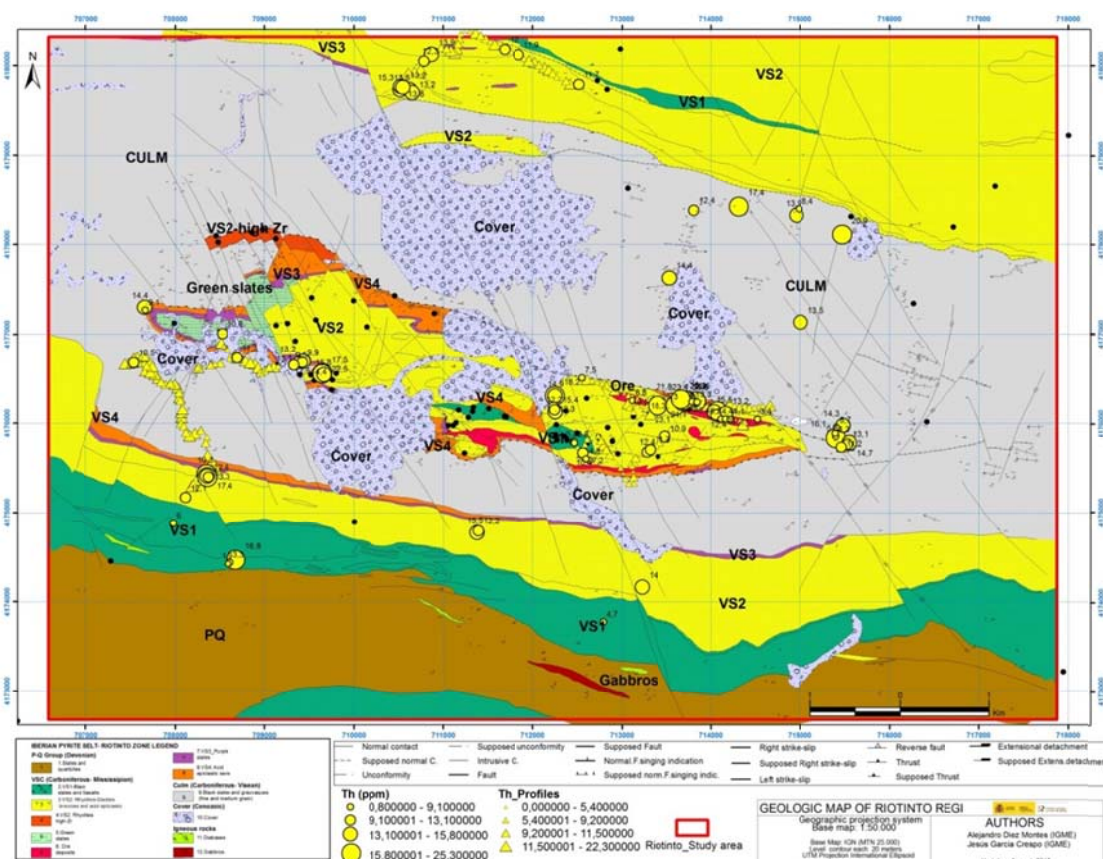
Figure 4.16. Thorium radiometry measurements on the geological map.

VSC.VS4. Acid epiclastic serie

This unit (8 in Figure 4.2) included 27 samples of shale (5 samples), sandstone (1), rhyolitic tuffs (8), basic tuffs (1) rhyolites (8) and dacites (4). Density ranges vary between 2.84 and 2.31 g/cm^3, averaging 2.63 g/cm^3. Except most of the slates and 2 samples of rhyolitic tuffs which have very low values (2.43g/cm^3), most of the samples fall around the mean value. The gravimetric response of the unit is diverse, showing a relative maximum area in the middle, but minimum zones in the north and east.

Regarding the magnetic properties of this unit, most samples are paramagnetic (k <ucgs 250 x 10-6), with only one sample (rhyolitic tuff) ranging from weak to moderately ferromagnetic (0.1 <Fe3O4 <1) (Figure 4.7). In the magnetic map (Figure 4.5) most of the outcrops of these rocks are within bands of relative minima except the westernmost outcrops and central outcrop area, wich are located within a maximum.

These rocks show relative minimum of U, Th and K in the radiometric maps (Figures 5.4, 5.5 y 5.6).

From this unit, 73 samples of natural gamma radiation have been taken, but only 3 are stand alone measures. The values are below average for all the elements, being very similar to those within the rhyolite-dacite group VS2: 1.7% K, 2.4 ppm U and 9.8 ppm Th. In Figure 4.8 a positive relationship between K and Th content can be observed, whereas in the Figure 4.10 the ratio of Th and U is negative, with decreasing content of U with increasing content of Th.

CULM

This unit (item 9 in Figure 4.2) includes 7 samples of black and green shales and greywackes of medium to fine grain. Density ranges vary between 2.70 and 2.24 g/cm^3, averaging 2.41 g/cm^3. This average density is higher because two of the samples included in the calculations present mylonitic textures slates (RTD-938-238-A and B). Excluding these samples, the average density would drop to 2.29 g/cm^3. The gravimetric response of this unit is diverse, probably influenced by the presence of volcanic rocks of subcropping mineralizations within the thrust fronts. In the map of Figure 4.2 this unis is related to both, relative maxima and minima.

The Culm comprises paramagnetic values (k <250 x 10-6 ucgs) for all samples, although the reduced to the pole magnetic map (Figure 4.6) shows relative maximum in the western and south eastern parts of the study area. These peaks might have the same origin as the gravimetric highs.

The radiometric maps of K and Th (Figures 5.4 and 5.5 respectively) show two areas of relative maxima in the east and west within this unit. This pattern appears also in the ternary map (Figure 4.8), with a central zone with green colors, which could correspond to an enrichment of U-Th.

From this unit, 88 samples of natural gamma radiation have been taken. They show values within average for K (2.1%), under average for U (2.6 ppm) and a bit higher to average for Th (12.2 ppm) (Table 4.IV). All the graphs show positive correlations between the different elements. In figure 4.11 the sample num. 861 has been because corresponds to a fault zone in *Peña del Hierro*, north of the study area. This sample presents a slightly higher then the average U value.

Cover & Tailings

27 samples of natural gamma radiation have been taken for the cover aand tailings. The measured values are close to average, with 2.4% of K, 3.9 ppm 10.3 ppm U and Th and also show a positive correlation between all the elements (see Figures 4.8 to 4.13).

In Figure 5.7 (Ternary map) the cover and tailings present light green colors, which allow to differenciate them from the other lithologies.

5.   UNDERSTANDING REGIONAL GRAVITY, MAGNETIC AND RADIOMETRIC MAPS OF THE RÍO TINTO AREA

5.1.   Bouguer and residual anomaly maps

A strong, some kilometers long, gravity gradient is observed in Figure 5.1 from the northeast to the southwest into the frame of the northern geological limit of Iberian Pyrite Belt (Río Tinto Zone). This gravity gradient comprises positive values between +20 and +36 mGal.

Taking into account the outcropping geology of the area (see geological map, Figure 4.2) there is not a clear correspondence between the Bouguer anomaly and the outcropping materials: low anomaly areas (below 27 mGal) located in the northeast are related to the black slates and greywackes of the Culm facies (Carboniferous-Visean group), also outcropping in the southwest of the area (in this case associated to higher values of Bouguer anomaly, red-pink colours). This fact and the long wavelength of the anomalies inform us of the deeper and regional origin of the Bouguer anomalies, being necessary to isolate the residual Bouguer anomaly to analyse gravity results (residual gravity anomaly between -3.2 and +3.6 mGal, map in Figure 5.2).
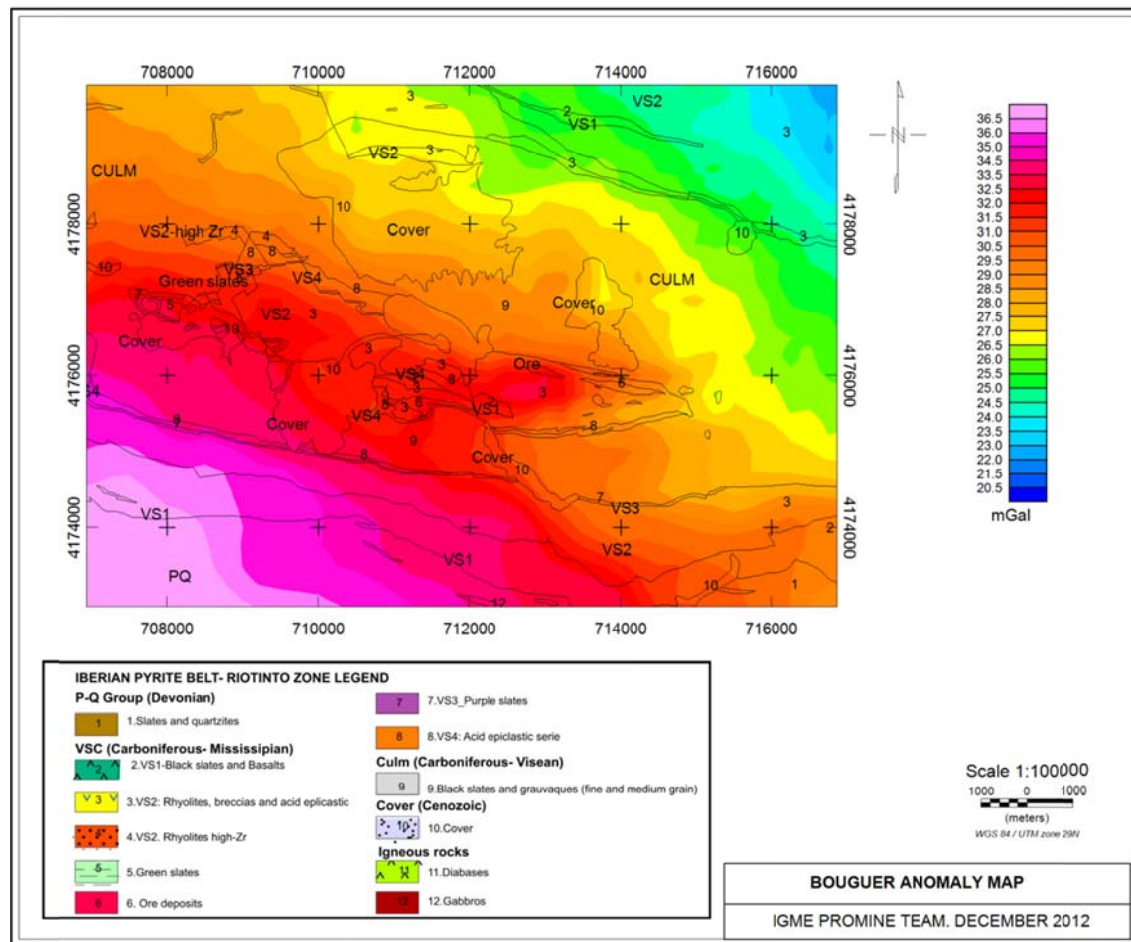
Figure 5.1. Bouguer Anomaly Map (2012) of the Río Tinto Area

On the basis of anomaly intensity, three zones can be distinguished in the residual anomaly map (Figure 5.2):

a) North zone between 0 and -3.2 mGal (yellow-blue colours) related toblack slates and greywackes (Culm facies, Carboniferous-Visean) and the rhyolites, breccias and acid epiclastic (VS1) outcropping. The metasedimentary character of these materials are in good concordance with the low density values, but the emplacement of the Río Tinto ore mine disturbs the low values in density providing an outstanding maximum (over 4.5 mGal) in the centre of the area.

b) Centre zone occupied by the Río Tinto ore mine depicts more than 3.5 mGal of positive anomaly coinciding with the outcropping of ryolites, breccias and acid epiclastic (VS2 and VS4) and some massive sulphurs (Ore deposits in the map). The outstanding character of the anomaly implies either the wider outcropping or the subcropping of the massive sulphurs not yet mapped. Westward the high density materials of purple slates and jasper enriched in

43

magnesium (VS3) provide positive values (+1, +1.5 mGal) of anomaly. The Río Tinto mine is formed by the outcropping of ore deposits, purple slates and acid epiclastic.

c) South zone between 0 and +2.6 mGal (orange-red colours) coinciding with the Devonian slates and quarzites (P-Q group), black slates and basalts (VS1) and the western part of the rhyolites, breccias and acid epiclastic (VS2). The mapped limit (east-west trend) between the discordance Culm facies and the volcanosedimentary complex is clearly reflected in the residual Bouguer anomaly map delimiting maximum values on the south where green and black slates basalts outcrop.
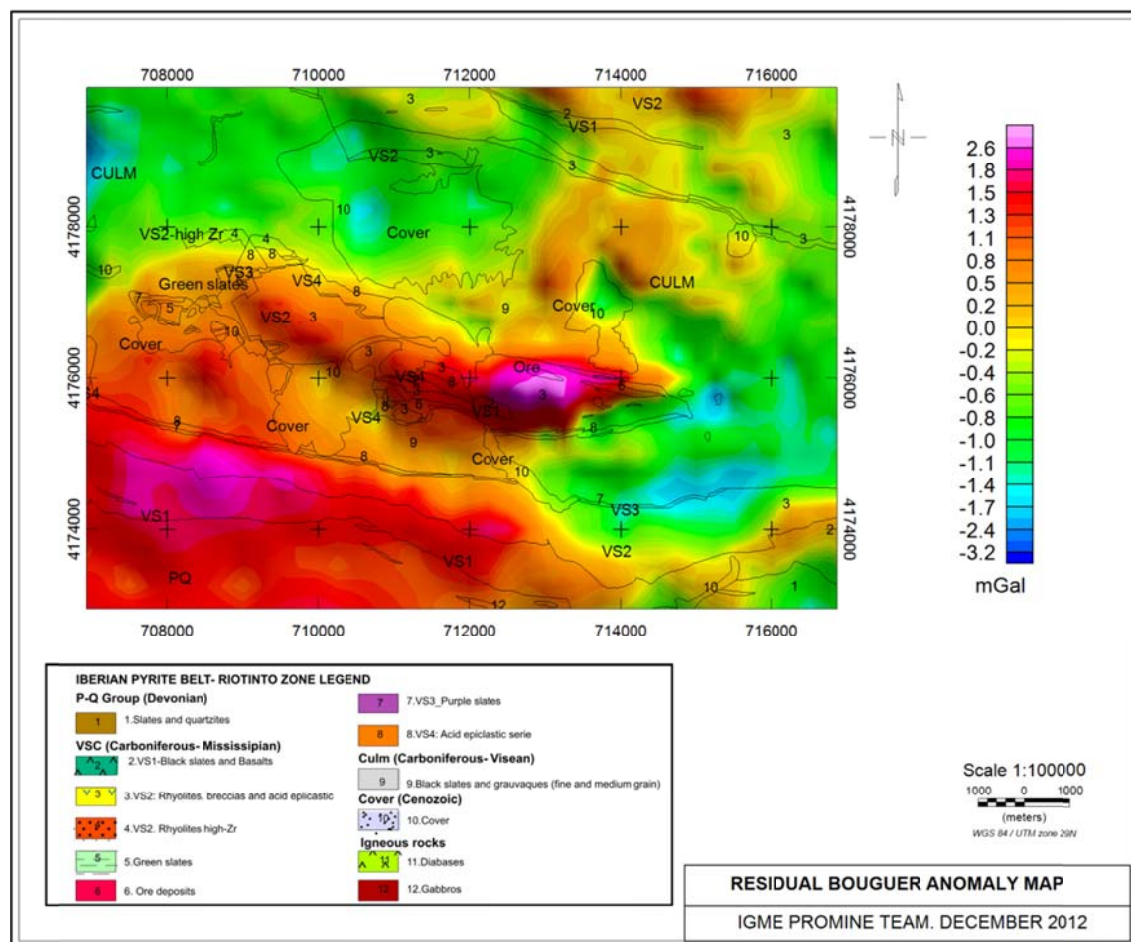
Figure 5.2. Residual Bouguer Anomaly Map (2012) of the Río Tinto Area

To sum up residual Bouguer anomaly map reflect together metasedimentary low density in the north, the superposition of high density materials (outcropping of the Río Tinto ore mine) over the Culm facies (characterized by medium values of Bouguer anomaly) in the centre and the high density materials on the south coinciding to Devonian slates, limestones and quartzites.

5.2. Airborne Geophysics

5.2.1. Reduced to the pole aeromagnetic map

Reduced to the pole (RTP) aeromagnetic map of Río Tinto region (Figure 5.3) is a portion of the geophysical flight over the Spanish Pyrite Belt and southern areas of OMZ (Ossa-Morena Zone) carried out between November 1996 and April 1997 with a line spacing of 250 m, and altitude clearance of 80 m (Figure 2.1).
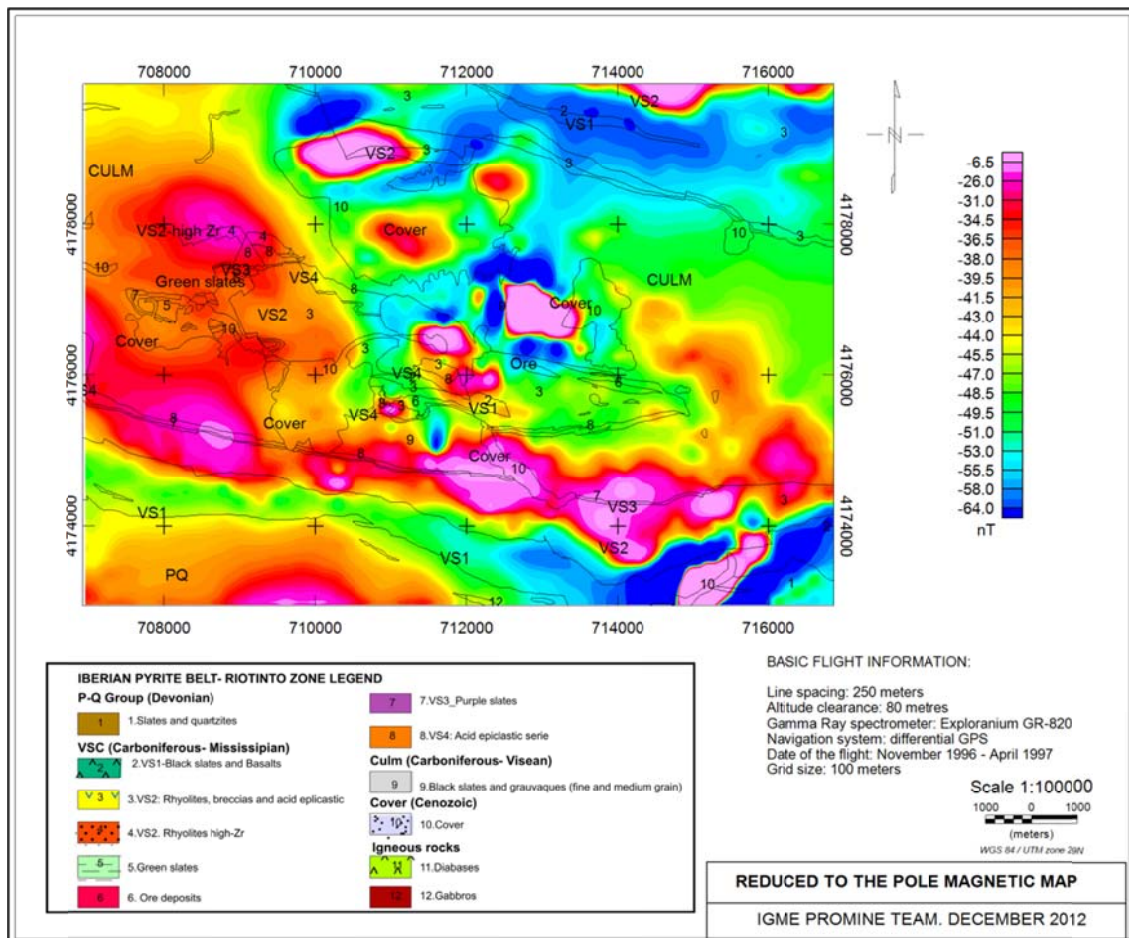
Figure 5.3. Reduced to the pole magnetic map of the Río Tinto area

As in the case of the residual Bouguer anomaly map, on the basis of anomaly intensity, two zones can be established in the total field reduced to the pole aeromagnetic map on the basis of total intensity:

1) Low field areas of intensity below -45 nT (green-blue colours). Located in the north of the map the low magnetic anomaly values are a consequence of the low magnetite (also low density) contents of the Culm facies (black slates and greywackes, petrophysical chapter). Also rhyolites, breccias and acid epiclastic (VS2) provide values lower than 53 nT in contrast to the high magnetite content of the same series in the southern outcropping unit.

45

Nevertheless a few spots of high magnetic intensity are also visible overlapping the paramagnetic values of the centre-north part of the studied area.

2) High field areas of intensity over -45 nT (yellow-red colours). In the south of the area, the complex unit composed by rhyolites, breccias, tuffs and acid epiclastic of the Carboniferous-Mississippian (VS2) depicts continuous maximum values E-W trending as part of the volcano-sedimentary complex (as these materials are mainly paramagnetic, VS1 basalts must be involved in depth, as seen in gravity residual map).

Accounting the fewspots of high magnetic intensity, the most remarkable one (a few kilometres wavelength) is the one located on the west of the area (red colours) related to the outcropping of the purple slates, jasper enriched in magnesium (VS3) and green slates as part of the outstanding ore mineralization in the area (jaspers are the likely source of these signatures). Some shorter wavelength magnetic anomalies are related to shallower bodies whose main characteristic is the unclear correspondence between the anomalies and the mapped formations. Some of those maximum appear on the Cenozoic cover and black slates and greywackes of Culm; considering that those units are mainly paramagnetic the rarely outstanding maximum could be explained as being the anthropic dumping of the ore deposits.

Summarizing paramagnetic materials (and also low density materials) coincide with the Culm facies and rhyolites, breccias and acid epiclastic metasedimentary units in the north area. The mining ore deposit of Río Tinto depict both magnetic (massive sulphurs and purple slates and jasper enriched in magnesium) and paramagnetic response. In the case of density this area depicts high density values. In the south rhyolites, breccias and acid epiclastic show high magnetite response probably related to an E-W band of purple slates mapped between VS2 and Culm facies. On the contrary the green and black slates show paramagnetic response. This bimodal magnetic response does not coincide with a bimodal density since homogeneous high values are showed in this area. A few shortwavelength high magnetic anomalies are depicted in the centre of the area probably related to some dumpling materials from the mine working.

5.2.2. Potassium, Thorium and Uranium contents

Airborne radiometric informs of the first few dozen centimetres in radiometric content. In the case of potassium radiometric map (Figure 5.4, values between 0 and 7.5 % of K) two areas can be distinguished.

1. Low concentration of potassium, less than 4% (yellow-green-blue colours) corresponds to the metasedimentary units (Culm facies, rhyolites and breccias and black-green slates and basalts). The lowest values (less than 1% of K, blue colours) coincide with some accurate mapped units, as black-green slates and basalts (see VS1 in the south) and the quaternary cover (Co). Also an important minimum coincide with the high density value anomaly in the centre of the Río Tinto ore mine (see residual Bouguer anomaly map, Figure 5.2).

2. High concentration of potassium, more than 4% (orange-red colours) are widespread in the west part of the map. The most outstanding (over 7 % of K) is located in the southeast over the rhyolites, breccias and acid epiclastic (VS2), probably due to the ore mine damping and over the massive sulphurs of the ore deposits.

The thorium values (Figure 5.5) range between 0 and 29 ppm Th. High values (over 17 ppm Th, orange-red colours) are located in some of the metasedimentary units (Culm facies, rhyolites and breccias and black-green slates and basalts) not following a clear pattern. The most outstanding anomaly (more than 27 ppm Th) is located, the same as in the potassium map over the massive sulphurs of the ore deposits. The lowest concentration in thorium (less than 2 ppm) is located in two spots in the north in good coincidence with the aforementioned low values in potassium.

The uranium anomaly map (Figure 5.6, values between 0.5 and 11 ppm U) shows the prevalence of very low concentration in uranium, the majority of the area has less than 5 ppm U (green and blue colours). As in the potassium and thorium the lowest values are located in the north mapping the shape of the Cenozoic cover. The highest concentration (orange-red colour) is located in the mine exploitation where a maximum in thorium was also located.

Ternary map. Most of the map area (Figure 5.7) is occupied by predominance of K+Th signatures (red colours). Basic materials in the south (VS1) are perfectly mapped by a white band indicating the absence of radiometric elements. The places with high concentrations in Th+U are located in the cover (Co, formed by the mine dumping) and the mining site itself.
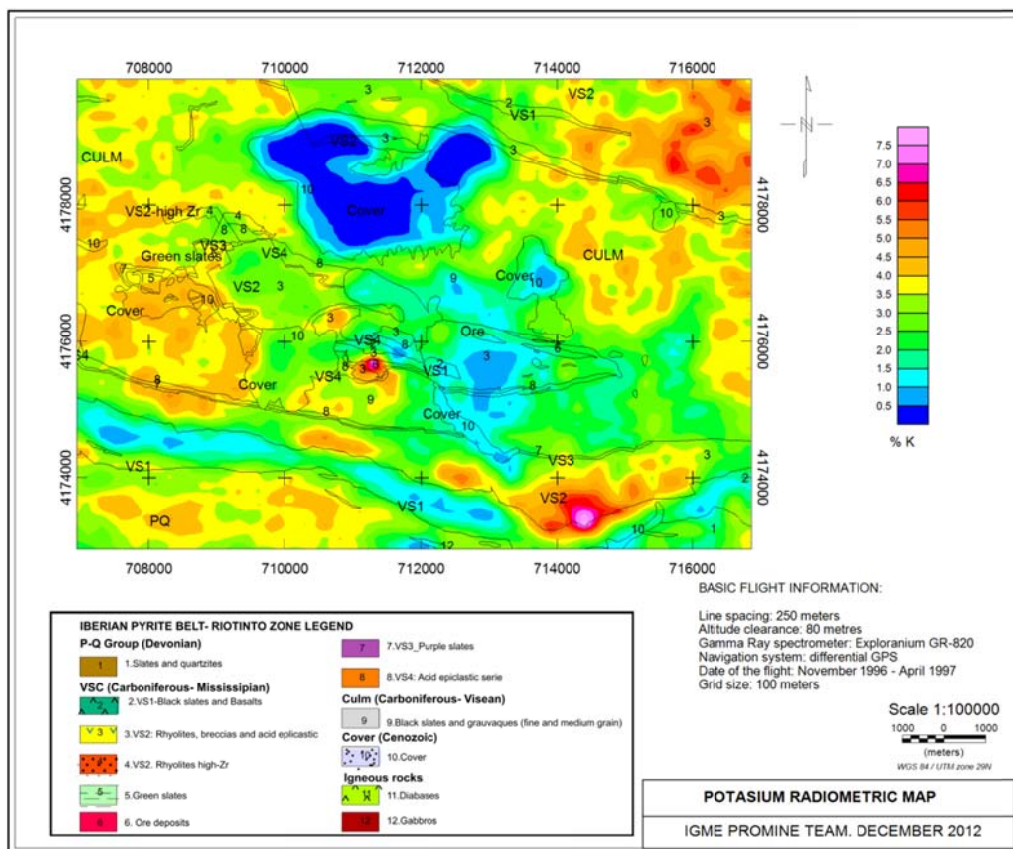
Figure 5.4. Potassium map of the Río Tinto zone
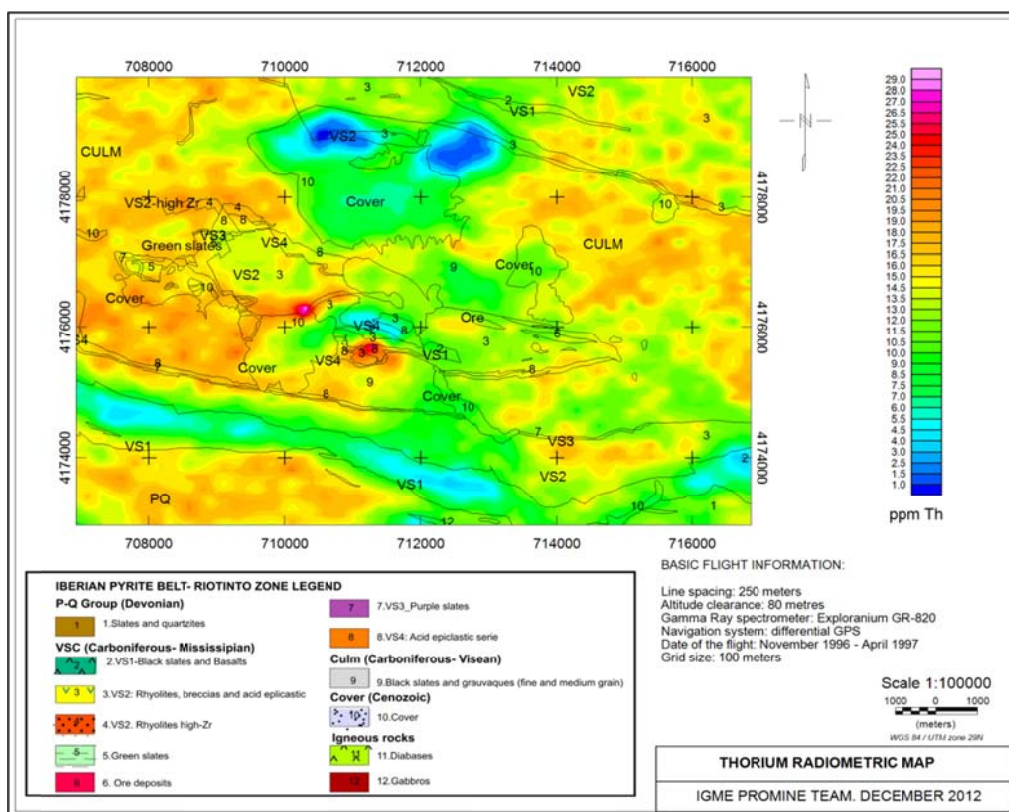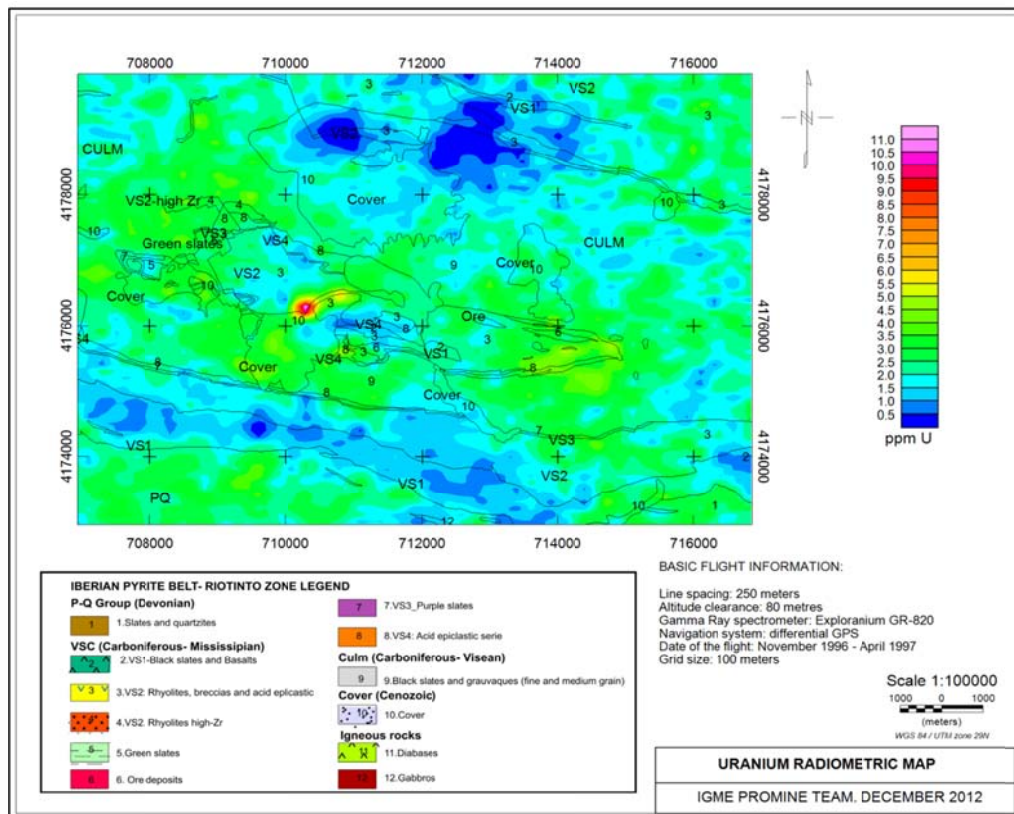

Figure 5.5. Thorium map of the Río Tinto zone
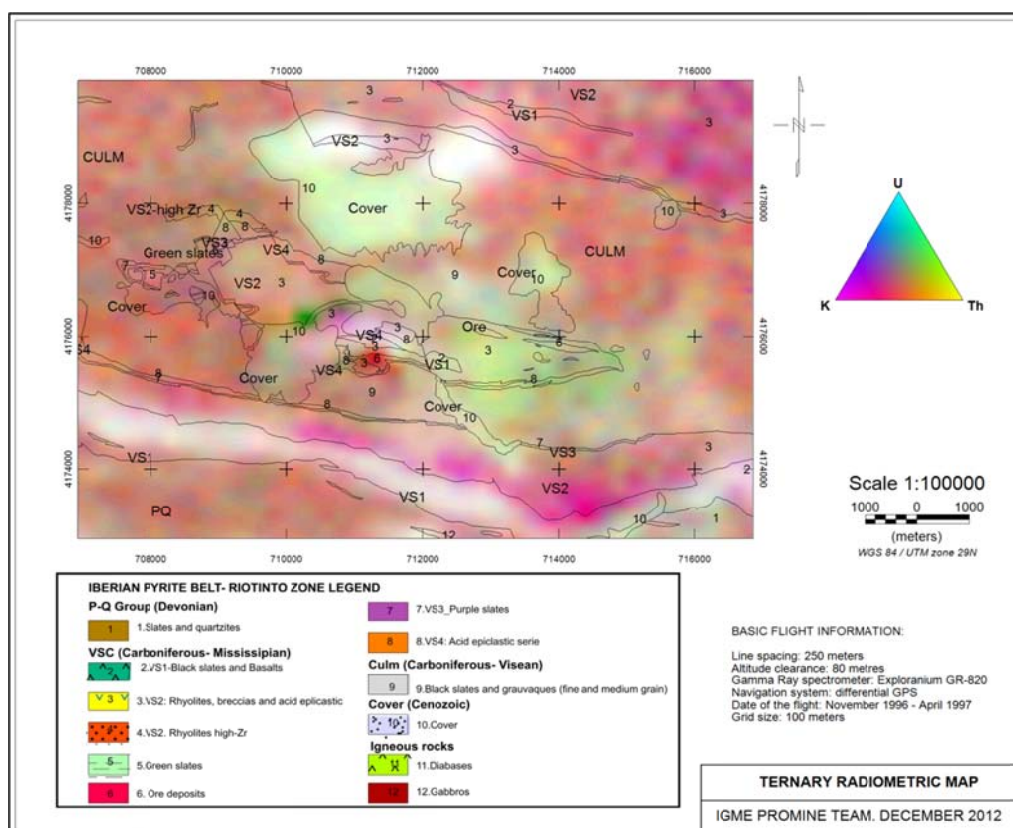
Figure 5.6. Uranium map of the Río Tinto zone

Figure 5.7. Ternary map of the Río Tinto zone

6. 3D POTENTIAL FIELD MODELLING OF RÍO TINTO AREA. NEW INSIGHTS INTO ITS GEOLOGICAL STRUCTURE.

6.1. Introduction

Río Tinto area is located central of SPZ (Figure 6.1, Zone B). During the ProMine Project a new geological map (1:10.000 scale, Figure 6.2) and new structural data were collected in the field, with structural measurement stations, petrographic, lithogeochemistry, microstructural analysis and petrophysical measures. On the other hand, new geophysical data have been acquired during the project.
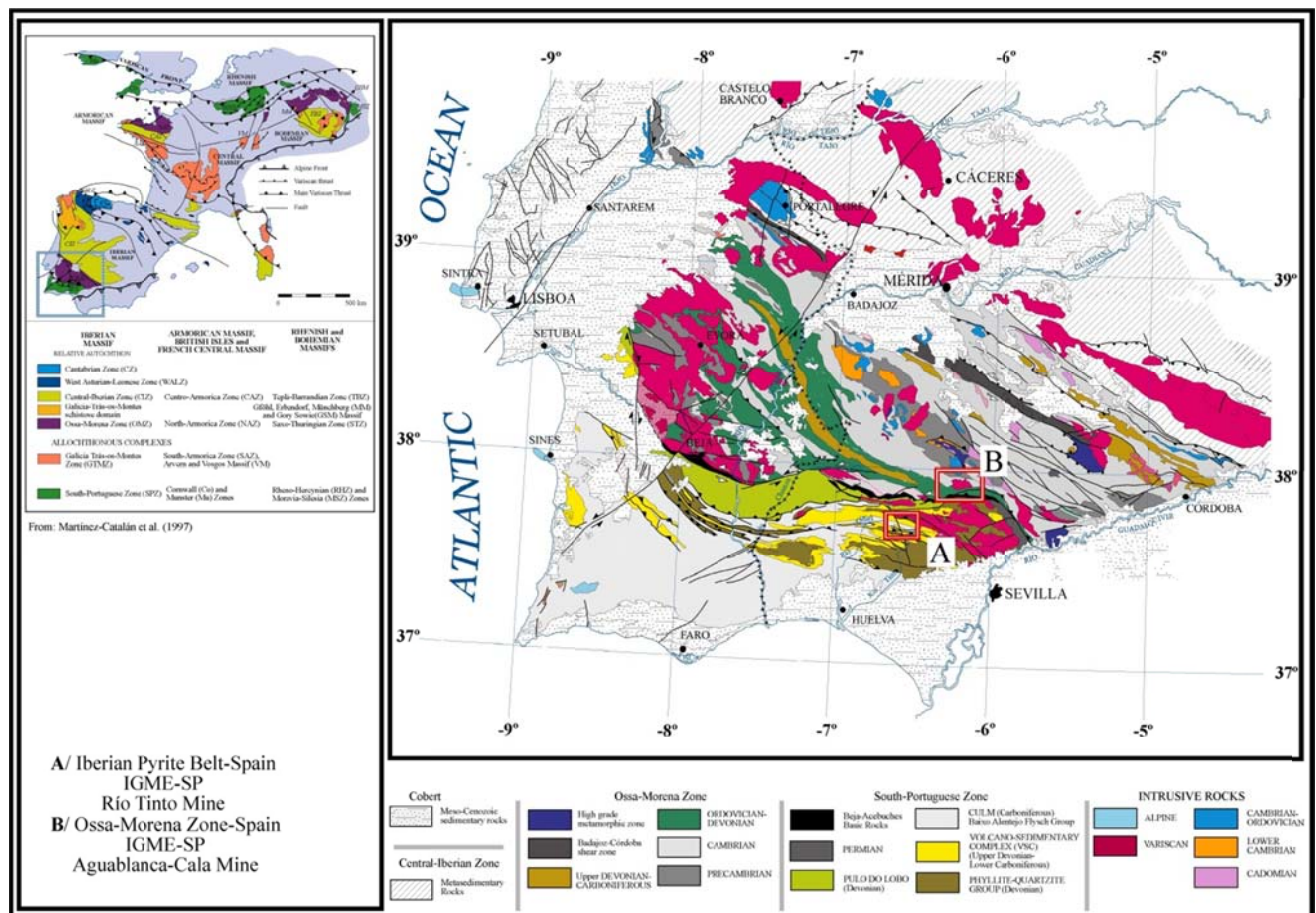
Figure 6.1.- A) General location of the study area in the European geological context; B) In the Variscan belt. The letters in figure indicate different studied zones in the ProMine project

The Río Tinto mine is located in the Río Tinto syncline where the core is formed by Carboniferous metasediments (Culm) (Navarro Vázquez and Ramírez Copeiro del Villar, 1982). But this syncline is not simple, in its central part outcrop volcanic rocks of the VSC through a thrust which formed the Río Tinto anticline (antiformal stack, González-Clavijo and Díez-Montes, 2010). The deformed stratigraphic succession of Río Tinto includes the Upper Devonian to Lower Carboniferous age, and

where the regional mapping in the IPB has identified a relative simple stratigraphic sequence, this comprises three major lithostratigraphic Paleozoic unit (Schermerhörn, 1971): Phyllite-Quartzite Group (PQ), the Volcano-Sedimentary Complex (VSC) and a sequence Carboniferous (Culm). These lithostratigraphic units have been described in the geological setting. To build the 3D model of the Anticline of Río Tinto, the lithostratigraphic units represented in Figure 6.2 have been simplified shown in the legend of Figure 6.3. The description is as follows.
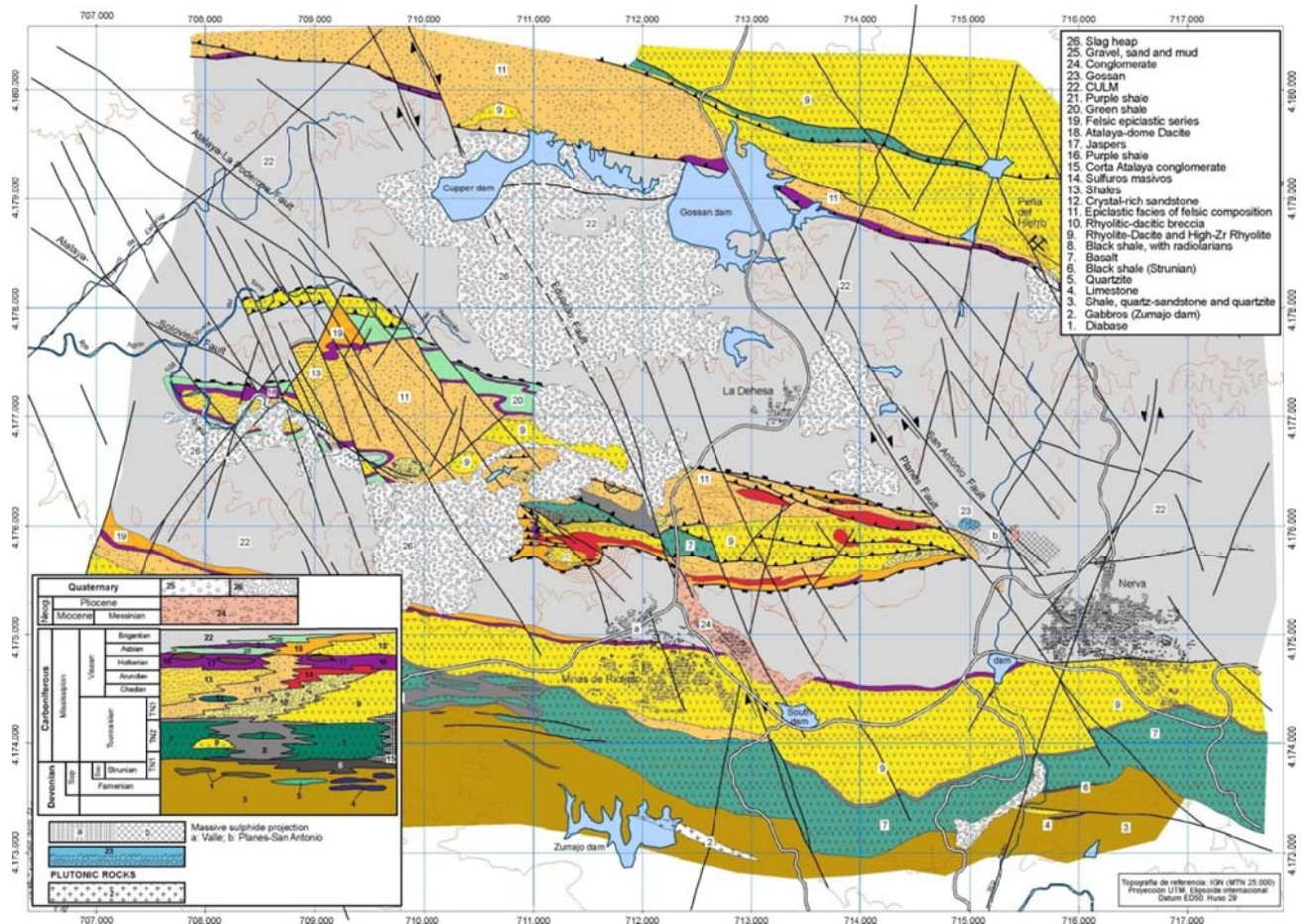
Figure 6.2. Geological map of Río Tinto area.

In the "Corta Atalaya" (Figures 6.2 and 6.4A) outcrops conglomerates with shale matrix of black colour, with edges of slate, quartzite and massive sulphides are exposed. This conglomerates type could correspond to other conglomerates described by other authors on all SPZ. These conglomerates are on top of P-Q Group and they mark the onset of instability of the basin and related to the first stages of the volcanism of the SPZ.

Overlying the P-Q Group is the **Volcano-Sedimentary Complex** (VSC). This unit is a submarine succession dominated by basic and felsic volcanic rocks, which are interbedded in mudstones and volcaniclastic sediments. The VSC has been dated as Late Fammenian to Late Visean (Oliveira, 1990; Rodríguez et al., 2002; Barrie et al., 2002; Dunning et al., 2002; Rosa et al., 2009; Valenzuela

et al., 2011). The volcanic lithostratigraphic units that have been used to build the 3D model of Río Tinto are from bottom to top, basalts (VS1), felsic rocks (VS2, rhyolite-dacite massive, volcanic breccias, epiclastic rocks) and finally the purple slates (VS3) and the transition series (VS4). This latter type of rocks (VS3 and VS4) represents the only guide level of the SPZ. Sometimes it was not possible to differentiate VS3 and VS4, combining both into a single unit (see cross-section in Figure 6.4B).

The **P-Q Group** outcrops south of Minas deRío Tinto village. On top of the P-Q Group and in contact with the bottom of the CVS (basalts) there is a level of black shales of Strunian age (Rodríguez et al., 2002).

Finally, stratigraphically overlying the VSC is a sedimentary sequence, the **Culm Group**. It is the uppermost IPB unit, consists of shale, litharenite and rare conglomerate with turbiditic features. The Culm Group ranges in age from Late Visean to Middle-Late Pennsylvanian; it is interpreted to represent a synorogenic flysch related to the Variscan tectonic event.

A)

LEYENDA

Cuaternario	25	26		
Terciario / Neógeno / Mioceno / Superior	Plioceno			
	Messiniense	24		

23

Carbonífero / Mississippiense / Viseense	Brigantian	22		
	Asbian	21 / 20	20	19 / 18
	Holkerian	17 / 16 / 17	15	17 / 16
	Arundian	13	11 / 14	
	Chadian	12 / 10	9	
Tournaisiense	TN3			
	TN2	8 / 7 / 9		6
Devónico / Superior	TN1 / Struniense	5	5 / 5	5
	Fameniense	3		

CULM
22. Pizarras negras y grauvacas de grano medio a fino
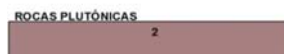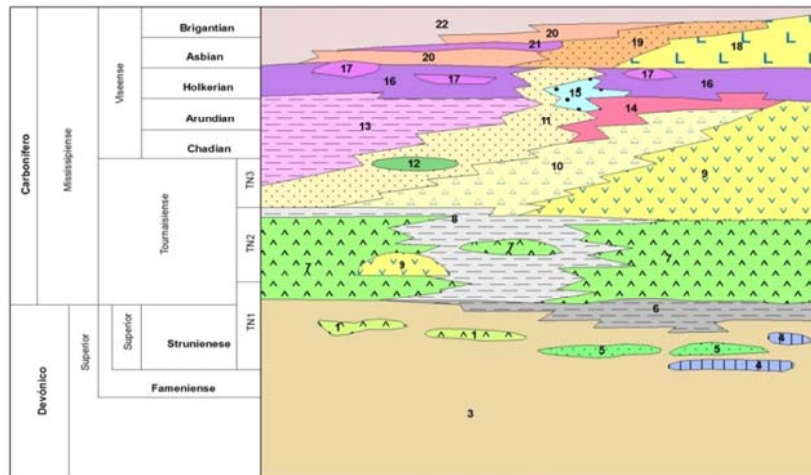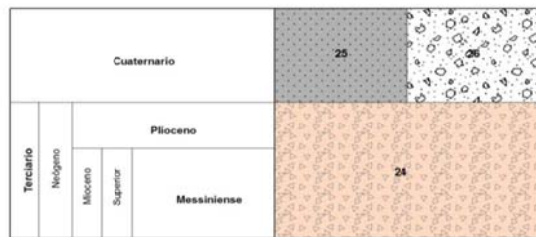
26. Escombreras (Antrópico)
25. Gravas, arenas y lutitas (Aluvial)
24. Conglomerados con cemento ferruginoso y capas de óxidos
23. Gossan

21. Pizarras moradas
20. Pizarras de tonos verdosos
19. Serie epiclástica de composición riolítica
18. Riolita
17. Jaspes ricos en manganeso
16. Pizarras moradas
15. Conglomerado de "Corta Atalaya"
14. Sulfuros masivos
13. Pizarras, tonos verdosos (Tobas epiclásticas pizarrosas)
12. Tobas epiclásticas de composición básica
11. Serie epiclástica de composición riolítico-dacítica
10. Brechas riolítico-dacíticas
9. Riolita-Dacita
8. Pizarras negras con capas de radiolarios
7. Basalto

COMPLEJO VULCANO-SEDIMENTARIO

GRUPO P-Q
6. Pizarras negras
5. Cuarcitas
4. Calizas
3. Pizarras, cuarcitas y grauvacas
2. Gabros (embalse del Zumajo)
1. Diabasa

ROCAS PLUTÓNICAS
2

ROCAS FILONIANAS
1

B)

	Culm
	VS4-Transition series
	VS3-Purpura shales
	Ore deposits
	VS2-Rhyolites-Dacites
	VS1-Black slates and Basalts
	P-Q group
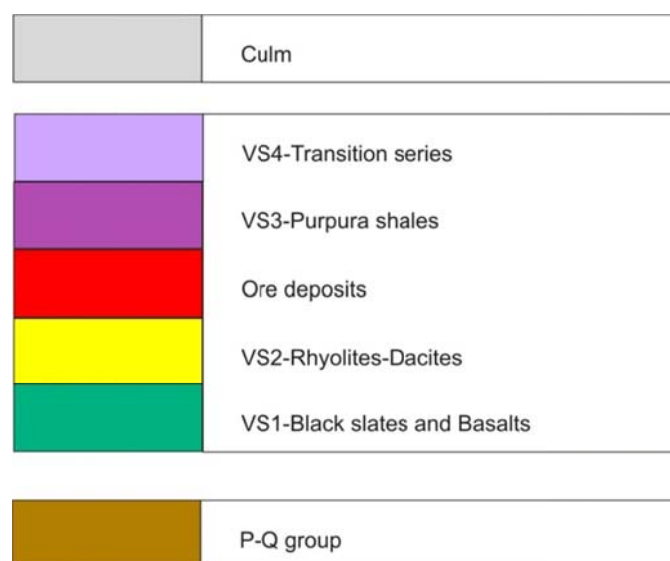
Figure 6.3. A) Geological legend of the study area (see geological map, figure 6.1 on this report).B) Groups in 3D model.

53
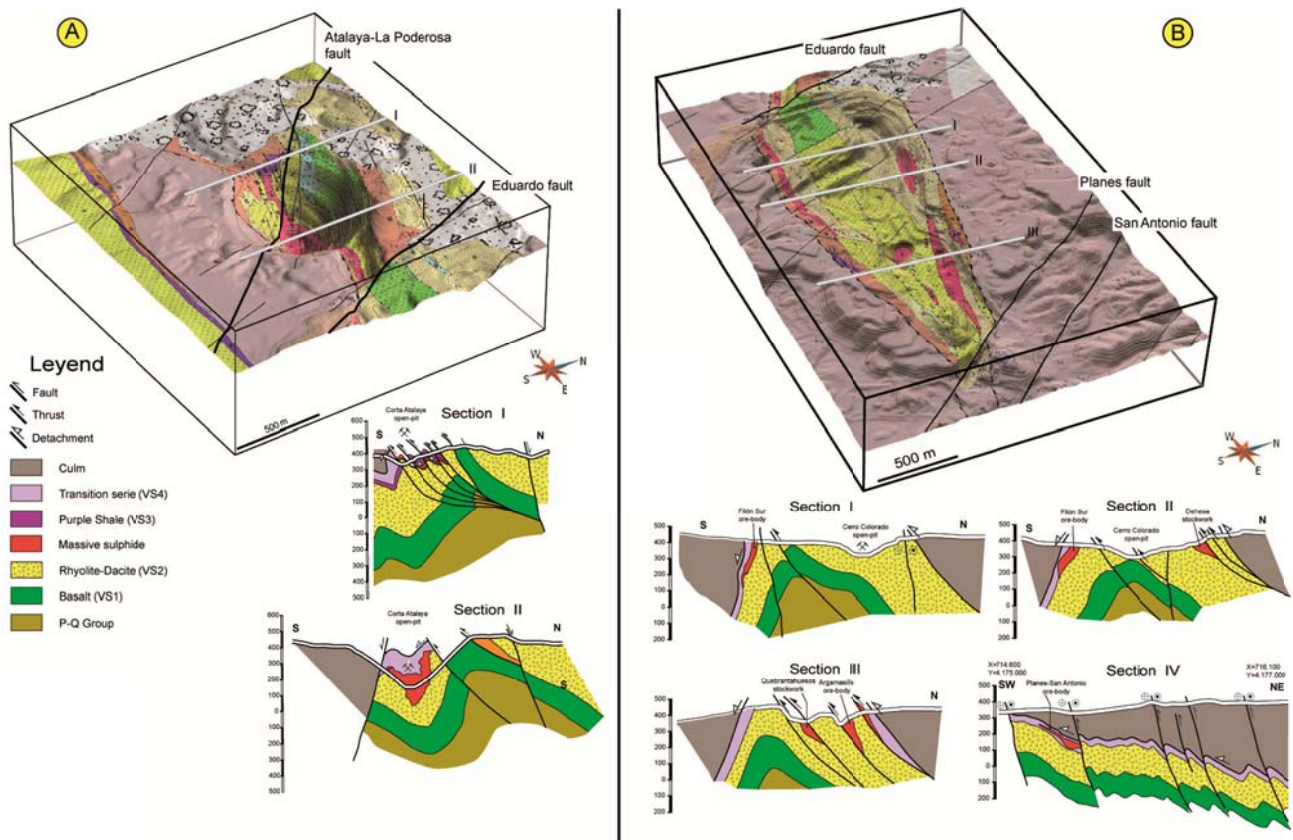
Figure 6.4. A)3D geological map of "Corta Atalaya" open-pit and two examples of the geological cross-sections for building the 3D model of this zone. Simplified legend used to build the 3D model of Río Tinto.B)3D geological map of "Cerro Colorado" open-pit and four examples of the geological cross-sections for building the 3D model of this zone.

The Iberian Massif is deformed mainly by the Variscan Orogeny. The tectonic evolution of the SPZ shows the characteristic features of a foreland fold-thrust belt dominated by thin-skinned tectonics model (Ribeiro and Silva, 1983; Silva et al., 1990; González-Clavijo et al., 1994; Quesada, 1998). This tectonic deformation has been confirmed by studies of deep seismic reflection profiles (Simancas et al., 2003). Three major tectonic domains have been established in the South Portuguese Zone on the basis of cartographic, stratigraphic, lithologic, structural and metamorphic criteria. They are from north to south and from the upper to lowest tectonic position: Northern Domain, Central Domain or Iberian Pyrite Belt and Southern Domain (Mantero et al., 2007). Río Tinto is located within the Central Domain or Iberian Pyrite Belt, characterized by having a high intensity of deformation, which decreases towards the southwest. Structural development of the SPZ is characterized by south-westward vergent folding and thrust displacement.

In this area, the first episode of the variscan deformation generates S to SSW vergence, thin-skinned fold and thrust belt that propagated southwards and formation of the mylonitic foliation. Structurally, at high levels the structure proposed for Río Tinto area mainly consists of south-vergent folds with sub-horizontal axes and oriented according to N90°E to N120°E. In general, the folds have only

normal flank, while short or inverse flank are rarely seen in this area. An antiformal stack Río Tinto is located in the central part of this synclinal where volcanic rocks outcrop (Mellado et al., 2006; González-Clavijo and Díez-Montes, 2010). The geometry of the antiformal stack km-scale system and the lateral variations of the fold axes are well shown in Figure 6.3. In this antiformal stack, the core is mainly formed by mafic and felsic volcanic rocks showing hydrothermal alteration and stockwork type mineralization.

The main tectonic structure of Río Tinto area is represented by the detachment at the contact between the volcanic rocks and the Culm (Figure 6.3A and B). This detachment had already been proposed by Quesada (1998) for all IPB. The detachment is not only at the bottom of the Culm, but also at the top of the VSC, affecting the purple shale and the top of the massive sulphide bodies developing mylonites and ultramylonites. This detachment seems to develop well in those areas where there are large massive sulphides bodies, and it has also been described in other areas of the IPB, e.g. in Masa Valverde Deposit (Castroviejo et al., 2010). It is interrupted by ductile thrusts (Figure 6.4A, section I) where the stockwork lies parallel to the main foliation. The detachment and the ductile thrust are interrupted by other out of sequence east-west thrusting with fragile-ductile character.

Finally, develops a conjugate system of faults with NW-SE dextral and NE-SW sinistral trend. In the Río Tinto area there is a predominance of the faults with NW-SE direction. Atalaya-La Poderosa, Eduardo, Planes and San Antonio are examples of this type of fault (Figure 6.2).

6.2. Dataset and methods used to build the 3D models

Traditionally, geological map has been the main tool to represent geological features and the relationships between lithologies. It is often accompanied by cross sections to help to understand how rocks and structures behave in the subsurface.

Today, new technologies provide new tools which make easier the representation and the understanding of the geology. Traditional tools along with new ones lead to new approaches to widen the geological knowledge.

Nowadays, most of the cartography, including geological maps, is available in GIS formats and the use of tools to analyse the data linked to them are widespread. Recently, new software has been developed, allowing managing 3D data, making easier to interpret geological structures. So, the use of both technologies makes possible new interpretations and the reconstruction of geological bodies in the subsurface. To achieve the modelling goals, two softwares have been used. ArcGIS has been employed for extracting data from previous layers loaded in geodatabase format, that were used to

build up the geological maps. After the adequate field work, these maps were reviewed and recompiled, both in stratigraphic and structural terms. gOcad has been the 3D modelling software used to load the data coming from ArcGis (i.e., geological limits, faults) and 3D data like drillings, dip points, and geological cross-section. A modelling study, integrating results from structural geology and petrology, was performed with gOcad, in order to decipher geometrical and geological relationships between different rocks and mineralization zones.

The input data used in this study are the topographic reference (as DEM of 100x100 m, basic datum of all the 3D features), reviewed geological map, structural data and samples for petrological and petrophysical characterization, geophysical data with corresponding interpretations and models, and borehole data (source data of Figure 6.5A). So the first step of the proposed methodology refers to the creation of a geological database, which includes all the information needed for 3D modelling. Six main typologies of geometric features and related attributes are exported from an ArcGIS-geodatabase:

1- Topographic data: topographic data as points from a digital elevation model.

2- 2D linear features from geological maps (stratigraphic and intrusion boundaries, fold axial traces, faults, foliations, etc.): a geological map with stratigraphic, tectonic and intrusion boundaries, linear features as 2D polylines.

3- 2D polygonal features of outcropping units, and 2D geological cross-sections.

4- Petrological and petrophysical samples, for laboratory determination of properties (densities, magnetic susceptibilities) from some surface rocks of the studied area, and natural gamma ray-measurements.

5- Geophysical data and interpretation.

6- Data from drill-hole and old maps, vertical sections, and horizontal slices of ore-bodies in some cases.

All these data are the source of our initial geological model. The processing of previous data generates new layers of information, which step by step are (Figure 6.5B):

- 3D geological maps and cross-sections. Building of a set of 3D parallel geological cross-sections across the analysed structures and intrusions constitutes the first basic step of our methodological approach.

- 3D pointsets. These correspond mainly to borehole intersects of top/bottom limits of selected units, and to 3D layers of dip points and structural measurements, needed for surface interpolation.

- Petrological, petrophysical samples and radiometric measures

- Geological cross-sections that come from 2.5D potential field modelling.

- All these layers are processed within the gOcad environment with adequate interpolators to generate 3D layers of curves and surfaces, and finally voxels of the modelled bodies (Figure 6.5C).
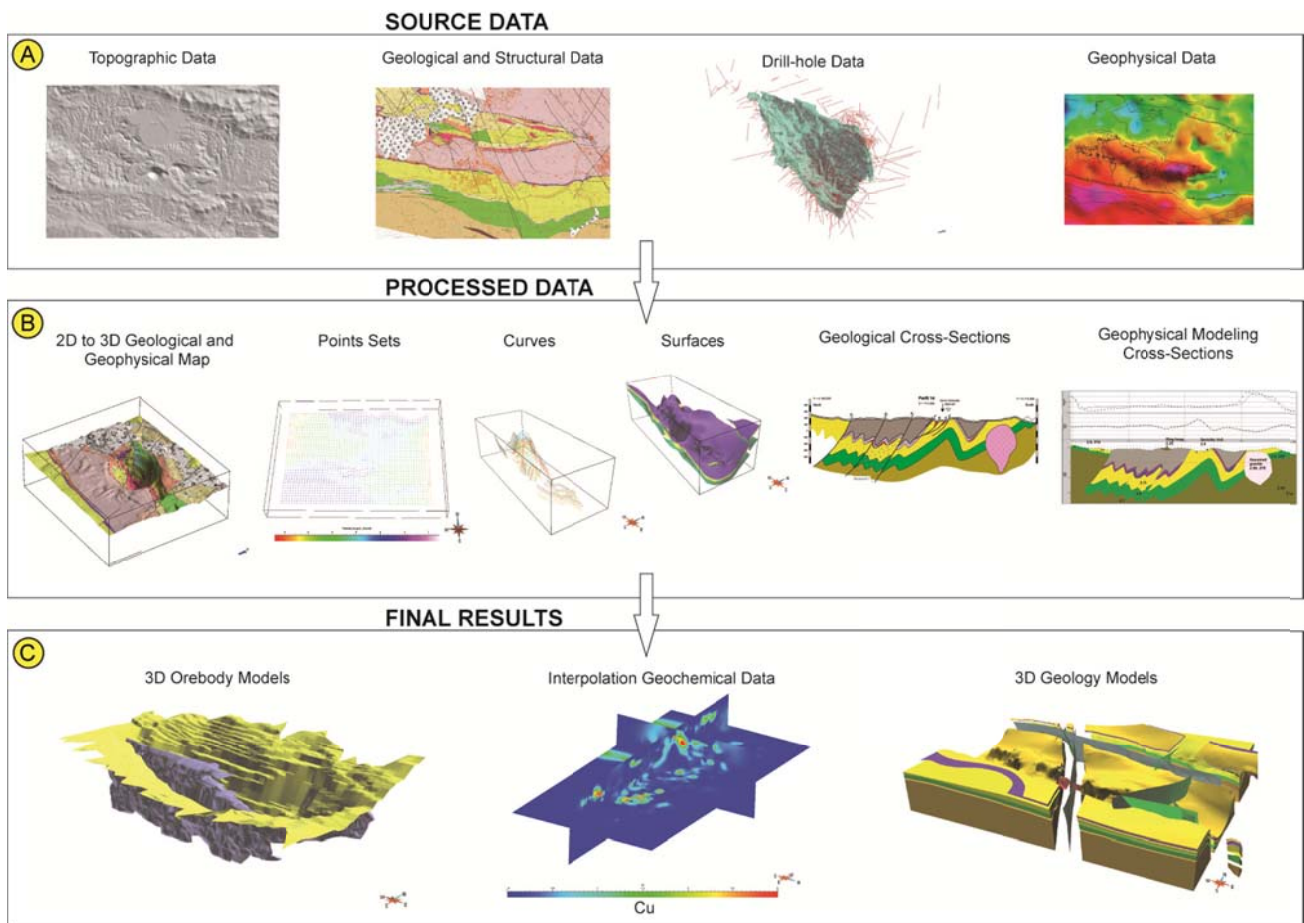
Figure 6.5. Schematic flow-chart for 3D modelling through data integration between source data, GIS and gOcad.

Existing geophysical coverages were densified with new acquired data. Although these were non-seismic surveys, they are sufficiently precise to solve the faced problem. New acquired geophysical surveys consisted of a gravity and natural gamma ray data. These surveys were interpreted qualitatively first, and then by geophysical inversion processes adapted to the problem to solve.

Geophysical modelling defines the correlation between a model of the subsurface and the geophysical data acquired, usually, on the surface. Working with potential fields, the subsurface

geology is investigated taking into account the variations that occur in the earth's gravitational and magnetic fields due to the density and magnetic susceptibility distribution in depth.

The final 3D geological models were obtained mostly from geological cross-sections that were adjusted to fit potential field anomalies. After calculating the gravimetric responses from the initial geological model (direct problem), we proceeded to the review of the initial deep structural cross-sections and new ones were built with the support of the geophysical models (see following section 6.3.2).

6.3.   3D modelling results

6.3.1. Initial 3D geological model

In the Río Tinto geological 3D modelling several steps are involved, but, first of all, the available information must be gathered in a suitable way in order to facilitate the analysis and avoid losing relevant data.

The mining company (EMED-Tartessus) currently carrying exploration task has provided part of the information. The rest of the information has been acquired from surveying.

Topographic data

For the Río Tinto area, EMED Tartessus Company provided an updated survey (2010) that covers the area immediately next to the site of mining interest. However, given the regional nature of the project ProMine, new data of a larger surrounding area has been included. The cartography produced by the ICA (Cartographic Institute of Andalucía) was chosen. All the maps of this Autonomous Community are available on line at 1:10,000 scales.

The topographic data processing includes several steps, beginning with the format conversion from CAD to GIS format. For this transformation, FME software has been used, creating a filter that extracts only the topography curves and points. Further coordinate transformation has been necessary to project data from WGS84 to ED50 Zone 29.

Once in GIS, lines and points have been transformed to a grid using the "Topo to Raster" tool in ArcGis. The cell size has been established to 10m. Then, that ArcGis grid has been turned into a point grid, ready to use in gOcad.

Finally, the meshes have been imported and a topographic surface has been built in the gOcad software.

Geological data

One of the first tasks in the project was the elaboration of a new geological map of the area at 1:10,000 scales. At the same time, 44 cross sections have been interpreted from the map, as input for the potential fields modelling, with special focus on the Río Tinto anticline (Figure 6.6). The geological map has been digitized and coded for GIS, using ArcGis software.

The geological map in ArcGIS format contains linear features such as stratigraphic boundaries, faults, structural measures, etc. that can be imported directly into gOcad and projected onto the topographic surface. Lines are then coded, separating them in different features, in order to create model surfaces.
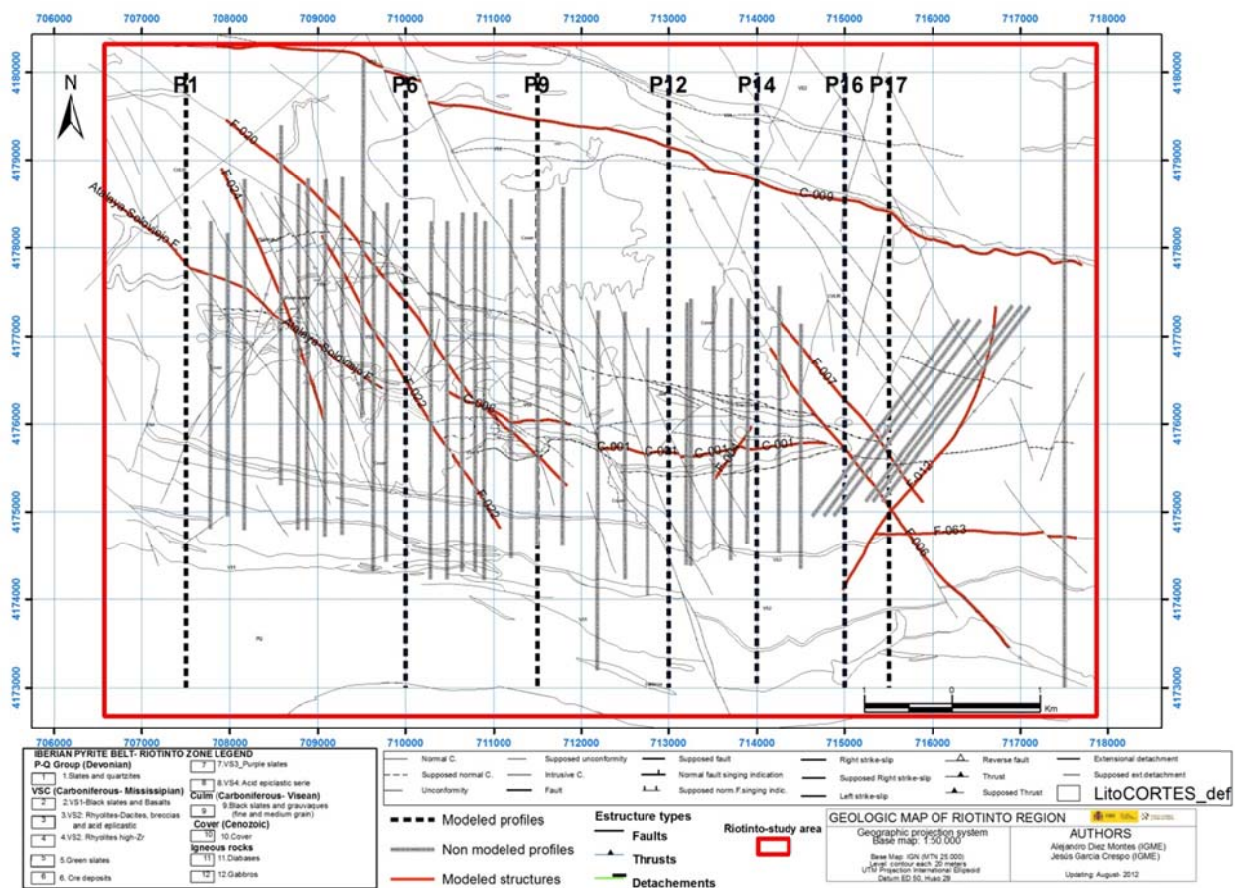
Figure 6.6. Location of the 44 geological cross sections in the studied area (black straight lines, either solid or dashed); dashed lines correspond to the modelled profiles. Thick lines in black and red are the main faults (red are the faults included in the regional 3D model). Red rectangle- 3D regional model;

The cross sections have been imported to gOcad for 3D vectorization. The lines drawn on the sections have been digitized and coded according with the geological legend.

The models incorporate the geophysical and petrophysical data described in sections 3 and 4 and interpreted in section 5. A summary of the analized samples used in this project is shown in Table 6.I

	Petrography	Chemical Analysis		Petrophysics		Natural gamma
	New	New	Compiled	New	Compiled	
RÍO TINTO	82	67	153	67	167	360
total	82	220		234		360

Table 6.I. -Summary of the samples used in the project

In Río Tinto area, 26 units have been distinguished on the geologic map: 13 are metasedimentary, 11 volcano-sedimentary and 2 plutonic. These groups have been grouped and reduced to the following 7 for 2.5D and 3D modelling: P-Q Group (PQ); CVS Group that is the host of major mineralizations, and includes VS1, VS2, VS3 and VS4; and finally Culm Group (Figure 6.3B).

Data from the subsurface mining works

During the active life of a mine abundant documentation is generated. This information includes detailed subsurface mapping. Such documents are useful in delineating the formations in depth.

In Río Tinto area several classified documents from mining activities have been made available, , like maps and sections of works, surveys, etc., from which valuable information has been extracted which has allowed the reconstruction of historical ore bodies.

The mine plans by level have being especially helpful. They contain the mine works at each level of the mine, with survey data, grades, lithological interpretations and maps showing the presence of sulphides masses. From them, the masses of sulphides have been drawn. Sections of the masses have been incorporated when available.

In this area, there are nine sites, currently abandoned, which extracted ore from several deposits. The traditional method for mapping involved the use of a local coordinate reference system for each site or group of sites. Thus, there is a reference system for Filón Sur, another one for San Dionisio and a different one for San Antonio. To georeference these cartographic documents, a two steps

transformation has been necessary: first from the local to the mine coordinates and second, into the UTM ED50 Zone 29.

The transformation parameters were obtained from measured points with total station and GPS with a precision of ± 7 to 5 meters. The digitization was done on the transformed documents. Sometimes this transformation involved translation, or translation and rotation to fit the data to a common mesh. Then, the transformation to UTM ED50 Zone 29 was carried out.

Drill holes data

In Río Tinto, documentation of about 6,700 drill holes was available. The majority was only location data without any valuable information. The filtering of the relevant information led to 2,658 drill holes with significant data. Fortunately, they had the deviation data of the well and, frequently, geochemical data.

The transfer of data from the surveys was done with the import tools that gOcad provides, after having structured the information in comma delimited files. Well objects have been used for loading the drill holes data. Such information allowed modelling the sulphides masses.

Geophysical Data

As already mentioned before have been used own project information, the data available in the database of the IGME (SIGECO, on line, 2014), as well as information collected from other companies who work in the area 6.3.2. Geophysical surveys. 2.5D modelling

6.3.2. Geophysical surveys. 2.5D modelling

Geophysical data are the result of sampling the distribution of a physical property of the Earth subsurface. Geophysical modelling defines the correlation between a model of the subsurface and the geophysical data. In potential fields, the subsurface geology is investigated taking into account the variations that occur in the earth's gravitational field due to the density and magnetic susceptibility distribution in depth.

The 2.5D potential field models described in this section are based on the cross sections build up from geological data and the observed gravity and magnetic data. Original geological cross sections were adjusted by geophysical inversion, changing mainly the geometry of the different geological bodies with the constraint of the physical properties measured in the laboratory from rock samples.

Once the RMS of the differences between observed and calculated anomalies was adequate, the modelled cross sections were "feed" into the gOcad software in order to build up the 3D model.

In the Río Tinto area, the geophysical and petrophysical available data used for the modelling have been described already section 2.3 Geological and Geophysical data, and also in chapters 3, 4 and 5.

The geophysical observables for the 2.5D modelling are the resudial Bouguer anomaly and the reduced to the pole magnetic map. More detailed information about the potential fields and radiometric data can be found in Chapter 5.

2.5D gravity and magnetic modelling

In the study area, eight N-S cross sections, approximately perpendicular to the strike of the gravity data, were extracted from the starting 3D gOcad model previously built from the available information as described in section 3.1. The profiles cross the main geological features and were selected in order to constrain the structures by 2.5 D gravity modelling. For that task we have used the latest GM-SYS software (by Geosoft), extending the models far enough at both ends of the profiles in order to avoid edge effects. The reduced to the pole magnetic field has been modelled with an IGRF of 43407 nT, I=90º, D=0º and considering that all the magnetic field is induced (i.e., no remanence). Calculations of the gravity and magnetic model response are based on the methods of Talwani et al., 1959, and Talwani and Heirtzler, 1964, and the algorithms described in Won and *Bevis, 1987*. In this work, we present the seven cross-sections modelled of the area: (Figure 6.7 to 6.13).

Densities and magnetic susceptibilities have been taken from the petrophysical data. Because the main uncertainties are the geometry of the bodies, for the densities, we have used its average in the majority of the cases (see Table II) or a value within the range of uncertainty (±0.05 mGal); for the magnetic susceptibilities we have employed values within the range of the measured values (Table II).

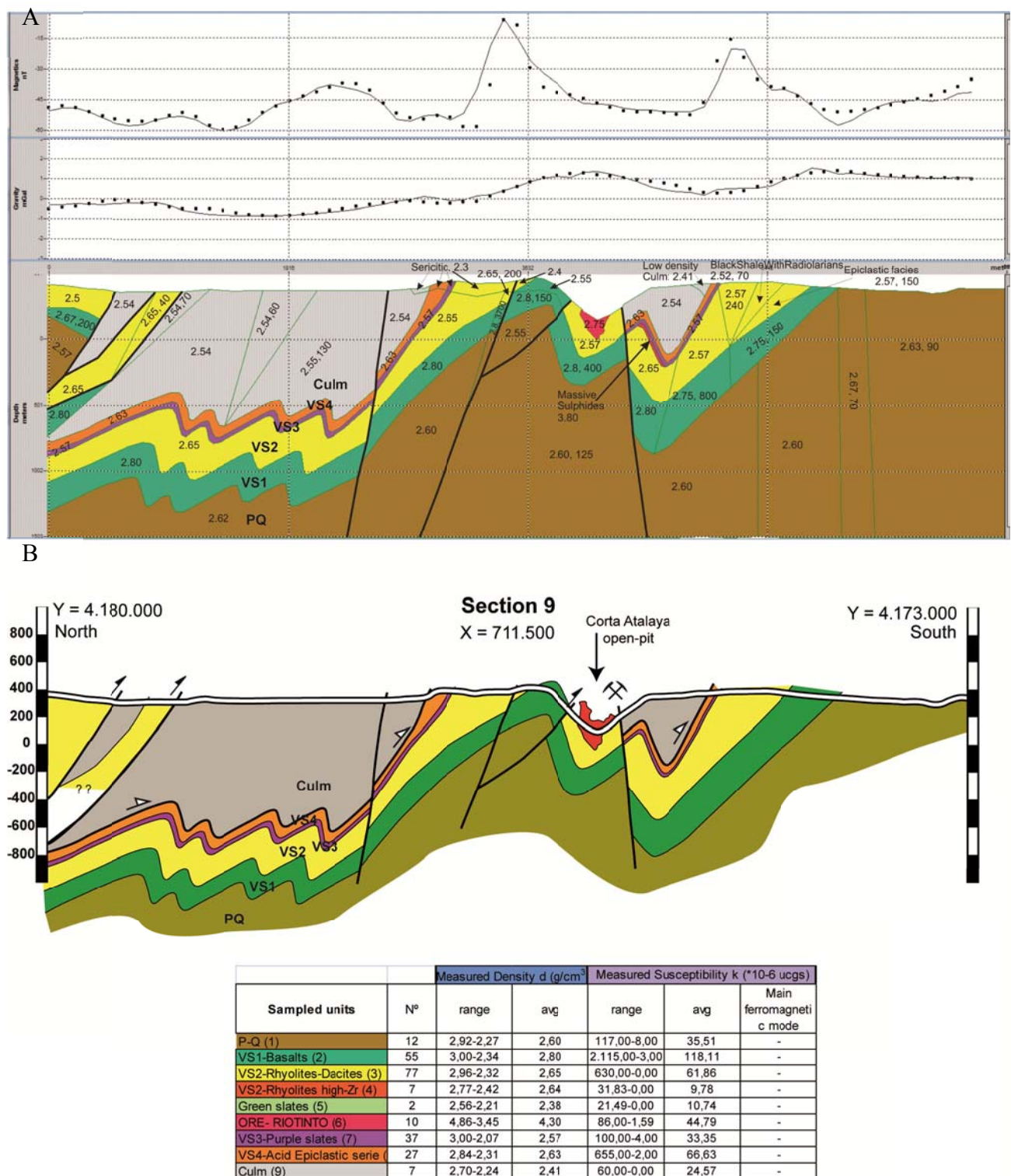The coordinates outlined in all the profiles are the UTM projection, zone 29. European Datum-1950.
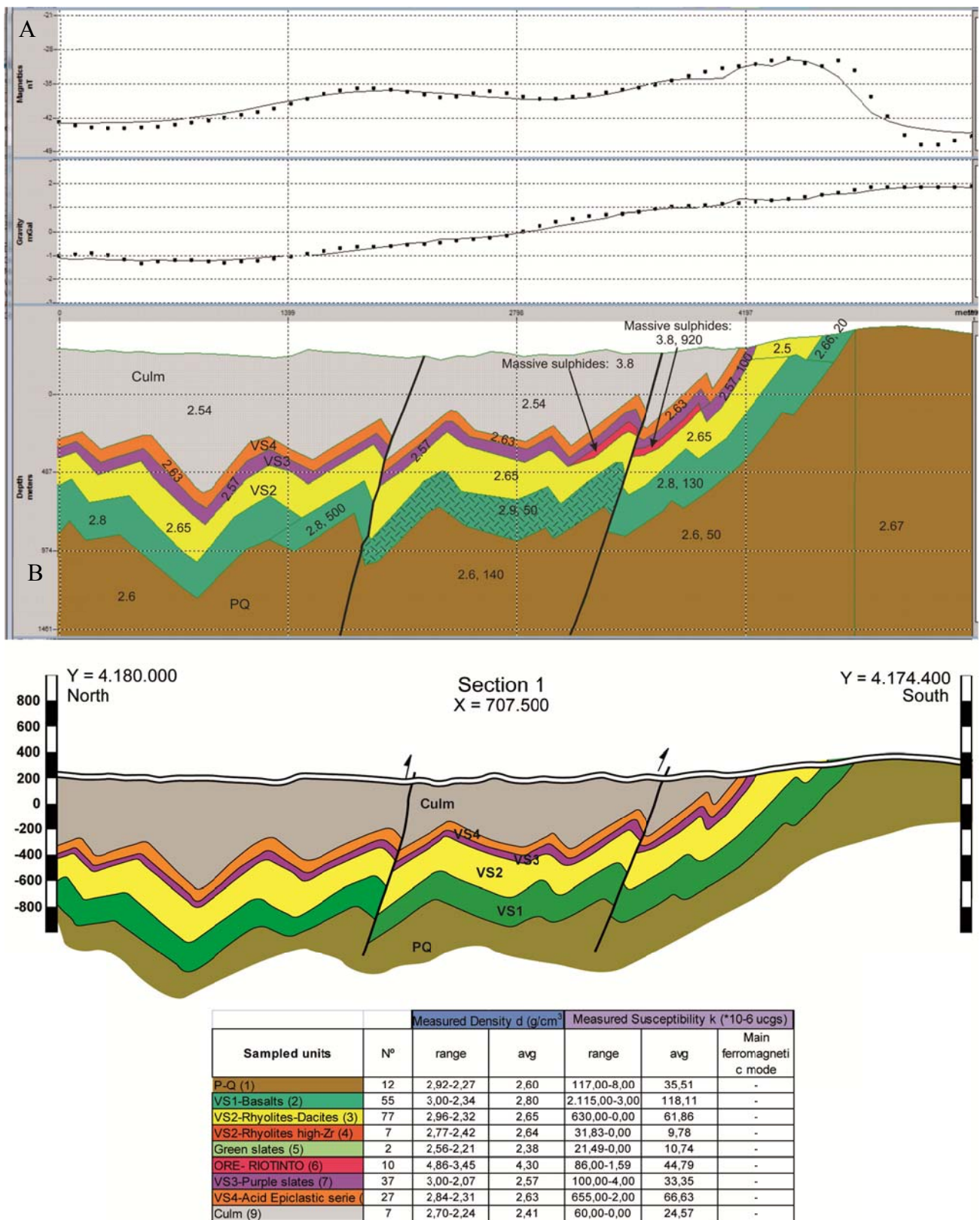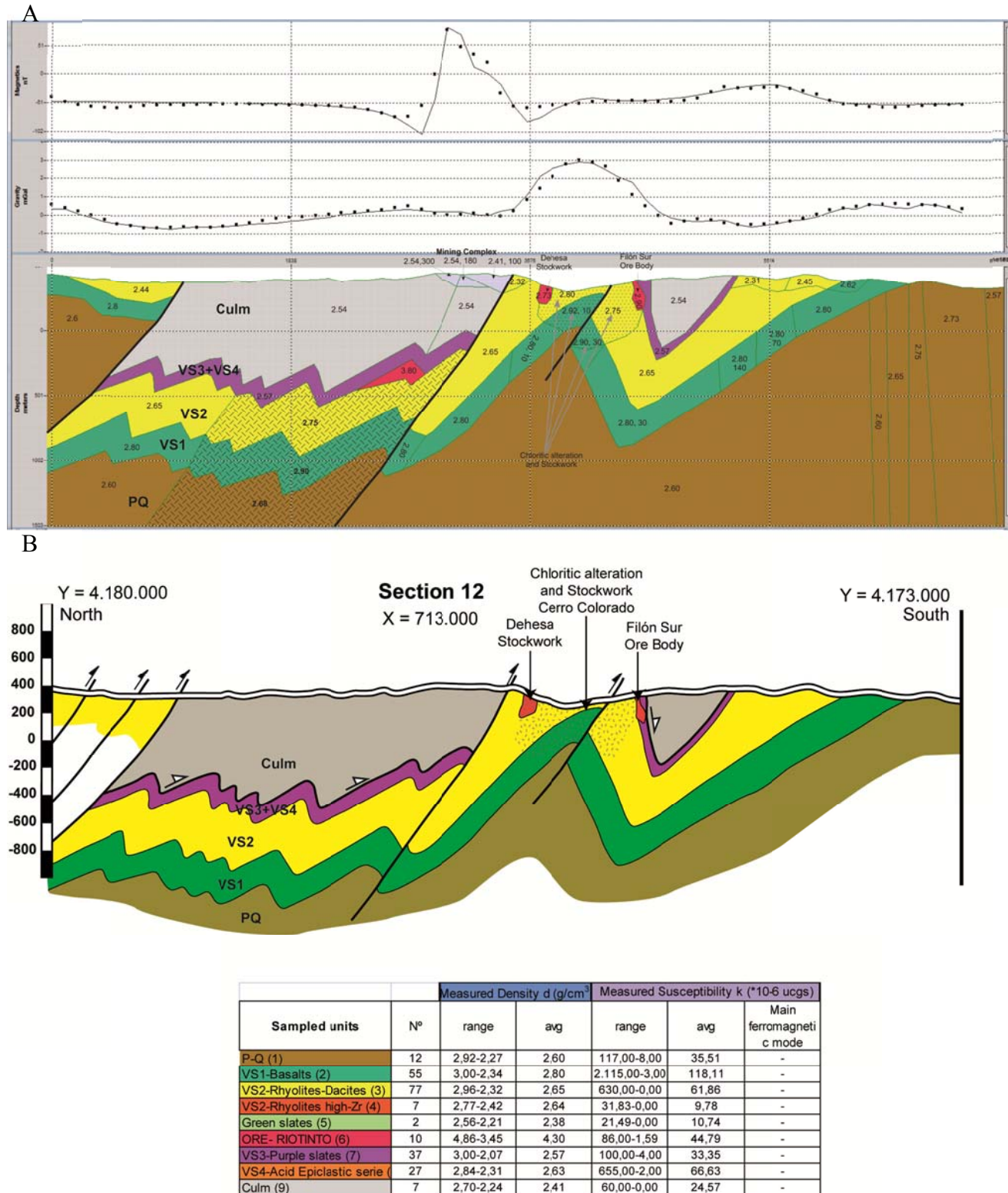
Figure 6.7. Profile 1. A) Fitted to gravity and magnetic anomalies cross-section model. Note the adjustment between measured (dotted line**)** and calculated (solid line) responses (magnetic above, gravimetric below). B) Geological cross-section. RMS of the gravity anomaly differences between

observed and calculated is 0.18 mGal. 2.54, 125= first number, density in g/cm^3; second number, magnetic susceptibility in cgs.
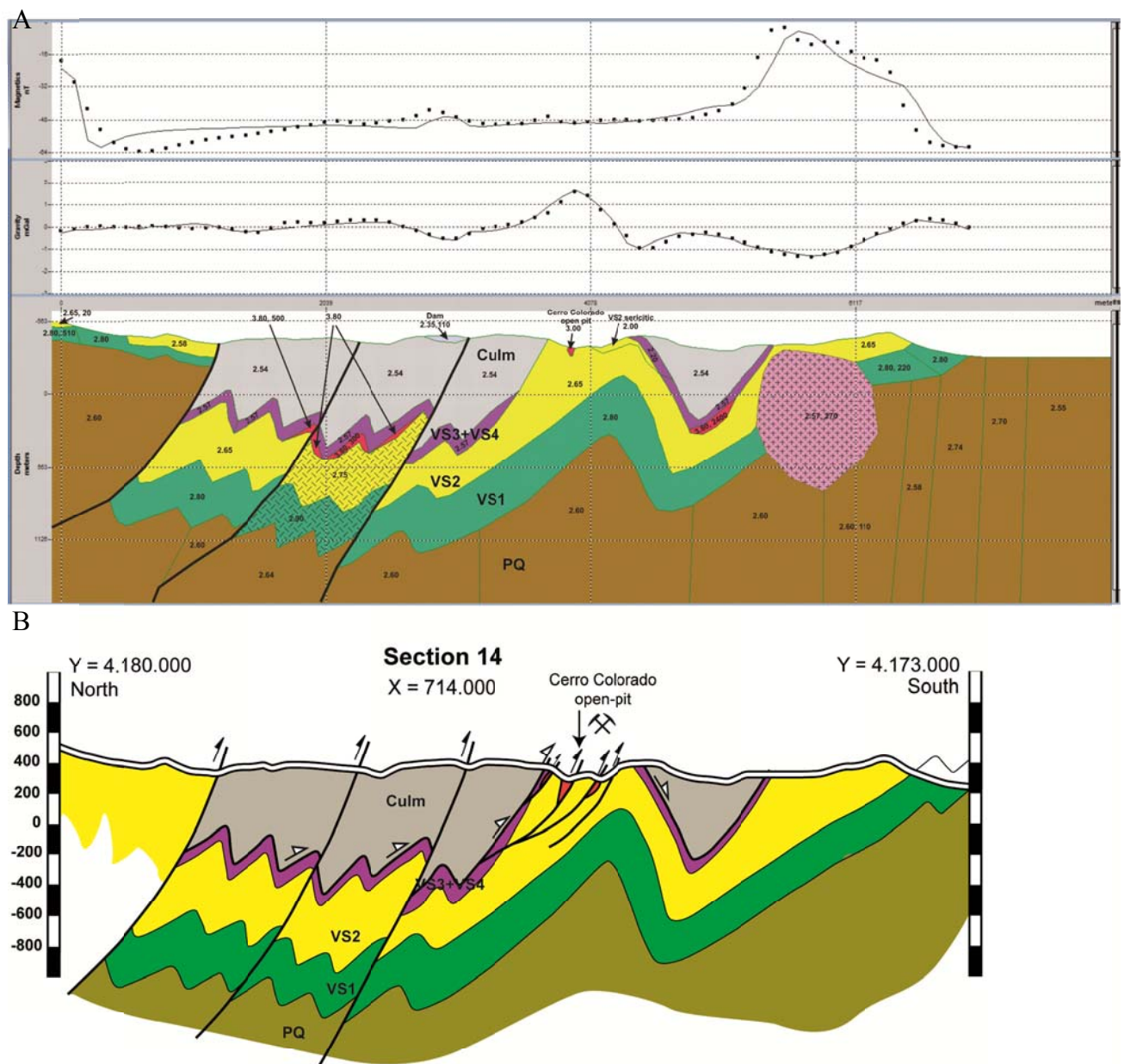
Section 1 (Figure 6.7) is characterized by a gentle N-S gravimetric slope from -1 to 2 mGal, due to the combination of the decrease in thickness of Culm and progressive shallowing of the PQ, since the thickness of the VS1, VS2, VS3 and VS4 is almost constant. Two additional features had to be modelled in order to fit the gravity data: an increase in the density of VS1 beneath the Culm, at the central part of the section, and two thin layers of massive sulphides with a density of 3.8 g/cm^3, beneath the VS3 and next to the southernmost fault.

The magnetic profile also shows a gentle N-S slope from -42 to c. -25 nT, with a sharp gradient at the boundary between the VS1 and the PQ, which leads to a minimum of c. -49 nT. That gradient and the minimum have been adjusted by the lateral changes in PQ magnetic susceptibility. The three relative maxima have been adjusted assuming lateral changes in the magnetic susceptibility of the VS1 and a high susceptibility in the massive sulphides south of the southernmost fault (Atalaya-Soloviejo fault; to see Geological Map, Fig. 6.2).

RMS of the gravity anomaly differences between observed and calculated is 0.1 mGal; RMS of the magnetic anomaly differences between observed and calculated is 1.3 nT

A

B

		Measured Density d (g/cm³)		Measured Susceptibility k (*10-6 ucgs)		
Sampled units	Nº	range	avg	range	avg	Main ferromagnetic mode
P-Q (1)	12	2,92-2,27	2,60	117,00-8,00	35,51	-
VS1-Basalts (2)	55	3,00-2,34	2,80	2.115,00-3,00	118,11	-
VS2-Rhyolites-Dacites (3)	77	2,96-2,32	2,65	630,00-0,00	61,86	-
VS2-Rhyolites high-Zr (4)	7	2,77-2,42	2,64	31,83-0,00	9,78	-
Green slates (5)	2	2,56-2,21	2,38	21,49-0,00	10,74	-
ORE- RIOTINTO (6)	10	4,86-3,45	4,30	86,00-1,59	44,79	-
VS3-Purple slates (7)	37	3,00-2,07	2,57	100,00-4,00	33,35	-
VS4-Acid Epiclastic serie (	27	2,84-2,31	2,63	655,00-2,00	66,63	-
Culm (9)	7	2,70-2,24	2,41	60,00-0,00	24,57	-

Figure 6.8. Profile 6. A) Fitted to gravity and magnetic anomalies cross-section model. Note the adjustment between measured (dotted line**)** and calculated (solid line) responses (magnetic above, gravimetric below). B**)** Geological cross-section. (Density in g/cm³. RMS of the gravity anomaly differences between observed and calculated is 0.18 mGal. 2.54, 125= first number, density in g/cm³; second number, magnetic susceptibility in cgs.

65

Section 6 (Figure 6.8) is characterized by a moderate gravity gradient from -1 to c. 1.8 mGal, due to the shallowing of the PQ. Superimposed to this signal, there is a relative maximum, located in the middle of the section originated by the central anticline, and flanked by two relative minima related with the different thickness of the Culm at both sides of the anticline. We haven't found any indication of the presence of massive sulphides along this section.

The main feature of the magnetic profile is a prominent maximum of c. 60 nT in amplitude, located above the Copper Dam (to which a susceptibility of 810 cgs has been assigned). The remaining part of the profile is rather flat (around -40 nT), with a succession of low amplitude maximum and minimum due to small variations in magnetic susceptibility within PQ and VS1.

RMS of the gravity anomaly differences between observed and calculated is 0.1 mGal; RMS of the magnetic anomaly differences between observed and calculated is 5.4 nT

A

B

Sampled units	Nº	Measured Density d (g/cm³)		Measured Susceptibility k (*10-6 ucgs)		Main ferromagnetic mode
		range	avg	range	avg	
P-Q (1)	12	2,92-2,27	2,60	117,00-8,00	35,51	-
VS1-Basalts (2)	55	3,00-2,34	2,80	2.115,00-3,00	118,11	-
VS2-Rhyolites-Dacites (3)	77	2,96-2,32	2,65	630,00-0,00	61,86	-
VS2-Rhyolites high-Zr (4)	7	2,77-2,42	2,64	31,83-0,00	9,78	-
Green slates (5)	2	2,56-2,21	2,38	21,49-0,00	10,74	-
ORE- RIOTINTO (6)	10	4,86-3,45	4,30	86,00-1,59	44,79	-
VS3-Purple slates (7)	37	3,00-2,07	2,57	100,00-4,00	33,35	-
VS4-Acid Epiclastic serie (	27	2,84-2,31	2,63	655,00-2,00	66,63	-
Culm (9)	7	2,70-2,24	2,41	60,00-0,00	24,57	-

Figure 6.9. Profile 9. A) Fitted to gravity and magnetic anomalies cross-section model. Note the adjustment between measured (dotted line) and calculated (solid line) responses (magnetic above, gravimetric below). B) Geological cross-section. (Density in g/cm³. Blue- assumed massive sulphides with a density of 3.8 g/cm³. RMS of the gravity anomaly differences between observed and calculated is 0.18 mGal. 2.54, 125= first number, density in g/cm³; second number, magnetic susceptibility in cgs.
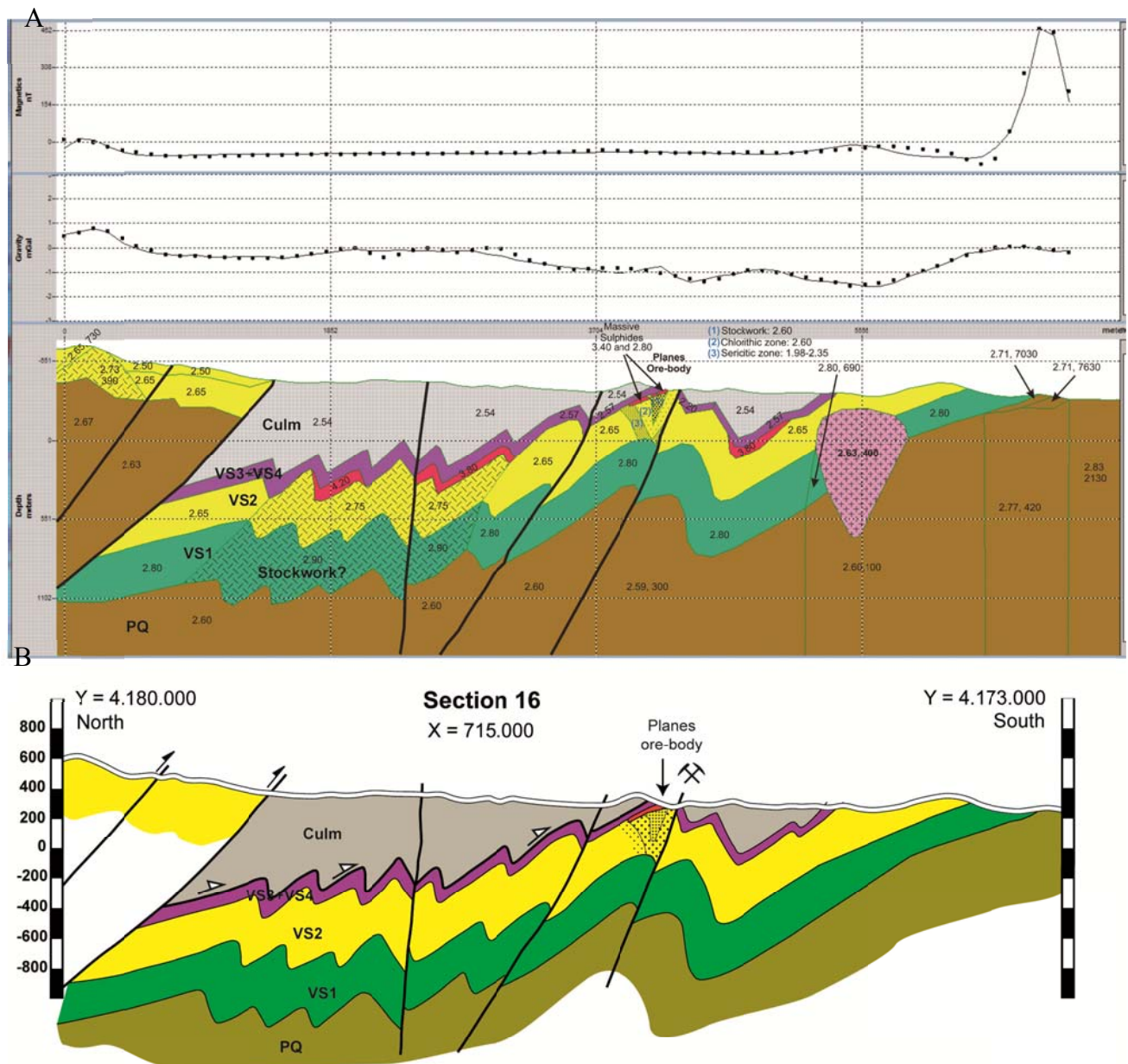
In section 9 (Figure (6.9), the gravity data is characterized by a subtle N-S gradient from -0.5 to 1 mGal with a succession of maxima and minima of different amplitudes and wavelengths. The first minima, about 0.7 mGal in amplitude and extending over a Culm outcrop has been assumed to be mainly due to its thickness, although a small increase in the PQ density is needed in order to improve the fitting of the anomaly in this area. In the neighbouring thrusts (c. 2570 and 4000 m in horizontal distance), as the volcanic suite, mainly VS2 and VS1 crops out, a certain alteration of the outcropping rocks is needed in order to fit the observed anomalies. The relative maxima centred on the Atalaya open-pit, about 1 mGal in amplitude, is primarily originated by the mineralization; because the mineralization is small compared with the grid spacing of the gravity data (0.5 km), it is not possible to model it with its real density, even limiting its lateral extension to 500 m. The transition to the following minimum is a local steep gradient that has been modelled assuming a thin layer of massive sulphides with a density of 3.8 g/cm^3. The aforementioned minimum is centred in an outcrop of VS2-VS3. It has been very difficult to adjust and finally we have settled by decreasing the density of the VS2 and VS1 by c. 0.05 g/cm^3, which is still within the range of measured densities. The southernmost end of the model adjusts the anomaly by slightly increasing the density within the PQ.

RMS of the gravity anomaly differences between observed and calculated is 0.1 mGal; RMS of the magnetic anomaly differences between observed and calculated is 4.2 nT

SECTION 12

A

B

Sampled units	Nº	Measured Density d (g/cm³)		Measured Susceptibility k (*10-6 ucgs)		Main ferromagnetic mode
		range	avg	range	avg	
P-Q (1)	12	2,92-2,27	2,60	117,00-8,00	35,51	-
VS1-Basalts (2)	55	3,00-2,34	2,80	2.115,00-3,00	118,11	-
VS2-Rhyolites-Dacites (3)	77	2,96-2,32	2,65	630,00-0,00	61,86	-
VS2-Rhyolites high-Zr (4)	7	2,77-2,42	2,64	31,83-0,00	9,78	-
Green slates (5)	2	2,56-2,21	2,38	21,49-0,00	10,74	-
ORE- RIOTINTO (6)	10	4,86-3,45	4,30	86,00-1,59	44,79	-
VS3-Purple slates (7)	37	3,00-2,07	2,57	100,00-4,00	33,35	-
VS4-Acid Epiclastic serie (	27	2,84-2,31	2,63	655,00-2,00	66,63	-
Culm (9)	7	2,70-2,24	2,41	60,00-0,00	24,57	-

Figure 6.10. Profile 12. A) Fitted to gravity and magnetic anomalies cross-section model. Note the adjustment between measured (dotted line) and calculated (solid line) responses (magnetic above, gravimetric below). B) Geological cross-section. (Density in g/cm³. Blue- assumed massive sulphides with a density of 3.8 g/cm³. RMS of the gravity anomaly differences between observed and calculated is 0.18 mGal. 2.54, 125= first number, density in g/cm³; second number, magnetic susceptibility in cgs.
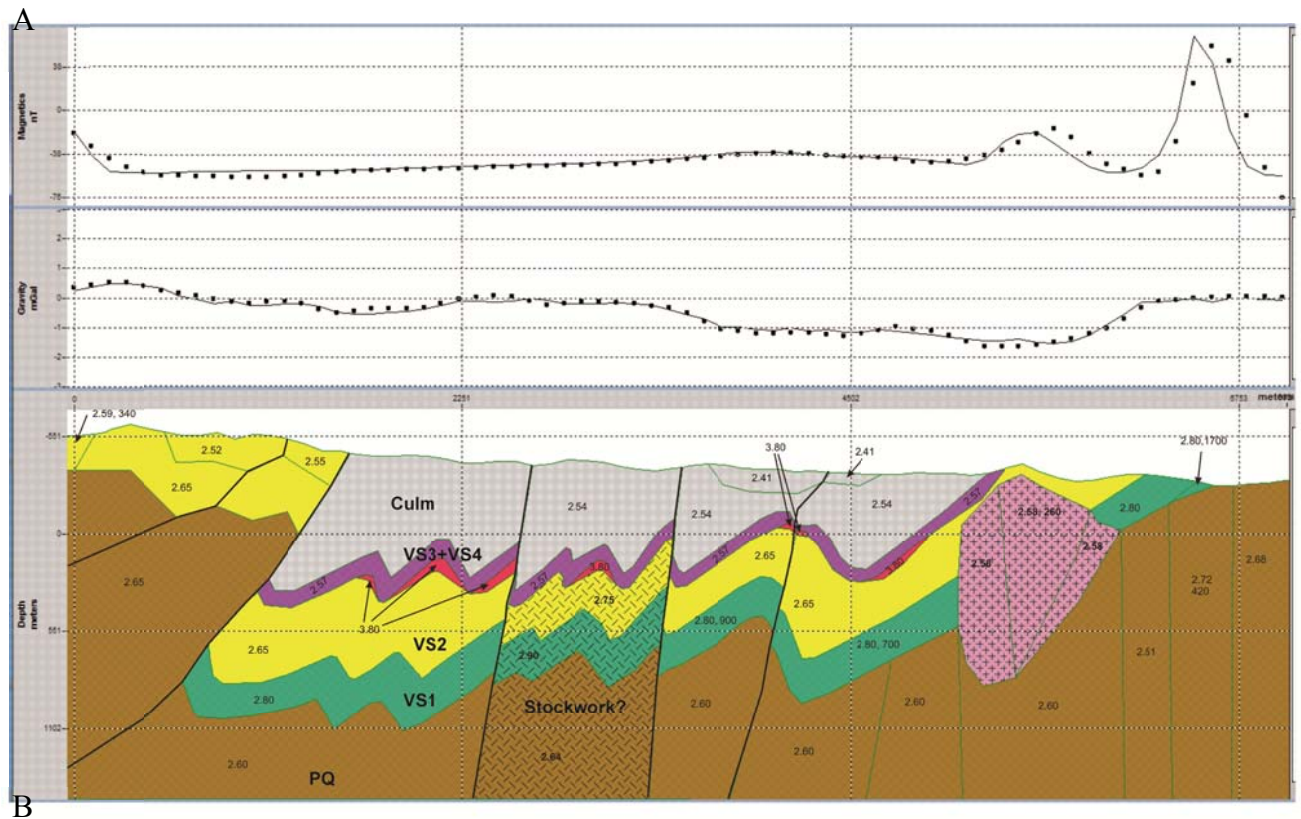
The most prominent gravimetric feature in the Section 12 (Figure 6.10) is the big maximum of c. 3 mGal in amplitude and about one km in length encompassing the Dehesa and Cerro Colorado stockwork and the Filón Sur ore-body. This maximum has been adjusted by assuming that the VS1 and VS2 are altered by chlorithisation and there is some stockwork within these formations, thus increasing its density up to 0.1 g/cm^3. Again, because both mineralization's are small in comparison with the gravimetric grid, the densities that have been assigned to them are unreal.

To the north, there is a small amplitude long wavelength minimum of c. 1 mGal that can be associated to a low density volcanics and the Culm nearby; superimposed to this minimum there is a steady gradient that ends up in a short wavelength maximum of c. 0.5 mGal in amplitude. The gradient has been associated to an increase of the density within the PQ, VS1 and VS2, that may be due to the existence of a stockwork, whereas the maximum has been adjusted assuming a small body of massive sulphides between the VS2 and VS3. To the south, medium wavelength small amplitude of minimum and maxima correspond to the combined effect of Culm and altered VS2, together with the shallowing of the PQ.

The magnetic profile almost flat, at c. 51 nT, with by two relative maximum superimposed, one of high amplitude (more than 150 nT), generated by the magnetic content within the Mining Complex, and another one of c. 25 nT in amplitude, that has been attributed to changes in magnetic susceptibility within the VS1.

RMS of the gravity anomaly differences between observed and calculated is 0.1 mGal; RMS of the magnetic anomaly differences between observed and calculated is 11 nT

SECTION 14

Sampled units	Nº	Measured Density d (g/cm³)		Measured Susceptibility k (*10-6 ucgs)		
		range	avg	range	avg	Main ferromagnetic mode
P-Q (1)	12	2,92-2,27	2,60	117,00-8,00	35,51	-
VS1-Basalts (2)	55	3,00-2,34	2,80	2.115,00-3,00	118,11	-
VS2-Rhyolites-Dacites (3)	77	2,96-2,32	2,65	630,00-0,00	61,86	-
VS2-Rhyolites high-Zr (4)	7	2,77-2,42	2,64	31,83-0,00	9,78	-
Green slates (5)	2	2,56-2,21	2,38	21,49-0,00	10,74	-
ORE- RIOTINTO (6)	10	4,86-3,45	4,30	86,00-1,59	44,79	-
VS3-Purple slates (7)	37	3,00-2,07	2,57	100,00-4,00	33,35	-
VS4-Acid Epiclastic serie (	27	2,84-2,31	2,63	655,00-2,00	66,63	-
Culm (9)	7	2,70-2,24	2,41	60,00-0,00	24,57	-

Figure 6.11. Profile 14. A) Fitted to gravity and magnetic anomalies cross-section model. Note the adjustment between measured (dotted line) and calculated (solid line) responses (magnetic above, gravimetric below). B) Geological cross-section. (Density in g/cm³. Blue- assumed massive sulphides with a density of 3.8 g/cm³. RMS of the gravity anomaly differences between observed and calculated is 0.18 mGal. 2.54, 125= first number, density in g/cm³; second number, magnetic susceptibility in cgs.

71

Along this section 14 (Figure 6.11), whose long wavelength component is almost constant at c. 0 mGal, the gravity anomaly shows a prominent central maximum of c. 1 mGal that can be associated to the combined effect of the mineralization Cerro Colorado stockwork and the VS2-VS1 anticline. North and South of this relative maximum, there are a set of maxima and minima of smaller amplitude (less than 0.7 mGal). In order to fit these anomalies, we have included three relevant features, deduced from the modelling, that weren't present in the initial geological model: **1/** the occurrence of a stockwork and massive sulphides, modelled as thin layers located between VS2 and VS3, **2/** the stockwork made of interbedded pyrite within the PQ, VS1 and VS2 that increases the density of those lithologies, located between faults and **3/** the presence of granites towards the southern end of the profile, which had been already predicted in other woks (e.g. Díez-Montes and Bellido-Mulas, 2008). A small amplitude (c. 0.5 mGal) and short wavelength gravity minimum located in the same place with high density VS1 and VS2, coincides with the dump of the mines, which is a low density area.

The SW magnetic maximum has been modelled as a more magnetic rock within the VS1; the prominent maximum towards the end of the profile has been modelled assuming slight ferromagnetic granitoid and some magnetization within the VS1. To the assumed massive sulphides, magnetic susceptibility varies between 0 and 2400 cgs.

RMS of the gravity anomaly differences between observed and calculated is 0.1 mGal; RMS of the magnetic anomaly differences between observed and calculated is 5.5 nT

A

B

Sampled units	Nº	Measured Density d (g/cm³)		Measured Susceptibility k (*10-6 ucgs)		
		range	avg	range	avg	Main ferromagnetic mode
P-Q (1)	12	2,92-2,27	2,60	117,00-8,00	35,51	-
VS1-Basalts (2)	55	3,00-2,34	2,80	2.115,00-3,00	118,11	-
VS2-Rhyolites-Dacites (3)	77	2,96-2,32	2,65	630,00-0,00	61,86	-
VS2-Rhyolites high-Zr (4)	7	2,77-2,42	2,64	31,83-0,00	9,78	-
Green slates (5)	2	2,56-2,21	2,38	21,49-0,00	10,74	-
ORE- RIOTINTO (6)	10	4,86-3,45	4,30	86,00-1,59	44,79	-
VS3-Purple slates (7)	37	3,00-2,07	2,57	100,00-4,00	33,35	-
VS4-Acid Epiclastic serie (	27	2,84-2,31	2,63	655,00-2,00	66,63	-
Culm (9)	7	2,70-2,24	2,41	60,00-0,00	24,57	-

Figure 6.12. Profile 16. A) Fitted to gravity and magnetic anomalies cross-section model. Note the adjustment between measured (dotted line) and calculated (solid line) responses (magnetic above, gravimetric below). B) Geological cross-section. (Density in g/cm³. Blue- assumed massive sulphides with a density of 3.8 g/cm³. RMS of the gravity anomaly differences between observed and calculated is 0.18 mGal. 2.54, 125= first number, density in g/cm³; second number, magnetic susceptibility in cgs.

Looking at the potential field's profiles, gravity and magnetic anomalies almost flat, it looks like an easy section to adjust. On the contrary, it has been very complicated, int the 16 section (Figure 6.12)

The pattern of the gravity anomaly shows a succession of relative maxima and minima of different amplitude and wavelength superimposed on a base line of c. 0 mGal. In addition of the three features deduced from the gravity data , the same as in Section 14 (the presence of massive sulphides as thin layers between VS2 and VS3; the stockwork of interbedded pyrite, but this time only within the VS1 and VS2 and the granite at the southern end of the profile) two additional features have been incorporated in the profile in order to adjust the gravity data: **1/** a high density VS2 at the northern end of the profile (we have assumed that the VS1 is absent in this part of the profile because a body of c.2.8 g/cm^3 makes impossible to match the observations); **2/** A combination of stockwork, chlorithic zone and sericitic zone, like a small anticline, have been necessary to adjust a very small amplitude maximum (not very well adjusted due to the undersampled gravity data that filters the effect of the Planes ore-body) and a small amplitude minimum next to it. The relative gravity maximum at the southern end of the profile has been associated to an increase in the PQ density.

The magnetic anomaly is flat except for a two short wavelength maximum located at both ends of the profile. The one at the north has small amplitude (tens of nT) and is related to the high density VS1. The one at the southern end has an amplitude of near 500 nT and has been modelled as two thin slices of high susceptibility PQ.

RMS of the gravity anomaly differences between observed and calculated is 0.1 mGal; RMS of the magnetic anomaly differences between observed and calculated is 15 nT

Figure 6.13. Profile 17. A) Fitted to gravity and magnetic anomalies cross-section model. Note the adjustment between measured (dotted line) and calculated (solid line) responses (magnetic above, gravimetric below). B) Geological cross-section (Density in g/cm³. Blue- assumed massive sulphides with a density of 3.8 g/cm³. RMS of the gravity anomaly differences between observed and calculated is 0.18 mGal. 2.54, 125= first number, density in g/cm³; second number, magnetic susceptibility in cgs.

Along this 17 section (Figure 6.13), whose pattern is similar to the ones in sections 14 and 16, the most relevant features deduced from the gravity modeling are: 1/ the occurrence of massive sulphides, modelled as thin layers located between VS2 and VS3, in slightly more quantity than in Profile 14, 2/ the stockwork made of interbedded pyrite within the VS1 and VS2 that increases the density of those lithologies, located between faults, 3/ the presence of a granitic body towards the southern end of the profile, which had been already predicted in other woks (e.g.: Díez-Montes and Bellido-Mulas, 2008).

The S magnetic maximum has been modelled as a variation in the magnetic character of VS2; in the central part of the profile, the magnetic data is fitted taking into account lateral variations in the magnetization of VS1; the medium amplitude and wavelength maxima on top of the granitoid is adjusted by a portion of the body with ferromagnetic properties. Finally, the prominent maximum at the end of the profile requires a high magnetization within VS1 (which is within the petrophysical range) but a higher than average magnetization within the PQ thus suggesting the possibility of intrusions within this formation (Tonalite-Trondhjemite-Granodiorite and Gabbros). To the assumed massive sulphides, magnetic susceptibility between 1000 and 2000 cgs has been assigned.

RMS of the gravity anomaly differences between observed and calculated is 0.1 mGal; RMS of the magnetic anomaly differences between observed and calculated is 11.7 nT

6.4.   The 3D model of the Río Tinto district

After importing the data corresponding to the lithological contacts from the map, they have to be projected on the topographic surface. This surface has been previously generated from the point grid generated in ArcGIS by direct triangulation. To reflect the slope variation, the contact curves have been densified before the projection. The codification of the lines is maintained since the import of the shape format, used for the translation between GIS and gOcad, keeps the fields used for the map. So, it is easy to filter the different types of curves. Afterwards, a manual edition is necessary to classify the curves as tops of each lithology.

As for the cross sections, the digitized curves have been classified in the same way as the contacts of the geological map. So, each surface can be generated from a set of lines coming from horizontal and vertical planes, when available. As limit for the model, a box, or Voxet, enclosing both kinds of curves has been created.

The surfaces or horizons have been generated as medium planes of each set of curves for each top and then each surface has been shaped using the D.S.I. (Discrete Smooth Interpolator), respecting the contact curves. To achieve this, the constraints to that curves must be established. To get a suitable surface, a succession of interpolations and triangle densifications has been used. Local edition has been necessary where some conflict has been detected, especially in reverse faults zones.

The faults system draw a complex pattern resulting in a difficult fault distribution hard to model. So, among all the existing faults, only the most relevant have been chosen. They have been created in a similar way as the horizons, taking fault traces from the map and fault interpretations from the cross sections. Again, the modelling using medium planes seems the best way to create these surfaces.

Intersections between fault surfaces have been constructed so that they respect the temporal relationships of the fault blocks and the lithological units. Surfaces are cut and their borders are linked to other surfaces or surface borders by means of constraints. Such constraints are the kind of border on surface or vector fault link. At the same time the constraints from curves and free borders are respected.

After the modelling of the faults, horizons have been cut by faults and constraints in faults borders have been established in order to recreate the fault slips. The horizons are thus defined by up to four types of constraints, namely, control points, border on straight line, border on surface and vector link on border, and where necessary, nodes have been blocked by control nodes.

The massive sulphide bodies are represented by surfaces with a different geometry mainly closed on it. They are generally well known as long as they have been mined and many data are available from drillings and level maps at large scale. The surfaces are thus constructed by triangulating between the outlines of two consecutive outlines among the pile of plans, so that a series of triangulated bands is got. Constraints can be set to the outlines and later interpolations led to a smoother surface that can be adjusted to other data, such us sections or drillings. And it has been possible to reconstruct the shape of the sulphide massive ore-body from drill-hole and plans of mine workings.

This procedure has allowed us to obtain a precise morphology of the massive sulphides that form the large ore-body of Río Tinto (Figure 6.14). All massive sulphides ore-body have been exploited by open-pit, except Planes-San Antonio which were exploited by underground mining. 'Corta Atalaya-San Dionisio', 'Filón Norte', 'Filón Sur' y 'Planes-San Antonio' are massive sulphides ore-bodies, while 'Mal Año-Dehesa', 'Salomón' y 'Quebrantahuesos' are intense stockwork, which can even replace the rock almost in its totality..
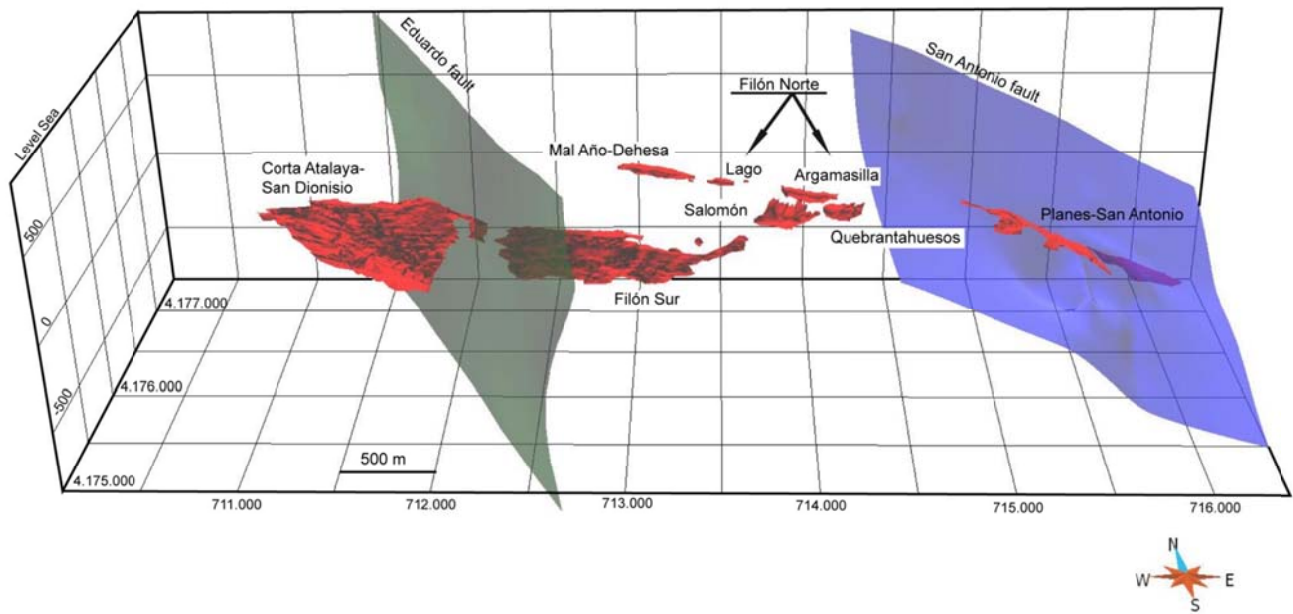
Figure 6.14. Visualisation from gOcad of the massive sulphide ore-body of Río Tinto.

goCad allows making models from a grid in order to make interpolations based on selected properties. Several simulations have been performed, in order to see if the variations in content of some elements are related to the geological structures in the area of study.

In gOcad, two types of cell distribution can be used: Voxet and SGrid. The latter (Stratigraphic GRID) has been chosen taking into account the bending of the anticlinal of Río Tinto. The SGrid is made of 79, 692, 500 cells and it has been built form a Voxet of 5x5x1 meters that has been deformed to adjust to the volume defined by the vulcano-sedimentary series. The method of interpolation used is the Discrete Smooth Interpolator. As a result, the simulation of the distribution of the elements adapts to the general structure.

The grades of the elements are hold as properties in the well objects in gOcad and are transferred to the cells prior to the interpolation.

Analytical contents of several elements of economic interest were available among the data provided by EMED Tartessus Company: Cu, S, Pb, Ag, Zn and As.The simulation shows the interpolation of the copper distribution in the Cerro Colorado open-pit. The correspondence between the zones of high grades and the ore-bodies is clear. The broad spread of the grades in the area is due to the stockwork and the chloritic alteration present in the central part of the anticline.The original data were taken from drilling campaigns previous to the open-pit, so the upper part of the structure is not present today. So, they have been useful to reconstruct the previous copper distribution.

78

Once the surfaces have been created and adjusted, a model can be constructed. The creation of a 3D model in gOcad implies the use of a number of regions in which the model is divided. Given the local nature of the model, a simplified stratigraphical column has been used, leaving seven major units (Figure 6.3), and the surfaces for these units have been created. In order to avoid unnecesary complexity in the eastern zone, when creating the 3D model in gOcad, six major units have been modelled, P-Q Group, basalts (VS1), rhyolites-dacites (VS2), sulphide massive, purple shales (VS3) and transition serie (VS4) (legend of the Figure 6.3).

The 3D model obtained shows the general structure in the area, a wide syncline with an anticline in the middle (Figure 6.15A) with the Culm formation above. The contact with the VSC is a detachment, eroding some parts of the underlying units. In order to make the figure easier to understand, this layer is not present in the figure, or the eroded upper part, so it becomes clear the folding at the central part and how it affects the sulphides. The sulphide massive ore-body is also shown, revealing their relationships with the acid volcanism and how they have been affected by the tectonics.

The 3D modelling of the Río Tinto geological structure and of the relationships between the thrusts and faults has greatly improved the understanding of this complex structure (Figure 6.15B). 3D modelling takes into consideration the strong lateral variations of the tectonic features and the thickness of each volcanic unit. Folded surfaces have been finally constructed in gOcad using cross-sections, fold axes and surface stratigraphic boundaries as constraints.
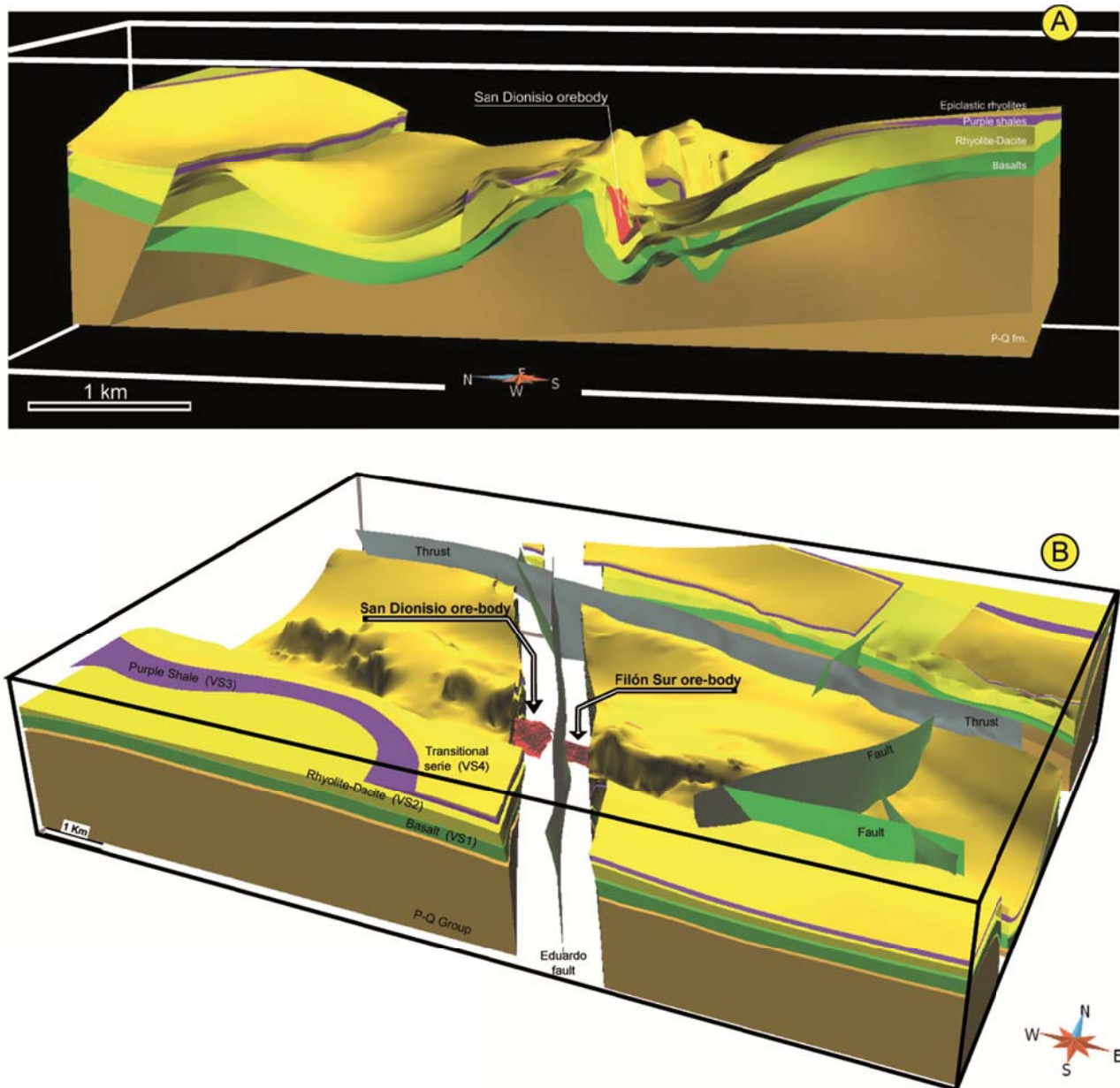
Figure 6.15. A)3D surface of structure Río Tinto N-S section.B). Visualisation of the 3D model of Río Tinto (See Annex VII).

7.   DISCUSSION AND CONCLUSIONS

7.1.   Petrophysics

Petrophysical data allows the geological interpretation of ground gravity and magnetic and radiometric high-resolution flights of the Río Tinto region. Furthermore, this dataset has been used to build up the 2.5D and 3D models of the area. From the analysis of the data the conclusions can be gathered in three groups:

A) Variability

- Lithologies and geological formations show a wide range of density, magnetic susceptibility and natural gamma radiation values; some of the lithologies are more homogeneous, displaying distinct physical properties, i.e., low magnetization, with moderate to high radioactive potassium content in rocks of VS2 and VS4. The Río Tinto rocks are in general low density paramagnetic rocks with a wide spectrum of radiometric signatures. The Ore deposits have very high values of density and very low susceptibility.

B) Petrophysical character

The petrophysical character of the main lithological groups and units has been established from the analysed data and their geophysical responses. Some remarkable differences between basic (VS1) (more dense and paramagnetic rocks) and VS2 (wide variability in density and magnetic susceptibility) have been observed.

- In the volcanic rocks, different types of alteration greatly modify the petrophysical response of density and magnetic susceptibility.
- The main geophysical markers of the Río Tinto region correspond to the ore deposits, depicting density maxima (4.30 g/cm^3) but being completely paramagnetic. Paramagnetic materials (and also low density materials) coincide with the Culm facies and rhyolites, breccias and acid epiclastic metasedimentary units of VS2-VS4. There are only a few strong ferromagnetic rocks in the sample, which correspond to the basic rocks of VS1 (a couple of basalts in Figure 4.7). Some jaspers can be also ferromagnetic (Plata and Navas, 1996), but these have not been sampled.
- Regarding gamma radiation in general, all the elements, especially U, are mobilized and concentrated in fault zones and / or contacts between the different units. Here the volcanic and volcanosedimentary rocks show gamma radiation values more similar to the average values presented by the granitoids of Cala area than the average values of metasediments (see García-Lobón et al., 2014).

7.2. Gravity, magnetic and radiometric maps

Bouguer anomaly reflects the contribution of the sources from the entire crust. Residual Bouguer, on the other hand, reflect the density distribution from shallower sources: metasedimentary low density in the north, the superposition of high density materials (outcropping of the Río Tinto ore mine) with the Culm facies (characterized by medium values of Bouguer anomaly) in the centre and the high

density materials at the south coinciding to Devonian slates, limestones and quartzites. A conspicuous minimum towards the southeast has been attributed to the presence of buried granites.

- Paramagnetic materials coincide with the Culm facies and rhyolites, breccias and acid epiclastic metasedimentary units in the northern area. The mining ore deposit of Río Tinto depict both magnetic (massive sulphurs and purple slates and jasper enriched in magnesium) and paramagnetic responses. In the south rhyolites, breccias and acid epiclastic show high magnetic intensity probably related to an E-W band of purple slates. The green and black slates are paramagnetic.

- Radiometric data show the predominance of K+Th signatures. Basic materials in the south are perfectly mapped by a white band indicating the absence of radiometric elements. The places with high concentrations in Th+U are located in the cover and the mining site itself

7.3.   Potential Resources Assessment

We have build up a predictive model which is based on the following assumptions:

1/ There are two styles of volcanogenic massive sulphide mineralization in the Iberian Pyrite Belt and located in different positions within the volcanic sequence. The first one includes dominantly exhalative shale-hosted deposits of likely late Strunian age and located at or near the PQ Group - Volcano Sedimentary Complex contact. This style of mineralization is located in the southern IPB and includes some major deposits such as Las Cruces, Aznalcóllar-Los Frailes, Sotiel-Migollas, Masa Valverde, Tharsis or Neves Corvo (Figure 6.1). The second style of mineralization includes the deposits located in the northern part of the IPB; they are usually hosted by glassy/pumice-rich rocks domes of dacite-rhyolite composition and of early Tournaisian age. The most significant deposits are San Telmo, Aguas Teñidas, Concepción and San Platón (Figure 6.1). Both Río Tinto and La Zarza belong to this group but have a shale-hosted exhalative zone above a volcanic-hosted remplacive one. Both styles of mineralization have an underlying stockwork.

2/ The estimated total tonnage of the already discovered deposits (including both the stockwork and the massive sulphides) is ca. 852 Mt in the southern zone and 1085 Mt in the northern zone.

3/ Thus, there are two major ore-bearing horizons: The shale and volcanic rocks near the PQ Group - VS Complex contact in the southern zone and the hanging wall of a dacite-rhyolite unit in the northern zone. These two metalotecs are reasonable well explored and is unlikely that there are undiscovered masses at depths, on average, above 800 m near the ore deposits and 200 m away from them. For the estimation, unknown new deposits should be at depths higher than 600 m.

4/ The final assumption is that deposits located at depths near 1000-1200 m can be mined if grades and tonnages are enough.

Assuming these assumptions are correct, then the amount of undiscovered massive sulphides is ca. 1.7 Gt in the southern part and 2.1 Gt in the northern part. These estimations include both massive sulphides and stockwork zones.

Specifically in the Río Tinto area, from the 2.5 D potential field modelling, we have been able to identify two areas of great interest (Figure 7.1, zones A y B) due to the possible presence of massive sulphides and stockwork zones, as we can see in some of the profiles (Sections 1, 9, 12, 14, 16 and 17; Figures 6.7; 6.9; 6.10; 6.11; 6.12 and 6.13). It has been neccesary to add these masses of massive sulphides and stockwork in the models in order to better fit the gravimetric data. The massive sulphides have been added on top of the VS2 whereas the stockwork is widespread within the VS1and VS2 (see its distribution on the figures). The 2.5D modelling has also revealed the existence of a buried granite (sections 16 and 17, figures 6.12 and 6.13), that had previously predicted by Díez-Montes and Bellido-Mulas (2008).

Also from the detailed geological field work and the study of fractures, we have identified two other possible areas of potential interest (Figure 7.1, zones C y D). These areas are associated with two faults that link of Atalaya-San Dionisio massive sulphide ore-body with other worked mineralizations located to the NW (La Poderosa mine and Soloviejo mine).
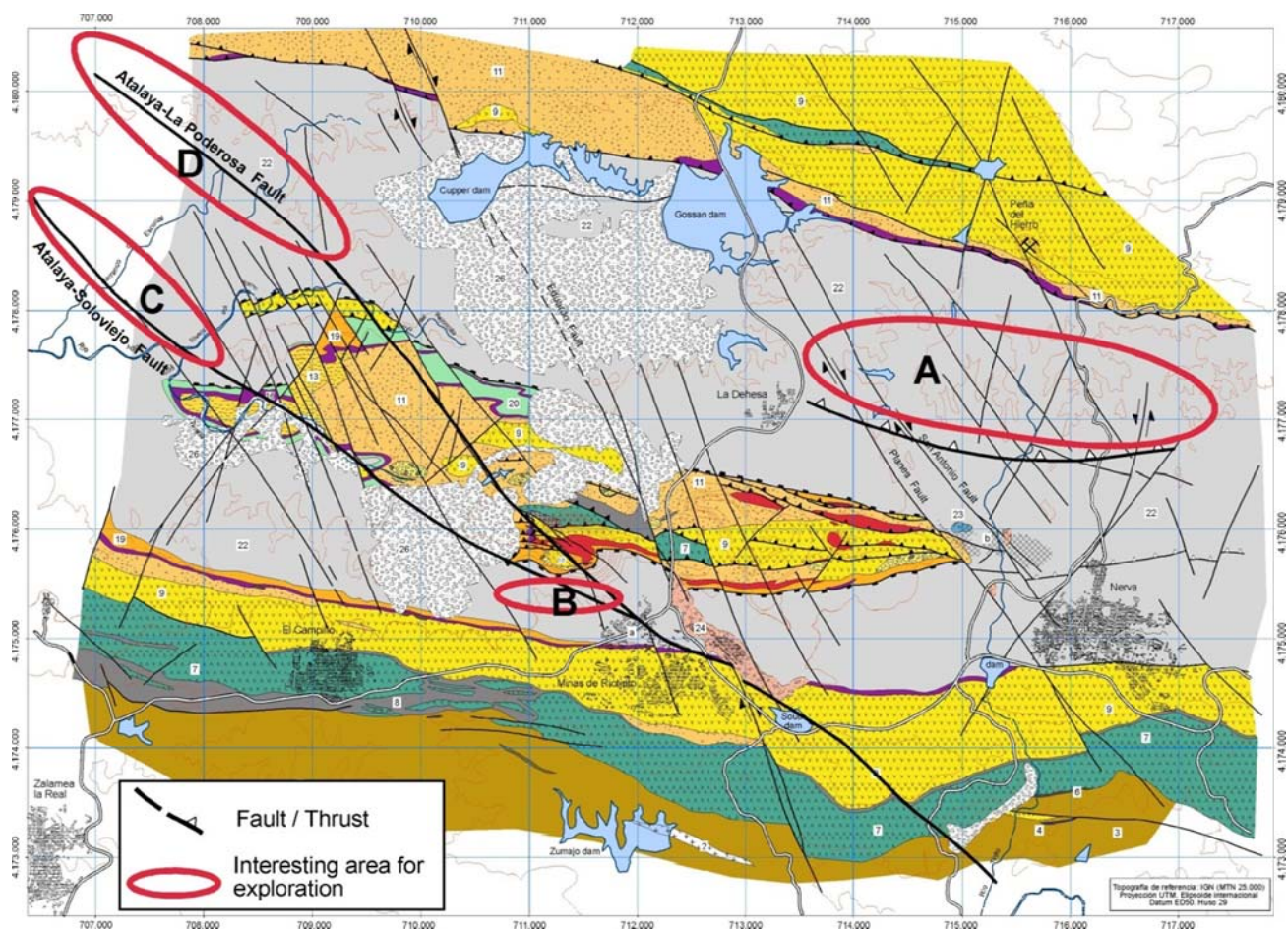
Figure 7.1. Potential interest areas next to Río Tinto mining district (Legend as Figure 2).

With the combination of geologic, magnetic and gravity anomalies, together with results in the ternary map, the areas outlined in the Figure 7.1 are considered to be as potential places for mineral exploration. These possible mining places require further investigation and its limits could be better defined using radiometric maps.

7.4. Concluding remarks

The detailed map of the Río Tinto anticline reveals the complex tectonics of this zone. We have been able to identify the detachment which is located at the contact between CVS and the Culm. This detachment is folded and cut by ductile thrust and then by out of sequence thrust. Detachment and thrust can produce a tectonic stacking. This tectonic stacking can contribute to vary the tonnage of a VHMS deposit.

The 2.5D modelling results indicated that a further revision of the initial geological model was necessary in order to fit the anomalies:

- The relative minimum located to the SW in the residual Bouguer anomaly requires the presence of buried granite in order to be adjusted in a "geological fashion" without having to draw unrealistic geometries to the volcanosedimentary sequences or unlikely low densities to the PQ. This granite was already postulated by Díez-Montes and Bellido-Mulas (2008).

- Some of the profiles have required an increase in the density of the PQ, VS1 and VS2 beneath the central part of the northern outcropping Culm facies, which have been assume to have massive sulphides and stockwork and to be within a thrust that was not considered before because there is difficult to distinguish on the field.

- Some of the small amplitude relative maxima have been adjusted by assuming the presence of massive sulphides between VS2 and VS3. Again this is required in order to preserve the consistence between geometries and physical properties and avoid unrealistic scenarios.

The 3D model shows the location and dimensions of the orebodies and has been used to estimate the tonnage of new possible mining areas and also as an input for the 4D modelling

The 4D modelling is a way to understand the deformation processes and how the mineralized bodies have reached their actual position. They can also be used as a way to predict where other mineralisation's can be found.

Acknowledgements

8.   REFERENCES

Barrie, C.T., Amelin, Y., Pascual, E. 2002. U-Pb Geochronology of VMS mineralization in the Iberian Pyrite Belt. Mineralium Deposita, 37: 684-703.

Bates, M., García-Lobón, J.L. 1998. Exploration of Pyrite Belt and surrounding areas concerning aeromagnetic and radiometric data. IGME documentary Report (SID Nº. 40464. Madrid). Available on line:http://www.igme.es/internet/sistemas_infor/Sid.htm

Broome, J.H. 1987. A modified ternary radioelement mapping technique and its application to the south coast of Newfoundland. Geological Survey of Canada, paper 87-14.

Broome, J.H. 1990, Generation and interpretation of geophysical images with examples from the Rae Province, north western Canada Shield. Geophysics, 55, 977-997.

Castroviejo, R., Quesada, C., Soler, M. 2010. Post-depositional tectonic modification of VMS deposits in Iberia and its economic significance. Mineralium Deposita, DOI: 10.1007/s00126-010-0306-7.

Darnley, A. & Ford, K. L.1989.Regional airborne gamma-ray surveys: a review. Exploration 87 Proceedings: Third Decennial International Conference on Mineral and Groundwater Exploration. Geophysical methods: advances in the state of the art. G.D. Garland (ed.), Ontario Geological Survey, 3, 229-240.

de la Rosa, J.D. 1992. Petrología de las rocas básicas y granitoides del Batolito de la Sierra Norte de Sevilla. Zona Surportuguesa, Macizo Ibérico. Tesis Doctoral, Universidad de Sevilla, 312 p. y anexos.

Díez-Montes, A. y Bellido Mulas, F. 2008. Magmatismos TTG y Al-K en la Zona Surportuguesa. Relaciones entre plutonismo y vulcanismo. Geo-Temas, 10: 1449-1452.

Díez-Montes, A., Bellido, F., Sánchez, T., Tornos, F., García Crespo, J. (2014). Lithogeochemistry of volcanic rocks in the Río Tinto Mine, Iberian Pyrite Belt, Spain (ProMine project). Serie de Informes técnicos 9, ISSN 1889-576X, IGME, Madrid, Spain, 1-59.

Dunning, G.R., Díez Montes, A., Matas, J., Martín Parra, L.M., Almarza, J., Donaire, M. 2002. Geocronología U/Pb del volcanismo ácido y granitoides de la Faja Pirítica Ibérica (Zona Surportuguesa). Geogaceta, 32: 127-130.

Fairhead, J. D., C. M. Green, and D. Blitzkow. 2003. The use of GPS in gravity surveys: The Leading Edge, 22, 954–959.

H Hammer, S., 1939. Terrain corrections for gravimeter stations. Geophysics, 3, 184-194.

IGME, 1982. Síntesis Geológica de la Faja Pirítica del SO de España. Instituto Geológico y Minero de España, Madrid. 106 pp.

Jorge, R., Fernandes, P., Pereira, Z., Oliveira, J.T. 2007. A late Famennian age storm-dominated succession at Berrocal, Iberian Pyrite Belt-Spain. In: Z. Pereira, J, T., Oliveira, R. Wicander, CIMP Lisbon 07- Joint Meeting of Spores /Pólen and Acritarch Sub-commissions. Abstracts, 83-87.

Mantero, E.M., García Navarro, E., Alonso-Chaves, F.M., Martín Parra, L.M., Matas, J., Azor, A. 2007. La Zona Sudportuguesa: propuesta para la división de un bloque continental en dominios. Geogaceta, 43: 27-30.

Mellado, D., González Clavijo, E.J., Tornos, F., Conde, C. 2006. Geología y estructura de la Mina de Riotinto (Faja Pirítica Ibérica, España). Geogaceta, 40: 231-234.

Navarro Vázquez, D. and Ramírez Copeiro del Villar, J. 1982. Mapa y Memoria de la Hoja nº 938 (Nerva). 2ª serie del Mapa Geológico Nacional a escala 1:50.000 (MAGNA). Instituto Geológico y Minero de España, Madrid.

Oliveira, J.T. 1990. South Portuguese Zone: Introduction. Stratigraphy and synsedimentary tectonism. In: Dallmeyer, R.D. & Martínez García, E. (eds.). Pre-Mesozoic Geology of Iberia. Springer, Berlin, 333-347.

Oliveira, J.T., Horn, M., Paproth, E. 1979. Preliminary note on the stratigraphy of the Baixo Alentejo Flash Group, Carboniferous of Portugal, and on the paleogeographic development compared to

corresponding units in northwest Germany. Comunicações Serviços Geológicos Portugal, 65: 151-168.

Pereira, Z., Matos, J., Fernandes, P. Oliveira J.T. 2008. Palynostratigraphy and Systematic Palynology of the Devonian and Carboniferous Successions of the South Portuguese Zone, Portugal. Memória N.º 34 do INETI, p.: 1-176.

Plata, J. L., 1991. Programa CCT (cálculo de la corrección topográfica por el método de Hammer). Documento interno Área de Geofísica, IGME.

Plata, JL.; Marcuello, A.; Madrid, A.; 2002. Informe Geofísica del Proyecto Geotermallorca. N.F.D. del IGME 62534

Plata, J.L.and Navas, J. 1996. Proyecto integrado de estudio Geológico y Metalogenético de la Faja Pirítica. Geofísica. Parte II: Caracterización petrofísica de unidades y edición digital de Cartografía Geofísica. IGME internal report SID 40454.

Quesada, C. 1998. A reappraisal of the structure of the spanish segment of the Iberian Pyrite Belt. Mineralium Deposita, 33: 31-44.

Ribeiro, A., Silva, JB. 1983. Structure of the South Portuguese Zone. In : Sousa MJL, Oliveira JT (Eds). The Carboniferous of Portugal. Mem.Ser.Geol.Port., 29, 83-89.

Rodríguez, R.M., Díez-Montes, A., Leyva, F., Matas, J., Almarza, J., Donaire, M. 2002. Datación palinoestratigráfica del volcanismo en la sección de la Ribera del Jarama (Faja Pirítica Ibérica, Zona Surportuguesa). Geogaceta, 32: 247-250.

Rosa, D.R.N., Finch, A.A., Andersen, T., C. M. C. Inverno, C.M.C. 2009. U–Pb geochronology and Hf isotope ratios of magmatic zircons from the Iberian Pyrite Belt. Miner. Petrol., 95: 47-69

Schermerhörn, L.J.G. 1971. An outline of the stratigraphy of the Iberian Pyrite Belt. Boletín Geológico y Minero de España, 82: 239-268.

SIGECO Geophysical Dabase (on line). Geological Information System SIGECO. IGME (2014). Editor: J. Navas. Available in: http://cuarzo.igme.es/sigeco/default.htm

Silva, J.B., Oliveira, J.T., Ribeiro, A. 1990.Part VI: South Portuguese Zone. 3: Structural Outline. In: Dallmeyer, R.D. and Martínez García, E. (eds.). Pre-Mesozoic Geology of Iberia. Springer-Verlag Berlin Heidelberg, 348-362.

Simancas, J.F. 1983. Geología de la extremidad oriental de la Zona Sudportuguesa. Tesis Doctoral, Univ. Granada, España, 439 pp.

Simancas, J.F., Carbonell, R., González Lodeiro, F., Pérez Estaún, A., Juhlin, C., Ayarza, P., Kashubin, A., Azor, A., Martínez Poyatos, D., Almodóvar, G.R., Pascual, E., R. Sáez, R., Expósito, I. 2003. Crustal structure of the transpressional Variscan orogen of SW Iberia: SW Iberia deep seismic reflection profile (IBERSEIS). Tectonics, 22 (6), 1062, doi: 10.1029/2002TC001479.

Somigliana C., 1929. Teoria generale del campo gravitazionale dell' ellisoide di rotazione, Mem. Soc. Astron. Ital., Vol. IV.

Talwani, M., Heirtzler, J. R. 1964. Computation of magnetic anomalies caused by two dimensional bodies of arbitrary shape. In: Parks, G. A. (Ed.), Computers in the mineral industries, Part 1. Stanford University Publications, Geological Sciences, 9: 464-480.

Talwani, M., Worzel, J. L., Landisman, M. 1959. Rapid gravity computations for two dimensional bodies with application to the Mendocino submarine fracture zone. Journal of Geophysical Research, 64: 49-59.

Tornos, F., Casquet, C., Relvas, J.M.R.S. 2005. Transpressional tectonics, lower crust decoupling and intrusion of deep mafic sills: A model for the unusual metallogenesis of SW Iberia. Ore Geology Reviews, 27: 133-163.

Valenzuela, A., Donaire, T., Pin, C., Toscano, M., Hamilton, M.A., Pascual, E. 2011. Geochemistry and U–Pb dating of felsic volcanic rocks in the Riotinto-Nerva unit, Iberian Pyrite Belt, Spain: crustal thinning, progressive crustal melting and massive sulphide genesis. Journal of the Geological Society, London, 168: 717-731.

Velasco, F., Sánchez-España, J., Boyce, A.J., Fallick, A.E., Sáez, R., Almodóvar, G.R. 1998. A new sulphur isotopic study of some Iberian Pyrite Belt deposits: evidence of a textural control on sulphur isotope composition. Mineralium Deposita, 34: 4-18.

Won, I.J., Bevis, M. 1987. Computing the gravitational and magnetic anomalies due to a polygon: Algorithms and Fortran subroutines. Geophysics, 52: 232-238.

9.   ANNEXS

I. Staff

The staffs involved in this work have been:

-Main team:

José Luis García-Lobón (jl.garcia@igme.es: Head of the project. Data interpretation. Petrophysics.
Teresa Sánchez García (t.sanchez@igme.es): Petrophysics. Data interpretation and modelling
Concepción Ayala Galán (c.ayala@igme.es): Gravity, data processing and modelling. Petrophysics.
Alejandro Díez Montes (a.diez@igme.es): Geology and modelling. Data interpretation. Petrophysics.
Jesús García Crespo (garcia.crespo@igme.es): Modelling and geology
Félix Bellido Mulas (ffbbmm50@gmail.com): Data interpretation.Geology
Carmen Rey Moral (c.rey@igme.es): Data interpretation
Félix M. Rubio (fm.rubio@igme.es: Geophysical survey coordinator. Topography and data processing
-Office support team:

Israel Pérez Ortiz (i.perez@igme.es): Processing and database management

Maria Isabel Reguera (mi.reguera@igme.es): Processing and database management

-Field workers (gravity-GPS surveyors):

José María Llorente Delgado (jm.llorente@igme.es).

Agustín González Durán (ag.gonzalez@igme.es).

II.   Measurements

Measured units used in this work are:

Gravity:	mGal (normal value g ~ 980.000 mGal)
Magnetic field:	nT (10^{-9} Teslas)
Distance and altitude:	m (meters)
Density:	g/cm^3 (gram/c. cubic)
Natural gamma radiation:	% K, ppm U, ppm Th
Coordinates:	UTM Zone 29 North referring to ED50 metres system

IV.   List of Tables

V. 3D Model

It contains 3D models in 3D pdf format of Río Tinto zone. Adobe Reader XI is recommended.

www.igme.es/Publicaciones/PubliGratuitas.htm/Informe8_Annex_V_RioTinto3D_IGME_SP_3D_1 7042013.pdf?dl=0

www.igme.es/Publicaciones/PubliGratuitas.htm/Informe8_Annex_V_RioTinto_IGME_SP_3D_1704 2013.docx?dl=0

It includes a video-clip of 4D evolution of Río Tinto zone and Santa Olalla de Cala-Aguablanca areas.

www.igme.es/Publicaciones/PubliGratuitas.htm/Informe8_10_Annex_V_Iberian_Belt_IGME_SP_4 D_17042013.avi?dl=0

www.igme.es/Publicaciones/PubliGratuitas.htm/Informe8_10_Annex_III_Iberian_Belt_IGME_SP_4 D_17042013.docx?dl=0